

*Institute of
Geophysics and
Planetary
Physics*

*Lawrence Livermore
National Laboratory*

1998
Annual Report

*October 1, 1997 through
September 30, 1998*

*Edited by
Frederick J. Ryerson, Kem H. Cook, and Jan Tweed
Institute of Geophysics and Planetary Physics
University of California*

Acknowledgments

This report was edited and produced by Jan Tweed, who also prepared the manuscript and graphics. Special thanks go to Marsha McNinnis, who offered her formidable expertise on the illustrations. Rick Ryerson and Kem Cook performed the scientific edits.

Section I. Overview _____ 1

Section II. Highlights of Fiscal Year 1998

Astrophysics Research Center _____ 3

Center for Geosciences _____ 11

Section III. Research Summaries of Collaborative Projects

Astrophysics

A VLA Survey of the Sky at 1400 MHz

Robert Becker, Wil van Breugel, Sally Laurent-Muehleisen _____ 29

Speckle and Adaptive Optics Imaging of Planets and Satellites

Imke de Pater, Seran Gibbard, Don Gavel, Bruce Macintosh, Claire Max, Henry Roe _____ 31

A Phonon-Mediated Particle Detector for Observational Cosmology
and Gamma-Ray Astronomy

Bernard Sadoulet, Carl A. Mears, Simon Labov, Matthias Frank, Sunil Golwala _____ 34

A Search for Red Quasars: The Radio-Loud Quasar Population at $z \geq 3$

Hyron Spinrad, Wil van Breugel, Daniel Stern _____ 37

Numerical Studies of Fragmentation in Star-Forming Regions

Christopher F. McKee, Richard I. Klein, Robert T. Fisher _____ 39

Geosciences

Geologic Constraints on the Magnitude, Age, and Rate of Slip along the
Cenozoic Karakorum Fault System in Western Tibet

A. Yin, T. M. Harrison, F. J. Ryerson, M. A. Murphy _____ 41

Molten Crust Beneath Tibet?

T. Mark Harrison, An Yin, F. J. Ryerson, Paul Kapp _____ 44

Application of the UC-LLNL Regional Climate System Model to the
Malibu Creek Watershed

John A. Dracup, Norman L. Miller, Thomas C. Piechota _____ 47

Noble Gases Dissolved in Groundwater from the Northern United States:
Tracers for Paleoclimate and Groundwater Flow

Jordan F. Clark, G. Bryant Hudson, Mark Caffee, Laura K. Rademacher _____ 50

Schumann Resonance Measurements and Climate Models

Steven Constable, Benjamin Santer, Martin Fullekrug _____ 51

Integrating Postseismic Relaxation into Crustal Stress Evolution Models <i>Louise Kellogg, William Foxall, Fred Pollitz</i>	54
Dynamic Earthquake Rupture Simulation on Dipping Faults <i>Ralph J. Archuleta, William Foxall, Larry J. Hutchings, Stefan B. Nielsen, Edward Zywicz, David D. Oglesby</i>	58
3-D Modeling of Structure in D" <i>Barbara Romanowicz, Doug Dreger, Shawn Larsen, Ludovic Bréger</i>	61
High-Resolution Study of Inner-Core Rotation <i>John E. Vidale, Doug Dodge, Fei Xu</i>	65
Controls of U Groundwater Chemistry Constrained by AMS ^{14}C and ^{36}Cl <i>James B. Gill, Gregory Nimz, Aaron O. Reyes</i>	68
Deformation of Olivine: Comparison of Predictions with Experiments <i>Hans-Rudolf Wenk, Bill Durham, Yanxia Xie</i>	71
<hr/>	
Section IV. IGPP–LLNL Seminars	75
<hr/>	
Section V. Bibliography	79
<hr/>	
Section VI. Fiscal Year 1999 IGPP–LLNL University Collaborative Research Program	87

Section I. Overview

The Institute of Geophysics and Planetary Physics (IGPP) is a Multicampus Research Unit of the University of California (UC). IGPP was founded in 1946 at UC Los Angeles with a charter to further research in the earth and planetary sciences and related fields. The Institute now has branches at UC campuses in Los Angeles, San Diego, and Riverside, and at Los Alamos and Lawrence Livermore national laboratories.

The University-wide IGPP has played an important role in establishing interdisciplinary research in the earth and planetary sciences. For example, IGPP was instrumental in founding the fields of physical oceanography and space physics, which at the time fell between the cracks of established university departments.

Because of its multicampus orientation, IGPP has sponsored important interinstitutional consortia in the earth and planetary sciences. Each of the five branches has a somewhat different intellectual emphasis as a result of the interplay between strengths of campus departments and Laboratory programs.

The IGPP branch at Lawrence Livermore National Laboratory (LLNL) was approved by the Regents of the University of California in 1982. IGPP–LLNL emphasizes research in tectonics, geochemistry, and astrophysics. It provides a venue for studying the fundamental aspects of these fields, thereby complementing LLNL programs that pursue applications of these disciplines in national security and energy research.

IGPP–LLNL is directed by Charles Alcock and was originally organized into three centers: Geosciences, stressing seismology; High-Pressure Physics, stressing experiments using the two-stage light-gas gun at LLNL; and Astrophysics, stressing theoretical and computational astrophysics. In 1994, the activities of the Center for High-Pressure Physics were merged with those of the Center for Geosciences.

The Center for Geosciences, headed by Frederick Ryerson, focuses on research in geophysics and geochemistry. The Astrophysics Research Center, headed by Kem Cook, provides a home for theoretical and observational astrophysics and serves as an interface with the Physics Directorate's astrophysics efforts.

The IGPP branch at LLNL (as well as the branch at Los Alamos) also facilitates scientific collaborations between researchers at the UC campuses and those at the national laboratories in areas related to earth science, planetary science, and astrophysics. It does this by sponsoring the University Collaborative Research Program (UCRP), which provides funds to UC campus scientists for joint research projects with LLNL. Additional information regarding IGPP–LLNL projects and people may be found at <http://www-igpp.llnl.gov/>.

The goals of the UCRP are to enrich research opportunities for UC campus scientists by making available to them some of LLNL's unique facilities and expertise, and to broaden the scientific program at LLNL through collaborative or interdisciplinary work with UC campus researchers.

UCRP funds (provided jointly by the Regents of the University of California and by the Director of LLNL) are awarded annually on the basis of brief proposals, which are reviewed by a committee of scientists from UC campuses, LLNL programs, and external universities and research organizations. Typical annual funding for a collaborative research project ranges from \$5,000 to \$30,000. Funds are used for a variety of purposes, such as salary support for UC graduate students, postdoctoral fellows, and faculty; and costs for experimental facilities.

A statistical overview of IGPP–LLNL's UCRP (colloquially known as the mini-grant program) is presented in Figures 1 and 2. Figure 1 shows the distribution of UCRP awards among the UC campuses, by total amount awarded and by number of proposals funded. Figure 2 shows the distribution of awards by center.

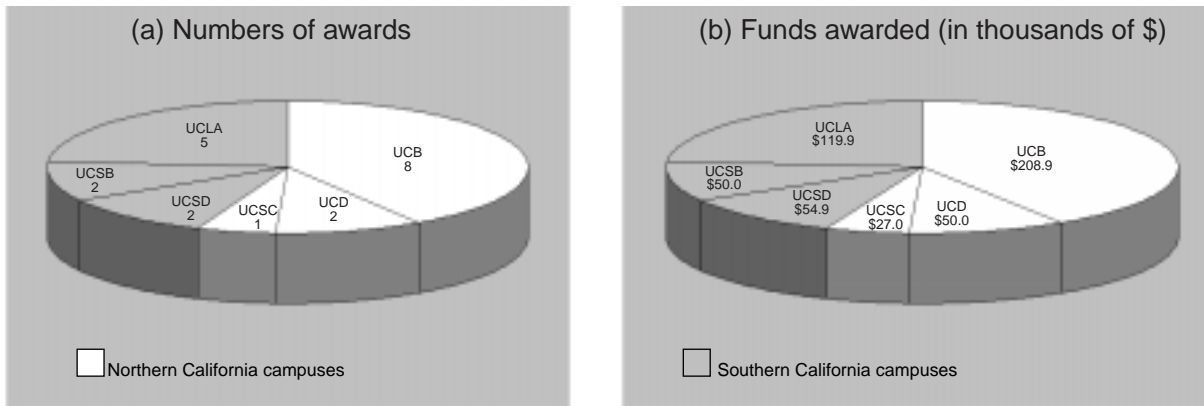


Figure 1. Distribution of FY 1998 UCRP awards to UC campuses from IGPP-LLNL.

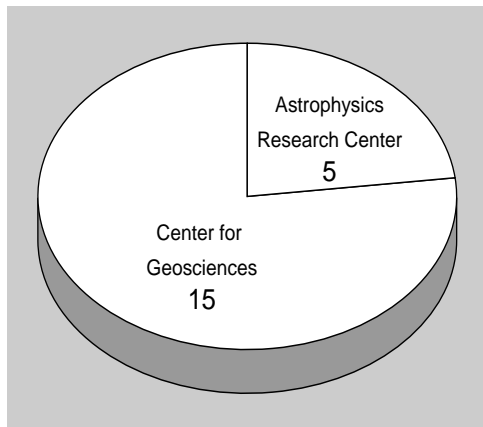


Figure 2. Distribution of awards by IGPP-LLNL center.

Although the permanent LLNL staff assigned to IGPP is relatively small (presently about 16 full-time equivalents), IGPP's research centers have become vital research organizations. This growth has been possible because of IGPP support for a substantial group of resident postdoctoral fellows; because of the 20 or more UCRP projects funded each year; and because IGPP hosts a variety of visitors, guests, and faculty members (from both UC and other institutions).

To focus attention on areas of topical interest in the geosciences and astrophysics, IGPP-LLNL hosts conferences and workshops and also organizes seminars in astrophysics and geosciences. Section IV lists the seminars given in FY 1998.

Since FY 1987, IGPP-LLNL has maintained a bibliography of published research papers resulting from UCRP projects and from research by the IGPP's staff, postdoctoral fellows, and con-

sultants. These lists are published each year in the annual report. Section V gives the bibliography for FY 1998. As a measure of research productivity, the results are gratifying. The abundance of publications from IGPP collaborative projects is a measure of the significance of the results obtained in these projects. The refereed-journal publication rate for IGPP-related projects corresponds to more than 1 paper per year for each faculty member, 2 papers per year for each IGPP postdoctoral fellow, and 2 papers per year for each IGPP staff member.

Figure 3 compares the total papers published in refereed journals or conferences for the last five years. (Note: Because of the extensive peer-review process for most scientific journals, several papers submitted by the principal investigators are still in progress. Therefore, we cannot give an accurate total of 1998 papers published until we receive formal notification from the journals and authors. Final 1998 totals will be available in our 1999 report.)

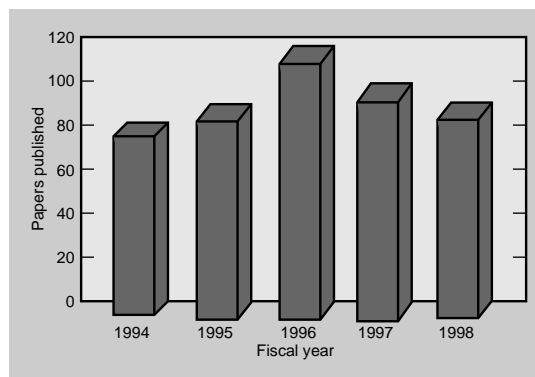


Figure 3. Total number of papers published in refereed journals and conference proceedings from 1994-1998.

Section II. Highlights of Fiscal Year 1998

Astrophysics Research Center

The Astrophysics Research Center serves the aims of IGPP–LLNL in astrophysics. These goals include managing the astrophysics part of the UCRP and facilitating contacts between UC scientists and their LLNL counterparts.

The Astrophysics Research Center also serves as the focus of astrophysics activities at LLNL by organizing the weekly astrophysics colloquium, hosting visitors and collaborators, editing an annual Observatory Report that covers astrophysics activities at LLNL (and is published in the *Bulletin of the American Astronomical Society*), and providing a variety of other service functions.

The staff and postdoctoral researchers of the Astrophysics Research Center carry out a significant program of research. The scientific staff of the Center are Kem Cook (Center Head), Charles Alcock, Seran Gibbard, Bruce Macintosh, Claire Max, Stuart Marshall, and Willem van Breugel. Administrative support is provided by Christina Budwine (Operations Manager), and by Institute Assistant Jan Tweed and Group Secretary Donna McCown. Ray Spence manages the network of computers in the center.

Postdoctoral fellows perform most of the research in the Astrophysics Research Center. Some fellows are supported entirely by IGPP funds, while some are supported partially by other groups at LLNL. In FY 1998, the postdoctoral fellows were Nahum Arav (U/Colorado), Michael Brotherton (U/Texas, Austin), Sally Laurent-Muehleisen (UC Davis), Dante Minniti (U/Arizona), Adam Stanford (U/Washington), and Hien Tran (UC Santa Cruz).

The Center hosts several scientific visitors, not only from the UC campuses but also from around the world. These visitors stay for a day to a year. Some who are affiliated with local institutions spend large, ongoing portions of their time in the center.

The Center and its offices are in Building 319, which is close to the offices of many LLNL astrophysicists and is subject to minimal access controls. These features make the center ideal for the many collaborations that have developed between UC researchers and LLNL scientists.

The Astrophysics Research Center has access to a variety of machines for computing. Most day-to-day work, which includes code development, image processing, and symbolic manipulation, is carried out on the center's network of Sun[™] workstations. This network has been used for large-scale processing by the exploitation of codes that utilize a large fraction of the network for parallel processing. This level of processing is especially effective at night, when most of the network is otherwise quiet and when the "invasive" code will not adversely affect the image-processing work. In addition, much greater computing power is available in other parts of LLNL.

RESEARCH HIGHLIGHTS

The Astrophysics Research Center has developed a research program that exploits the traditional strengths in astrophysics at LLNL and opens new areas of study. This research ranges from smaller-scale theoretical and observational projects to large collaborative ventures. The following pages summarize some of this research.

Laser Guide Stars

Claire Max, Scot Olivier, Jim Brase, Don Gavel, Bruce Macintosh, and Herbert Friedman, working with four LLNL collaborators and collaborators from three UC campuses, are developing laser guide stars for astronomical adaptive optics. The goal of this project is to improve the angular resolution achieved at ground-based observatories. If the project is successful, the angular resolution at major observatories might be improved by 10–100%.

The angular resolution of ground-based telescopes with apertures larger than 10–20 cm is limited to about a second of arc because of turbulence in the atmosphere. In principle, by deforming a flexible tertiary mirror to make the wavefront nearly flat, adaptive optics (AO) can be used to correct for the wavefront distortions, which are measured with a wavefront sensor. This correction would allow ground-based telescopes to be operated at or near their diffraction-limited bounds.

For example, at a wavelength of 1 μm , the diffraction-limited resolution would be 0.08 arcsec for a 3-m telescope and 0.02 arcsec for a 10-m telescope, which represent improvements in resolution of factors of 25 and 100, respectively, relative to the atmospheric resolution of about 1 arcsec.

To produce this correction requires a bright reference object within a few arcseconds of the object being imaged. The statistics of bright stars are such that only a few percent of the sky is accessible for diffraction-limited viewing using nearby bright stars as the wavefront reference.

To make up for the lack of bright reference stars, this consortium is developing the ability to produce artificial stars using a powerful laser. The idea is to use a laser tuned to the sodium D lines to resonantly excite the atmosphere's sodium layer at 90-km altitude, which makes an artificial star to serve as a reference beacon.

A wavefront sensor detects the tilts of the reference wavefront, and a wavefront computer uses the reference wavefront to calculate the adaptive-optics corrections. Finally, the correction is applied to a deformable mirror. The images recorded using the deformable mirror, with the telescope's primary mirror, have most of the atmospheric distortions removed.

A 20-W dye laser and an AO system (both developed at LLNL) have been installed on the Lick Observatory 3-m Shane telescope. The laser is based on technology developed for the LLNL Atomic Vapor Laser Isotope Separation (AVLIS) program and produces an eighth-magnitude artificial guide star, sufficient for adaptive optics cor-

rection of the 3-m telescope at wavelengths of 1–2 μm .

The system produced near-diffraction-limited images, in September–October 1996, using the laser guide star as a wavefront reference. This was the first-ever demonstration of a sodium laser guide star high-order adaptive optics system. During 1997–1998, the group worked to refine the system, improving its performance and reliability in preparation for our first laser guide star science observations in November 1998. The system was used to develop the calibration and observation techniques that all other laser guide star AO systems will need as they become operational on large telescopes. The system also demonstrates excellent performance using bright natural guide stars as references.

Natural-guide-star science programs studying young stellar objects (Fig. 1), binary stars, and the outer planets are being carried out in collaboration with Profs. Andrea Ghez (UC Los Angeles), Imke de Pater (UC Berkeley), and James Graham (UC Berkeley). Michael Liu and Jennifer Patience, students of Profs. Graham and Ghez, respectively, have carried out a systematic search for stellar companions to the stars known to have planets orbiting them (Fig. 2) in an attempt to see if perturbations by previously unknown stellar companions can explain the bizarre planetary systems recently discovered by Geoff Marcy and collaborators. Observations of the outer gas giant planets Neptune and Uranus (Fig. 3) are being fit to radiative transfer models developed by Prof. de Pater and her graduate student Henry Roe.

In 1998, science programs using the laser guide star to study fainter targets will also be carried out. The LLNL group is also working on the adaptive optics and laser guide star system for the 10-m W. M. Keck telescope, which was shipped to the Keck Observatory for integration into a Keck-built optics bench in spring of 1998; first light is expected on the Keck telescope in January 1999.

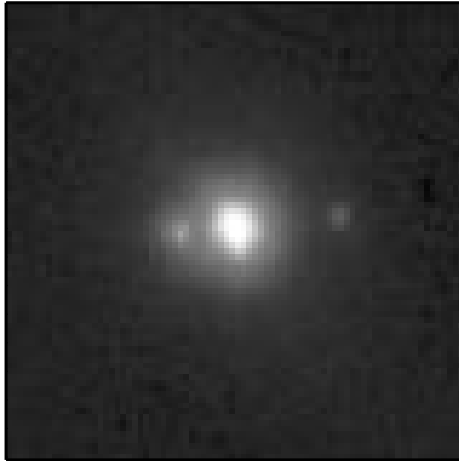


Figure 1. Faint companions to the young stellar object LkHa 234.

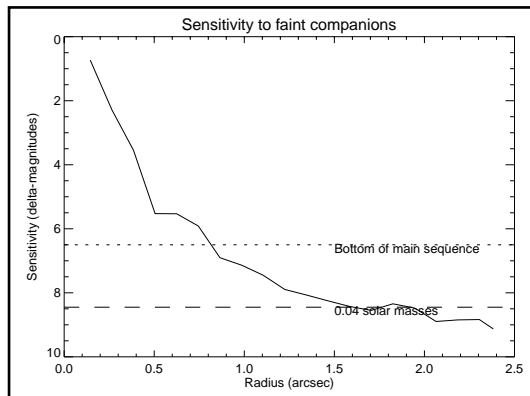


Figure 2. Sensitivity of the Lick AO system to faint stellar and brown dwarf companions.

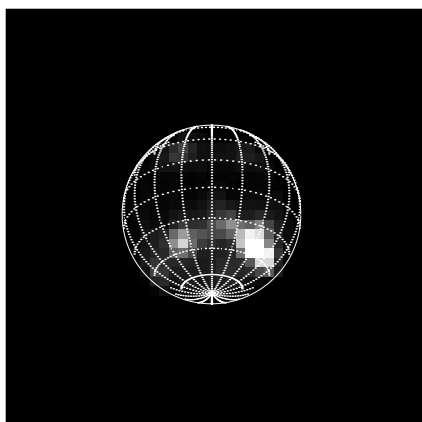


Figure 3. Near-infrared image of the outer planet Neptune from the Lick AO system, showing bright stratospheric storm features.

Speckle Imaging of Titan, Io, and Neptune

In FY1998, Claire Max, Donald Gavel, Bruce Macintosh, and Seran Gibbard, working with collaborators from UC Berkeley, NASA Ames, the Southwest Research Institute, and JPL, continued to observe solar system objects at very high spatial resolution using the technique of speckle imaging. Speckle imaging uses a series of very short exposures to “freeze” the turbulence of the Earth’s atmosphere, which limits the resolution of most ground-based observations to ≈ 0.5 arcseconds.

In October 1997 and July–August 1998, we made near-infrared observations (at the 10-m W. M. Keck Telescope) of Saturn’s moon Titan, Jupiter’s volcanically-active moon Io, and Neptune. The speckle imaging technique allows us to obtain spatial resolution near the diffraction-limit of the telescope (0.04 arcseconds at a wavelength of 2 microns).

Titan, which is Saturn’s largest moon, is unique among planetary satellites in possessing a thick atmosphere. Seen in visible light, Titan is shrouded in a featureless, orange haze. This haze is believed to be composed of organic compounds produced by the photolysis of methane. Models suggest that this haze gradually settles to Titan’s surface, and over long periods of time, could form oceans, lakes, or underground reservoirs of liquid.

In October 1997, we obtained excellent images of Titan’s leading (brighter) hemisphere, and in July–August 1998, we obtained images covering the darker trailing hemisphere.

Our data is taken through the K’ and H filters, which include both a strong methane absorption band (which gives us data on Titan’s atmospheric structure) and a window in the band through which we can see surface features on Titan. This technique allows us to obtain interesting information about both the surface and previously unknown characteristics of Titan’s atmosphere.

Our data clearly show a continent-sized bright-surface feature on Titan’s leading hemisphere that is consistent with icy or rocky highlands, as well as a very low albedo region that is consistent with the presence of liquid hydrocar-

bons on the surface. Titan's darker hemisphere has a very low albedo (< 0.05) overall, with some brighter areas. If Titan's dark areas are liquid hydrocarbons, this would be the first detection of surface liquids on a solar system body other than the Earth.

Io, the innermost large moon of Jupiter, experiences tidal stresses and enough internal heating to create volcanoes on its surface. By observing Io in the infrared while the Sun is eclipsed by Jupiter, emission from individual volcanoes can be imaged or even resolved.

We use these data to determine the time variations, size, spacing, and number of volcanoes, which in turn yields information about the nature of these volcanoes—particularly the high-temperature events thought to be silicate volcanism. Seventeen individual volcanic features on Io's surface were resolved in observations during an eclipse in July 1998 (Figs. 4a–c). Keck observations of Io represent the highest resolution infrared measurements available to date.

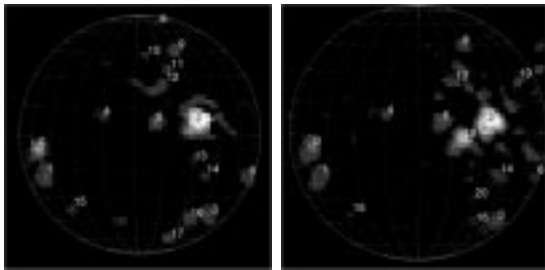


Figure 4a/b. Near-infrared images of volcanic hotspots on the surface of Io. Observed using the 10-m W. M. Keck telescope and LLNL's speckle interferometry software.

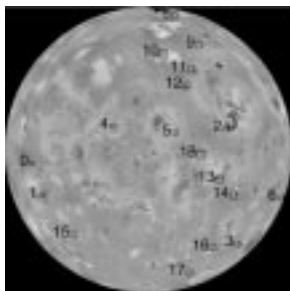


Figure 4c. Visible-light image of Io from the Voyager spacecraft showing the location of the hotspots detected in our Keck imaging.

Neptune is a very dynamically active planet about which little is known because of its small angular extent (2.5 arcseconds). Voyager 2 detected prominent dark and bright spots at visible wavelengths, as well as some bright wispy cloud features. These features change on timescales varying from hours to years.

Our goals in observing Neptune are to determine the altitude and composition of the material that makes up the infrared-bright features on the disk of Neptune; to determine the timescales over which these features evolve; to look for oscillations in spot size or shape; and, ultimately, to determine the contribution of these storms to Neptune's overall heat budget.

Speckle observations of Neptune at H band were made in October 1997 and July–August 1998. In addition, we observed Neptune in conventional mode using infrared narrow bands, which probe different heights in Neptune's stratosphere.

Using a model adapted from a Neptune radiative transfer code developed by Kevin Baines (JPL), we are able to constrain the number density of Neptune's stratospheric haze layers and to verify that the infrared-bright storm features are, indeed, located in Neptune's stratosphere rather than lower down in the troposphere.

The MACHO Project

The MASSive Compact Halo Objects (MACHO) Project is an experimental search for the dark matter, which makes up at least 90% of the mass of our galaxy. It was initiated at LLNL and involves Charles Alcock, Kem Cook, Stuart Marshall, and Dante Minniti (LLNL); Robyn Allsman, and Tim Axelrod (Mt. Stromlo Obs., Australia); David Bennett (Notre Dame); Mark Pratt (U/Washington); Christopher Stubbs (CfPA at U/Washington); Kim Griest (CfPA at UC San Diego); Doug Welch (McMaster University); Will Sutherland (Oxford University); and Kenneth Freeman, Bruce Peterson, and Peter Quinn (European Southern Obs., Chile).

The Milky Way's dark matter is thought to be distributed in a large, spherical halo. Its constitution is unknown, because it emits no detectable radiation. Before this Project, most hypotheses for its constitution involved speculations from particle physics. This experiment searches for planets, brown dwarfs, and black holes or any other massive objects (MACHOs) having a mass range of $10^{-7} M_{\odot} < M < 10 M_{\odot}$.

If the dark matter consists of MACHOs, it will occasionally magnify light from extragalactic stars by the gravitational lens effect. An event can be recognized by fitting a theoretical light curve to the observations (four-parameter fit) and by its lack of color variation (it is achromatic).

Unambiguous recognition of microlensing requires adequate data points on the light curve (10) and measurements in at least two filter bands. To detect events, one must monitor millions of stars for several years. The experiment has been operating for five years, and we have an agreement to operate through 2000.

The MACHO Project uses the 130-cm reflecting telescope of the Mt. Stromlo Observatory, near Canberra, Australia. Operating at prime focus with an innovative optical system gives a field of view 1 deg in diameter. We use a dichroic filter for simultaneous imaging in a blue and a red spectral band, doubling the effective exposure rate.

The MACHO Project has been monitoring fields in the Large and Small Magellanic Clouds (satellite galaxies of the Milky Way) as well as fields toward the center of the Milky Way. The Project has accumulated almost 6 TBytes of image data and about 600 Gbytes of photometry on about 70 million stars. Data is reduced in near real time, and microlensing events are often identified well before their peak.

The project sends out alert announcements to the world, which are also posted on its web site (<http://darkstar.astro.washington.edu>). These alert announcements are used by different groups throughout the world to search for planets and to study ongoing microlensing events in detail.

Planets can be detected via microlensing when they orbit the lensing object, and most of the lenses detected toward the center of the Milky Way are normal stars. Over 350 microlensing events have been recorded. Analysis of these events shows that planets and brown dwarfs are not significant components of the dark matter, but that ancient white dwarfs might be.

Ongoing microlensing has also been used to study the source star in greater detail than possible without the magnification. Members of the Project have obtained Keck echelle spectra of main sequence stars in the bulge of the Milky Way, getting scheduled time during the bulge season knowing that there would be ongoing microlensing events with main sequence source stars.

The large number of microlensing events toward the bulge has forced a revision in our view of the Milky Way's structure. It is now thought most likely that we live in a strongly barred spiral galaxy. The microlensing detected by the Project toward the Large Magellanic Cloud suggests that the halo of the Milky Way has a significant MACHO component. If the halo of our galaxy is assumed to be a relatively 'standard' halo, the MACHOs comprise about 50% of the dark matter and have masses of about $0.5 M_{\odot}$. This result is quite surprising.

The project has also detected two microlensing events toward the Small Magellanic Cloud. Both events were discovered by the alert system and were studied in detail by groups around the world. The project alerted the world that the second event was likely to be a binary lens-caustic crossing event and predicted the caustic-crossing time. This led to an intense observing program around the world. Analysis of this non-standard microlensing event has placed the binary lens in the Small Magellanic Cloud itself, along with the source star.

Comets in the Outer Solar System

Charles Alcock, Kem Cook, and Stuart Marshall are collaborating with teams at the Institute of Astronomy and Astrophysics and National Central University (both in Taiwan), and individuals at

UC Berkeley, on a novel survey of the outer solar system.

Following the detection of solid objects in the trans-Neptunian region, the observed frontier of the solar system progressed from about 10 AU in the early 1600s—when Kepler deduced his “laws” of planetary motion, only six planets were known to orbit the Sun—to about 50 AU today. During these four centuries, three planets, hundreds of comets, and thousands of asteroids have been detected in orbit about the Sun, and dozens of moons as well as four ring systems have been observed to orbit planets. Progress is very slow beyond Neptune because the objects are mostly small, solid bodies, and the brightness in reflected sunlight declines as the inverse fourth power of distance.

Although no objects have been observed beyond 50 AU, a rich population of comets has been inferred. This population acts as a reservoir from which new comets can enter the inner solar system, become active, and be discovered as their brightnesses increase by many orders of magnitude.

The populations and distributions of these objects are now known; in the case of the comets, the uncertainties span orders of magnitudes. Scientifically, these objects serve as probes to the primordial solar system because they preserve a record (in ice) of the conditions at that epoch. Programmatically, interest is growing regarding ways to mitigate the hazards of asteroid or comet collisions with Earth. The region of interest for us is the Kuiper Belt, which lies just beyond the observed frontier of the solar system. It is believed that there are between a billion and a hundred billion comets in the Kuiper Belt, in orbits with semi-major axes between 50 and 200 AU.

We have designed a novel survey for taking an inventory of the comets in the Kuiper Belt—we would use the occultation of nearby stars by the comets to estimate the total population of small (~2 km) objects. Our system consists of an array of telescopes at a dark site; each telescope has a wide-field-of-view, charge-coupled-device (CCD)

camera system pointed at the same region of the sky. Our design study determined the architecture and parameters of the system, that is, the number of telescope elements, the size of the telescopes, the kind of cameras, etc.

Three is the minimum number of telescopes for systematic control and measurement of the false-positive range; we adopted this minimum to minimize the overall cost of the array. With three telescopes—and the design goal of a false-alarm probability per measurement of about 10^{-12} —the false-alarm probability per measurement at one telescope should be no poorer than about 10^{-4} . This sets the signal-to-noise requirement for each telescope in the system. The optimum telescope for this design has an aperture of 50 cm and a focal length of approximately 95 cm. This couples well to a moderate-cost, commercially produced CCD camera.

We have completed the design for the three-telescope array. This included design of the optical corrector cell for the telescope system, which ensures that most of the flux from a star will be collected into one camera pixel over the entire three-square-degree field of view. We also (1) identified a small telescope manufacturer who can fabricate the needed telescopes at moderate cost, (2) selected the digital camera for the project, and (3) invented a novel photometry scheme that allows us to perform photometry on several thousand stars five times per second (much faster than allowed by conventional astronomical photometry schemes).

Searching for Asteroids

Kem Cook (LLNL), Christopher Stubbs and A. Diercks (U/Washington), and Ted Bowell and B. Koehn (Lowell Obs., Arizona) have completed an innovative 2048- × 4096-pixel scanning CCD camera, which operates at prime focus on an 18-in. Schmidt telescope on Anderson Mesa in Arizona.

This system is the heart of the Lowell Observatory Near-Earth Object Survey (LONEOS) and allows about 1000 square degrees per night to be

triple-scanned to detect near-Earth objects (NEO) through their rapid apparent motion.

The LONEOS system began taking data with the newly refurbished Schmidt telescope last year. It was decided, however, that the corrector and field flattener that were being used needed to be refabricated. These elements were reinstalled during the Winter of 1998, and the system has been operational for most of this year. This system discovered its first NEO 1998 MQ and four new NEOs this year.

A Spectacular Post-Starburst Quasar

One of the fundamental questions in astronomy is to understand the origin, and source of energy, of some of the most luminous objects in the universe—quasars. Quasars are thought to be massive black holes, which may have formed simultaneously with their host galaxies, or perhaps prior to that, during the very early stages of the Big Bang. There is circumstantial evidence that some quasars live in relatively young ‘starburst’ galaxies. Approximately 10% of the quasars emit bright, non-thermal radio emission. Radio source catalogs can therefore be used for identifying large numbers of quasars in a systematic way (without selection effects caused by cold gas and dust, which are normally thought to accompany large starbursts and which might obscure otherwise very luminous active black holes).

Brotherton (IGPP postdoc, presently at the National Optical Astronomy Observatories) and colleagues at IGPP, Oxford University (U.K.) and the Anglo-Australian Observatory (Australia) used the large NRAO VLA Sky Survey (NVSS) together with the AAO ‘ultraviolet-excess’ quasar survey to identify several hundred radio quasars. During follow-up observations with the Keck telescope, one of these quasars—UN J1025-0040—showed a very unusual spectrum.

The spectrum shows the broad Mg II 2800 Angstrom emission line and strong blue continuum characteristic of quasars, but it is dominated in the red by a large Balmer continuum discontinuity and prominent high-order Balmer absorp-

tion lines indicative of a substantial young stellar population. (see Figure 5 for a comparison between a normal luminous starburst [top] and the quasar starburst [bottom]). Stellar synthesis population models show that the stellar component is consistent with a 400 million year old, instantaneous starburst with a mass of 100 billion solar masses.

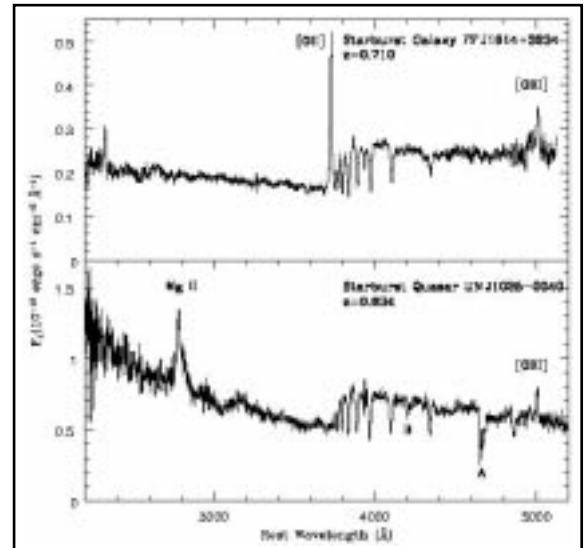


Figure 5. Keck spectra of an ultra-luminous starburst galaxy (FF J1614+3234, top), and the UV-excess starburst quasar (UN J1025-0040, bottom).

A deep near-infrared Keck image (Fig. 6) taken in 0.5 seeing shows a point source surrounded by asymmetric extended fuzz. Approximately 70% of the light is unresolved, the majority of which is emitted by the starburst. While starbursts and galaxy interactions have been previously associated with quasars, no quasar ever before has been seen with such an extremely luminous young stellar population.

This spectacular object may represent a transitional step in an evolutionary sequence between a massive starburst and active black hole, both of which may have been triggered by interaction or merging of its host galaxy with a nearby neighbor. The frequency of objects like UN J1025-0040 is unclear, as less extreme versions require detailed observations to recognize. A post-starburst quasar could have been found and misidentified in previ-

ous surveys because of low-quality spectra or limited wavelength coverage. Because of its young age, the starburst could only have been brighter and bluer in the past. Such extreme starbursts have not been identified in previous ultraviolet excess quasar surveys, suggesting that a younger version of UN J1025-0040 might be hidden as a dust-enshrouded infrared galaxy.

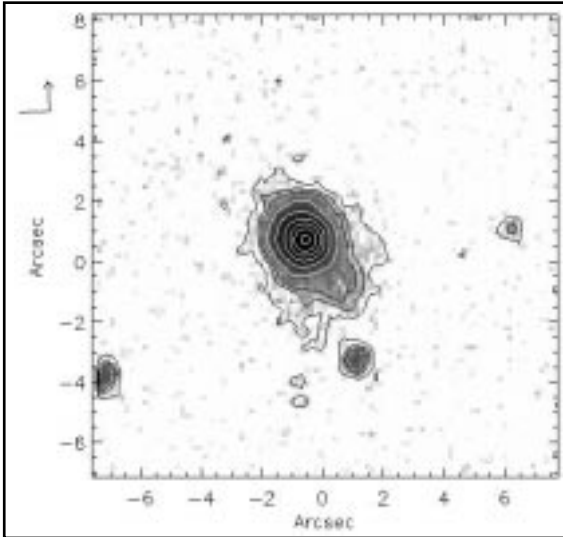


Figure 6. Keck near-infrared image of the starburst quasar UN J1025-0040, showing a point source surrounded by asymmetric extended fuzz with a feature suggestive of a dust lane, and a companion galaxy to the south-west.

Center for Geosciences

The Geosciences Research Center was formed to promote collaborative research in the geosciences among LLNL, the various UC campuses, and other scientific organizations both within the U.S. and abroad. LLNL's mission-oriented programs in national security and in environmental and energy research employ many disciplines within the geosciences. IGPP draws upon these capabilities and expertise and acts as a focal point for research in the more fundamental aspects of the earth sciences.

We hope to consolidate many unique talents and capabilities at LLNL and to provide an easily identifiable avenue for LLNL-UC collaborations. The Center for Geosciences is the focus of these interactions with visitors from academic (UC and other universities), industrial, and governmental research institutions. The Center's research emphasis is on the physics and geochemistry of the solid Earth, including seismology, geochemistry, experimental petrology, mineral physics, environmental geochemistry, hydrology, tectonics, and active tectonics.

The Center is housed in the Geophysics & Global Security and Geosciences & Environmental Technologies divisions of LLNL's Earth and Environmental Sciences Directorate (EES). It is involved with several programs within EES and also with the Isotope Sciences Division of LLNL's Chemistry and Materials Science Directorate, which is a major contributor in the area of geochemical expertise and analytical facilities. The Center also has active collaborations with the staff of LLNL's Center for Accelerator Mass Spectrometry (CAMS).

The scientific staff of the Center are Rick Ryerson (Center Head), Henry Shaw, Marc Caffee, Bob Finkel, Ian Hutcheon, and Douglas Phinney. Postdoctoral fellows during FY98 included Matt Kohn (Rensselaer Polytechnic Institute), who recently left the Lab to take a faculty position at the University of South Carolina; Dan Farber (UC Santa Cruz); and Adam Kent (Australian National University). Keith Putirka (Lamont-

Doherty Geologic Observatory) and Jerome Van der Woerd (Institut de Physique du Globe de Paris [IPGP]) also recently joined the Laboratory as postdocs. Putirka is working on developing and applying methods of phase equilibria to constrain the relative effects of melting conditions and mantle composition on the chemical diversity of basaltic lavas. Van der Woerd is working on the tectonics of northern Tibet using satellite image interpretation, field mapping, and cosmic-ray surface exposure dating.

Anne-Sophie Meriaux, a predoctoral fellow from IPGP, also spent the year at LLNL, working on surface dating of samples from the Altyn Tagh Fault, collaborating with Dan Farber and Bob Finkel on dating moraines in South America, and refining cosmogenic nuclide production rates.

Adam Kent has been working on the diffusion of cations in carbonate minerals found in 'Martian' meteorites as a means of constraining the thermal history of these samples and the implications for past life on Mars. He has also been using the ion microprobe to analyze volatile constituents in glass inclusions in phenocrysts from various lava suites.

Dan Farber has been working on the Holocene glacial history of the Andes, and also on the partitioning of trace elements between fluids and minerals in subduction zones.

RESEARCH HIGHLIGHTS

The current research within the Center for Geosciences is focused around two major projects—the Cenozoic and active tectonics of the Indo-Asian collision, and experimental determination of the partitioning of trace elements between minerals, fluids, and melts relevant to subduction zones and mid-ocean ridges.

The **Asian tectonics program** considers both the long-term evolution of the Tibetan Plateau and Himalaya, and the active tectonics of the region. Matt Kohn and Rick Ryerson are currently collaborating with Profs. Mark Harrison and An Yin (UC Los Angeles) on a number of problems in the

southern and central Tibetan Plateau. Liz Catlos, a graduate student from UC Los Angeles, has been working with Kohn on the determination of pressure-temperature histories of metamorphic rocks adjacent to the Main Central Thrust in Nepal.

The program in active tectonics is facilitated by the AMS facility at LLNL, allowing us to date surface features that have been disrupted by Quaternary seismic activity. Marc Caffee and Bob Finkel have been responsible for the development of these cosmogenic dating schemes at LLNL, and they are currently collaborating with Rick Ryerson and colleagues Paul Tapponnier (IPGP), Gilles Peltzer (Jet Propulsion Laboratory), and Jean-Phillippe Avouac (CEA Bruyères-Le-Chatel) to determine the rates of slip and shortening along major strike-slip faults and across young mountain belts, respectively, in central Asia.

During the summer of 1998, Rick Ryerson, Jerome Van der Woerd, and Anne-Sophie Meriaux joined a team from IPGP and the Chinese Seismological Bureau to collect samples for surface dating along the central segment of the Altyn Tagh Fault.

The effort in surface dating took a new direction this year with a collaboration recently initiated with Lewis Owen at UC Riverside. Bob Finkel and Mark Caffee accompanied Owen and coworkers on a trip to Pakistan in the spring of 1998 to collect samples from glacial moraines near Nanga Parbat. The effort aims to determine the climate history of the region. Lynn Gultieri, a postdoc from UC Riverside, spent 4 months at LLNL analyzing the samples collected on this trip.

The **experimental program** comprises the efforts of Henry Shaw, Ian Hutcheon, Douglas Phinney, Dan Farber, Keith Puritirka, and Rick Ryerson, who continue to work closely with Craig Lundstrom (a former predoctoral fellow who is

currently a postdoc at Brown University) and a former IGPP postdoctoral fellow, James Brenan (currently a faculty member at University of Toronto). Brenan was the recipient of the MSA Award of the Mineralogical Society of America presented at the 1998 Geological Society of America annual meeting in Toronto during the fall of 1998. This award recognizes the contributions of a young scientist.

The following pages highlight these projects and additional research conducted in the Center for Geosciences.

Geospeedometry: Dating Tectonic Deformation

The goal of this project is to develop and apply cosmogenic dating methods to better constrain rates of tectonic deformation across active faults and folds in the collision zone between India and Asia. Active faulting and seismicity show that deformation in Central Asia is partitioned between thrust faulting in mountain belts and lateral displacement along great strike-slip faults. The extent to which deformation is localized along these faults as opposed to homogeneously distributed throughout Asia is critically dependent upon the rates of slip, and bears upon the more general question of how the Earth's lithosphere deforms.

Rick Ryerson, Bob Finkel, and Marc Caffee, in collaboration with colleagues at UC Los Angeles, the IPGP, and the Chinese Seismological Bureau, are currently focusing their efforts on sites along the Tibet-Tarim Basin boundary, which is defined by the Altyn Tagh Fault System (ATF) (Fig. 1). The ATF runs along the northern edge of the Tibet-Qinghai highlands for nearly 2000 km, merging with various thrust and other strike-slip systems at its eastern and western termini. Eastward propagation of the ATF may be the primary mechanism by which the northern part of the plateau has grown.

In the first two years of this project, mapping and sampling was performed in a number of regions (Fig. 1):

1. The Kunlun Fault, a left-lateral strike-slip fault to which a portion of the displacement along the ATF is thought to be transferred.
2. The eastern terminus of the ATF in the Tang He Nan Shan, where strike-slip movement is transferred to thrusting and thickening.
- 3/4. The Aksay and Subei segments of the ATF near its eastern terminus.
5. The Karakax Valley segment of the ATF in the west.
- 6/7. The Tura and Shur Kholi regions along the central segment of the fault where the highest slip rates are expected.

Quartz-rich lithologies from surfaces that constrain either lateral or vertical offsets were dated using both ^{10}Be and ^{26}Al , and slip rates were obtained.

At its eastern termination, slip on the Altyn Tagh Fault is transferred to other strike-slip fault systems, such as the Haiyuan and Kunlun Faults, and to sub-perpendicular thrust faults such as those in the Tang He Nan Shan. Slip rates on all of these features are required to support this hypothesis. Left-lateral slip along the Kunlun Fault has

resulted in a number of terraces risers offset by various amounts.

The cosmic-ray exposure age of these features yield a slip-rate of 12 ± 2 mm/yr. This is the first quantitative measure of slip-rate on any fault in Asia, and the results from one site were recently published.¹ A second paper presenting identical rates over 600 km of the Kunlun Fault is in preparation.

The Tang He Nan Shan is a northwest-southeast trending mountain range roughly perpendicular to the ATF at its eastern terminus. Preliminary data demonstrate that terrace age increases, yielding an uplift rate of 0.5–1.0 mm/yr. Geometric constraints on the attitude of the thrusts coupled with these uplift rates implies the central part of the Tang He Nan Shan is being uplifted at a rate of 2.5 mm/yr.

This rate predicts initiation of uplift in the Tang He Nan Shan 5 million years ago, an event that would transform the Qaidam Basin into a closed drainage at that time. This prediction is consistent with a dramatic increase in sedimentation rates in the Qaidam Basin at 5 Ma.

Along its western segment, the ATF bifurcates, with the main branch of the fault turning to the north (the Karakax Valley segment) and smaller branches continuing to the southwest. We obtained an age of ca. 6 Ka for a riser offset by 140 m, yielding a slip-rate of ~2 cm/yr for the Karakax Valley segment.

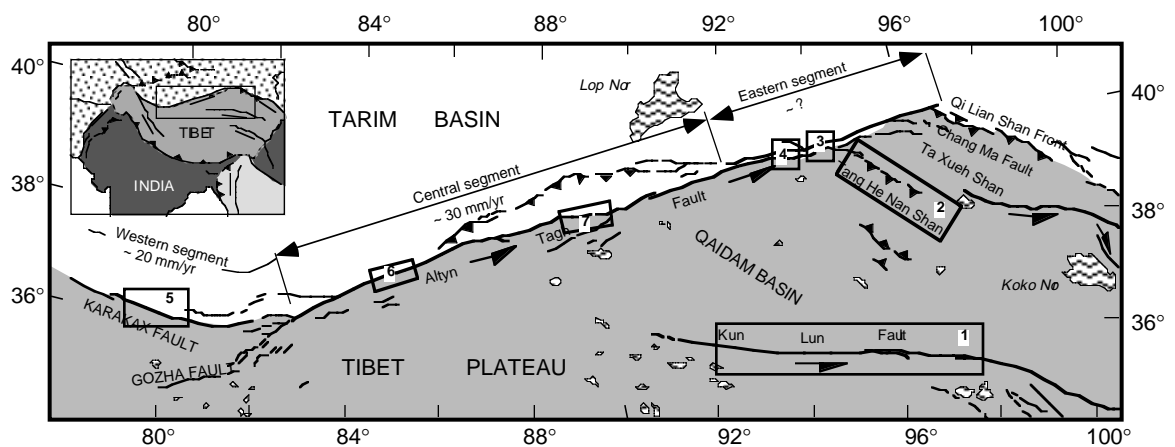


Figure 1. Generalized tectonic map of northern Tibet (area shown in box on inset map of Asia) indicating the areas under investigation in this project. We are attempting to determine rates of strike-slip movement along the Kunlun Fault (1), and the Aksay (3), Subei (4), Karakax Valley (5), Tura (6), and Shur Kholi (7) segments of the Altyn Tagh Fault and uplift along the borders of the Tang He Nan Shan (2).

Due to the western bifurcation of the ATF, the rate on the Karakax Valley segment sets a minimum rate for the central segment of the fault, which for rigid block kinematics must be accommodated to the lateral components on both the Karakax Valley plus the segments to the south.

One of the fundamental results of this ongoing investigation is the determination that the high slip rates are consistent with kinematic models, which assert that a large fraction of Indo-Asian convergence is accommodated by translation and rotation of rigid blocks, rather than by homogeneously distributed diffuse deformation of the Asian lithosphere.

Similarly, the high slip rates found imply that the ATF is responsible for the eastward extrusion of Tibet, which is in turn accommodated by crustal shortening along its eastern boundary, causing progressive northward growth of the Tibetan Plateau.

Estimating the Mineralogy of the Upper Mantle, and Partial Melting Depths and Temperatures of Oceanic Basalts

The formation of basaltic lavas represents the most important mode of mass transport on the terrestrial planets; partial melting and volcanism are the driving forces behind planetary evolution. To understand the evolution of Earth, it is thus critical to know the composition of Earth's mantle—the source region for all basaltic volcanism—as well as the depths and temperatures at which partial melting takes place.

To constrain these quantities, basaltic lavas from Hawaii and the East Pacific Rise (EPR) are compared. Lavas from these localities represent end-members in the production of oceanic crust: Lavas at Hawaii form by partial melting above a super-adiabatic thermal upwelling, or a 'mantle plume.'

The EPR, in contrast, is a passive spreading center; melting occurs when mantle of normal temperature rises to fill the void left by the separation of oceanic lithosphere. Since Hawaii is the result of a thermal upwelling, it is expected that

partial melting occurs at relatively high pressures (P) and temperatures (T) at Hawaii, and that Hawaiian lavas tap a deeper mantle source, compared to EPR lavas.

From prior geochemical work, it has been recognized that lavas from these two localities are different. Keith Putirka is considering two critical questions that arise from these observations: (1) Are the compositional differences between Hawaii and the EPR due to differences in the melting process (i.e., high P-T melting at Hawaii versus low P-T melting at the EPR)? or (2) Is the deep mantle source tapped by the Hawaiian plume fundamentally different in composition compared to the shallow mantle tapped by the EPR lavas?

Controversy surrounds the nature of geochemical heterogeneity in Earth's mantle. Differences in isotope ratios between Hawaii and the EPR require some heterogeneity in their mantle sources, because isotopes of an element are not normally fractionated from one another by partial melting. It has been proposed that isotopic differences are due to differences in mantle mineralogy.²⁻⁵

In this model, the normal mineralogy of peridotite (a rock consisting of olivine + clinopyroxene + orthopyroxene + garnet), contains an admixture of up to 5% eclogite (a rock consisting largely of clinopyroxene + garnet). The eclogite hypothesis is intriguing, because eclogite may be introduced into Earth's mantle through subduction of oceanic crust at convergent plate boundaries. However, isotopic differences need not be accompanied by substantial differences in mineralogy or bulk composition.⁶ Moreover, variations in the P-T conditions of partial melting can significantly affect basalt composition.^{7,8}

The nature and degree of mantle heterogeneity cannot be fully ascertained until such P-T effects have been evaluated. To estimate mantle heterogeneity, Putirka has developed melting models that explore the potential range of basalt compositions resulting from melting at varying P-T conditions. These models use Na, Ti, Hf, and rare earth element (REE) abundances, because

these elements have mineral/melt partition coefficients that are sensitive to both P and mineralogy. The models thus test whether differences in the P-T conditions of melting are sufficient to explain regional differences in basalt geochemistry. Any natural geochemical variations that are not explained by the models must be due to geochemical differences in the mantle source regions. Thus, by investigating the maximum effects of P-T on melt composition, minimum estimates may be placed on mantle heterogeneity.

Compared to the EPR, Hawaiian basalts have lower Na/Ti ratios due to higher Ti and lower Na (Fig. 2). Lower melt fractions at Hawaii could account for increased Ti, but not for Na, if Na is also incompatible.

This conundrum might be explained if mineral-melt partition coefficients for Na increase with increased pressure,⁸ which is observed for many high-pressure experiments.⁹ Hawaiian basalts also exhibit high Sm/Yb ratios compared to EPR lavas, and greater melting depths at Hawaii have been invoked to explain such differences.¹⁰ Finally, there exist significant inter-shield variations in Na/Ti at Hawaii; the melting models test whether the P-T conditions of melting can explain such local variations.

From Figure 2, it is apparent that variations in the P-T conditions of melting, using a depleted mantle starting composition, are sufficient to explain both local variation at Hawaii and large-scale geochemical differences between Hawaii and the EPR. This implies that bulk composition differences between Hawaiian and EPR source regions might be minimal. This result is consistent with near-uniform, but non-primitive, minor element ratios for oceanic basalts,¹¹ and high-pressure diffusion experiments that indicate efficient homogenization in parts of the upper mantle.¹²

Differences in isotopic ratios might have developed by metasomatism, a process that would not be expected to greatly influence mineralogy. It is also possible that re-equilibration and mantle mixing have obscured major element geochemical differences, without erasing isotopic signatures.

In Figure 3, melt compositions produced from eclogite and mineralogically similar garnet pyroxenite source regions are compared to natural lava compositions. Abundances of Na₂O, TiO₂, and REE at Hawaii are inconsistent with a variety of potential eclogite or garnet pyroxenite mantle sources.

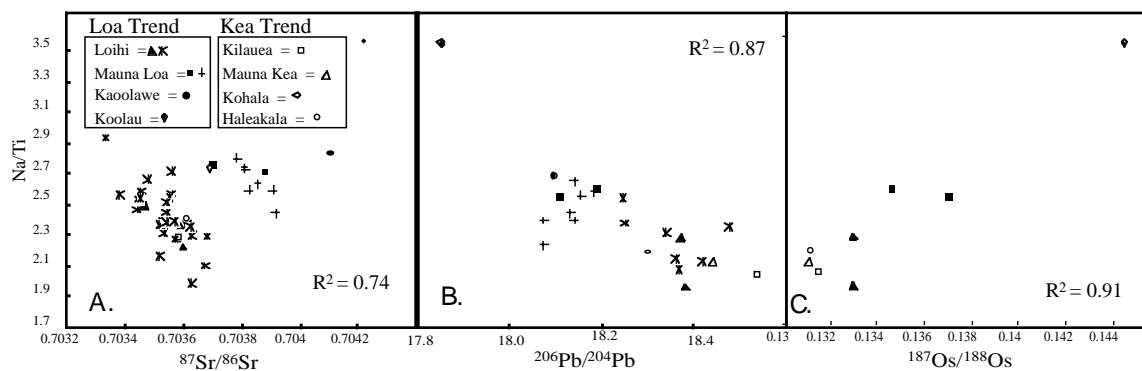


Figure 2. Aggregate melt compositions are calculated using a depleted peridotite source. High Na/Ti at Koolau may be explained by the presence of thinner lithosphere and cooler mantle temperatures. Intra-volcano variation probably reflects heterogeneity (mineralogical differences of up to 2% in the source region). ‘Bulk composition uncertainty’ reflects the increase in Na/Ti and Sm/Yb ratios that are obtained when an undepleted mantle source is input into the melting models. Note that almost the entire range of EPR and Hawaiian lavas can be produced from a depleted peridotite mantle source, simply by varying the P-T conditions of partial melting.

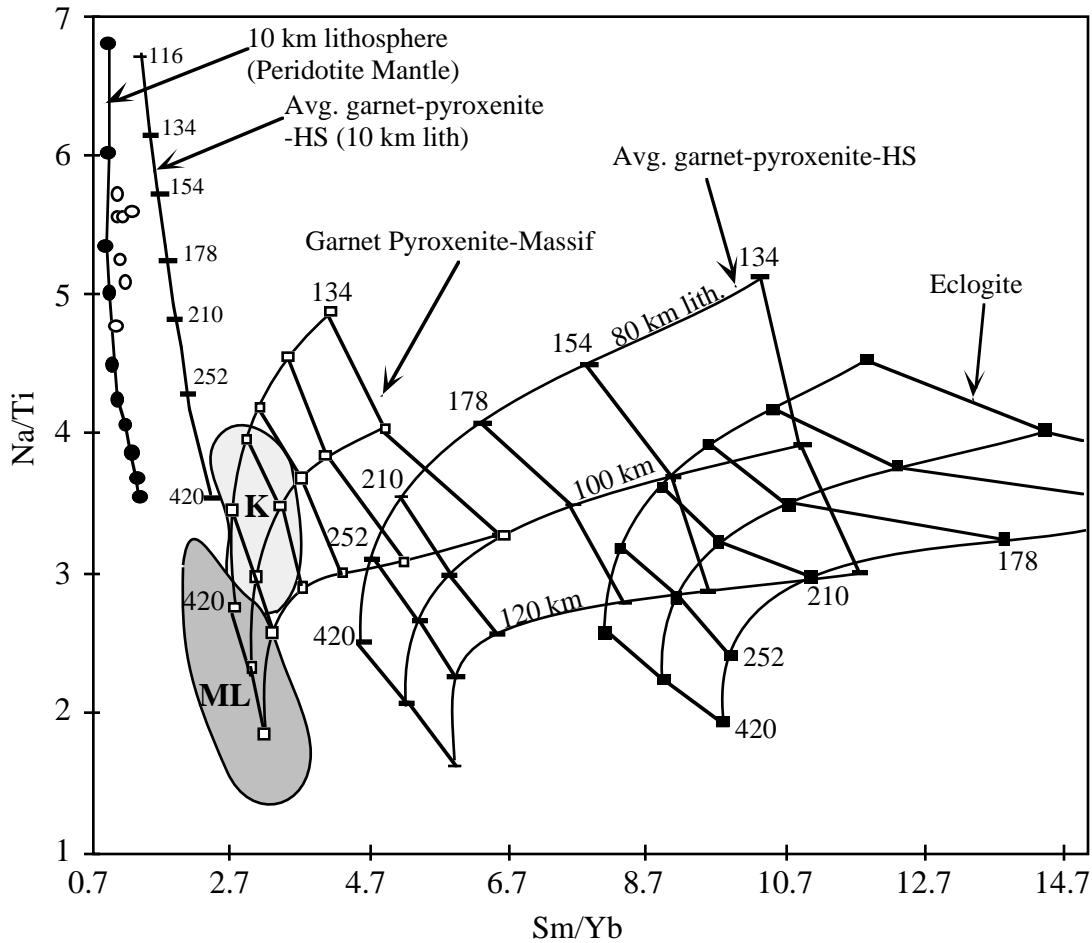


Figure 3. Calculated aggregate melts are shown for eclogite and garnet pyroxenite sources ('HS' is the average garnet pyroxenite from Hirschmann and Stolper;⁴ 'Massif' refers to garnet pyroxenites from massif peridotites; K is the Koolau, and ML is the Mauna Loa+Mauna Kea+Loihi fields, as in Figure 2). Na/Ti and Sm/Yb ratios at Hawaii overlap only with some massif pyroxenites, but the predicted Na, Ti, and REE abundances are too high compared to lava compositions. Eclogites and garnet pyroxenites are thus unlikely mantle components at Hawaii.

The mantle beneath Hawaii is undoubtedly mineralogically heterogeneous, but Hawaiian lavas were probably produced by partial melting of a peridotite mantle, with only minor differences in phase proportions.

While the models do not exclude eclogite in the EPR mantle source, it is conceivable that small differences in peridotite source region mineralogy (2%) could account for the range of EPR lava compositions. Thus, eclogite and garnet pyroxenite sources are not only unlikely at Hawaii, but are perhaps also unnecessary at the EPR.

If the mantle consists of depleted peridotite, then partial melting depths are also constrained by the models. Abundances of Na, Ti, Hf, and the REE for EPR lavas are best reproduced when melting begins at 120 ± 15 km, consistent with recent seismic work¹³ and prior depth estimates.¹⁰ In contrast, Hawaiian tholeiites can be modeled using a 100-km-thick lithosphere and initial melting depths of 200–400 km. This implies a temperature difference between Hawaii and the EPR of 300°C, close to estimates inferred from geodynamic studies¹⁴ and mantle tomography.¹⁵

Figure 4 shows how isotopic differences might be related to melting depth. At Hawaii, the average isotopic compositions of the volcanic shields correlate well with Na/Ti ratios, indicating that there is some vertical layering of isotopically distinct regions in the Pacific upper mantle. Individual lavas, though, from both Loihi and Mauna Loa volcanoes, show isotope versus Na/Ti correla-

tions that are opposite to the inter-shield trend. These intra-island trends are furthermore directed toward EPR isotope-Na/Ti values. The local trends appear to support the traditional view of a layered mantle, with the most depleted material occurring in the shallow mantle; the inter-island trend perhaps indicates significant lateral heterogeneity beneath the Hawaiian islands.

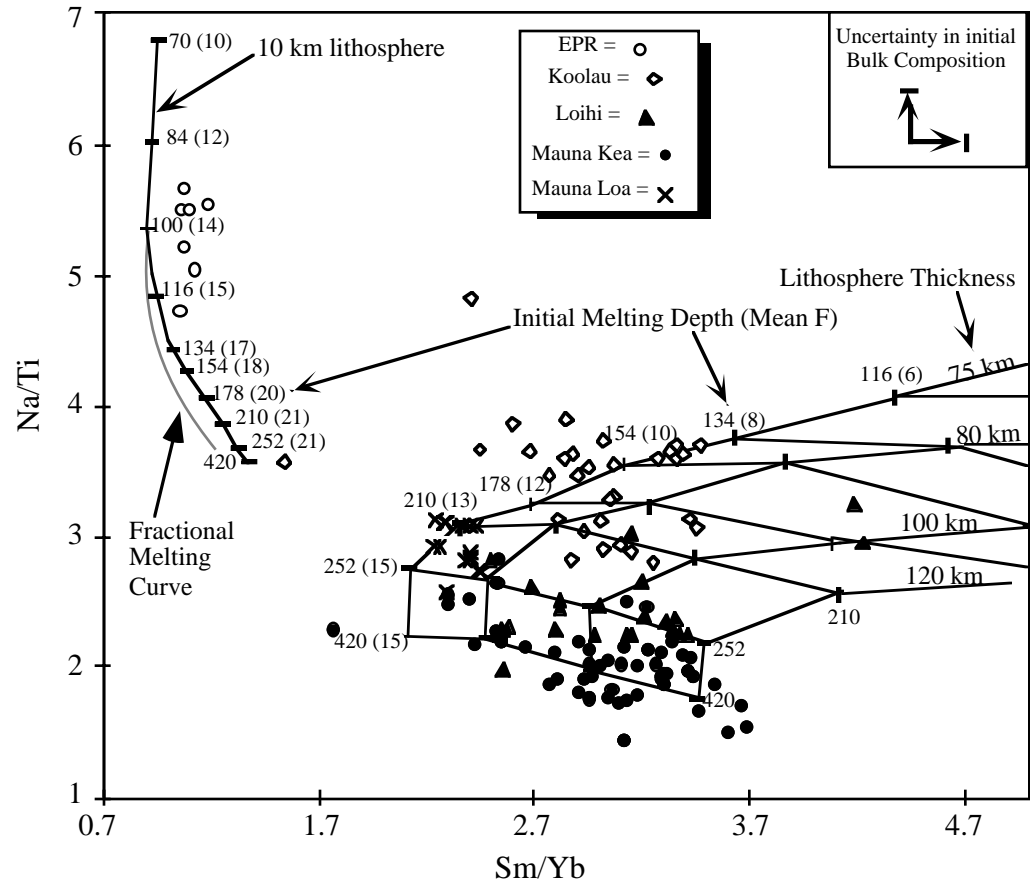


Figure 4. Hawaiian shield averages for isotopes and major oxides⁶ are compared to test for depth-dependent isotopic heterogeneity at Hawaii. Na/Ti ratios are correlated with $^{87}\text{Sr}/^{86}\text{Sr}$ (A), $^{206}\text{Pb}/^{204}\text{Pb}$ (B), and $^{187}\text{Os}/^{188}\text{Os}$ (C). (R^2 values are for shield averages). The Loa-trend volcanoes are consistent with two-component mixing between an upper, isotopically enriched mantle component, and a deeper, more isotopically depleted/less enriched source. Kea-trend volcanoes are not consistent with two-component mixing and may indicate a third component. Interestingly, Loihi and Mauna Loa lavas show local internal correlations for $^{87}\text{Sr}/^{86}\text{Sr}$ -Na/Ti that are opposite to the inter-shield trend, but directed toward EPR values.

Using Melt Inclusions to Investigate a Heterogeneous Mantle: An Example from Baffin Island, Northern Canada

Identification of chemical and isotopic heterogeneity within and between the mantle source regions of basaltic rocks provides the primary geochemical insight into the long-term dynamics of crust-mantle systems.¹⁶ However, recent studies suggest that estimates of basalt source region heterogeneity based solely on bulk-rock lava samples (as has traditionally been the case) may dramatically underestimate the diversity of melt compositions in a given system.¹⁷

The blending and mixing processes whereby individual melt batches combine during melt ascent and storage appear to homogenize much of the initial diversity of primary magma compositions, and this can destroy information about heterogeneity in a particular basalt source region. One way to circumvent this problem is to examine melt inclusions that are trapped prior to or during the homogenization process, as these can preserve some or all of the range of initial melt compositions.

An excellent example of the utility of melt inclusion studies for investigating melting of a heterogeneous source region is the Tertiary lavas of Baffin Island, northern Canada. Picritic basalts from Baffin Island comprise an interbedded suite of MORB-like lavas. Adam Kent has analyzed ~400 melt inclusions from 8 samples. The results indicate that the range of variation in geochemical enrichment between glass inclusions (as shown by K_2O/TiO_2 and La/Sm ratios) is a factor of ~50 greater than that between whole-rock lava samples.

Melt inclusions are interpreted to represent primitive melts that record melting of enriched and depleted zones within a heterogeneous mantle source. Calculations indicate that if the variations in K_2O/TiO_2 in melt inclusions correlate with Sr and Nd isotope composition in the same way as observed in whole rock lava samples, then the estimated Sr and Nd isotopic variation present in melt inclusions from a single sample is similar to that

observed in between whole rock samples from all major groups of oceanic lavas. These results outline the tremendous potential of melt inclusions studies for providing new information and insights into the chemical dynamics of the mantle.

Diagenetic Alteration of Tooth Enamel

The mineral in teeth and other biogenic phosphates is a hydrous calcium phosphate, called apatite, and the chemical and isotope composition of this apatite from tooth enamel is used in a variety of paleoclimate, anthropological, and paleodietary studies. However, successful application of chemical and isotopic analysis of teeth depends on the compositional resistance of enamel to alteration that can occur during burial and lithification.

Trace element and isotope geochemists differ strongly on the fidelity of trace and stable isotopes in biogenic phosphates during this diagenesis, some arguing for complete resistance, others for complete alteration. Unfortunately, most published data are from bulk materials, which does not allow direct investigation of diagenetic changes to mineralogy and compositions.

Measured compositions in "altered" materials could thus reflect either contamination by new minerals (i.e., mixed analyses) or chemical changes to the original biogenic apatite.

In this study, Matt Kohn used the ion microprobe, electron microprobe, and transmission electron microscope to compare modern and fossil teeth from northern and central Kenya (Fig. 5). Imaging and measured compositions confirm that fossil tooth chemistry is controlled not only by the diagenetic precipitation of secondary minerals but also by the chemical alteration of the biogenic apatite crystals themselves.

Increases in the concentrations of the elements Fe, Mn, Si, Al, Ba, and possibly Cu in fossil versus modern teeth reflect mixed analyses that include sub- μm , interstitial Fe-Mn oxyhydroxides, Fe-Mn silicates, and possibly clays, in amounts ranging from ~0.3% in enamel to ~5% in dentine.

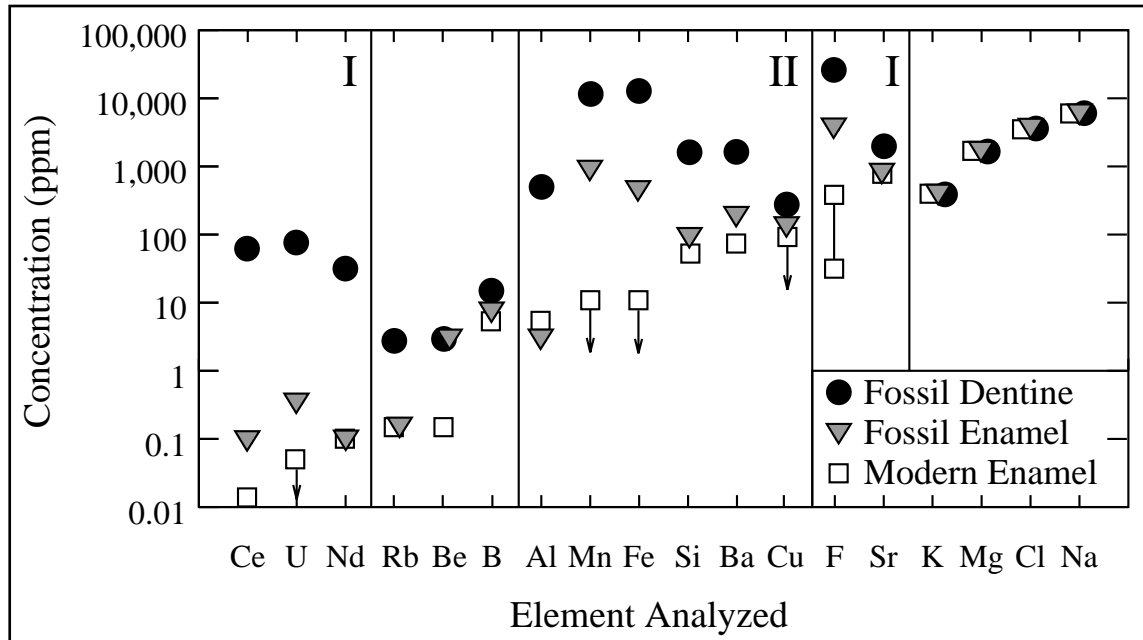


Figure 5. Ion microprobe analyses of composition vs. element for modern enamel (squares), fossil enamel (triangles), and fossil dentine (circles), showing strong increases in the concentrations of many trace and minor elements associated with fossilization. Regions denoted “I” correspond to elements likely associated with chemical alteration of apatite. The increased concentration of region “II” elements likely reflects mixed apatite and oxyhydroxide analyses. Although all fossil materials are altered, alteration is greater in dentine than in enamel.

Sub- μm crystals of Fe-bearing manganite [(Fe $^{3+}$,Mn $^{3+}$) O (OH)] and smectite were identified using the TEM. The pervasive distribution of these secondary minerals and their fine grain size indicate that mixed analyses are unavoidable in *in-situ* methods, even in ion microprobe spots only 10 μm in diameter, and that bulk chemical analyses are severely biased. However, increases in other elements, including the REEs, U, Sr, and F, apparently reflect additional alteration of the apatite crystals themselves. Extreme care will be required to separate secondary minerals from original biogenic apatite for paleobiological or paleoclimate studies, and nonetheless, bulk analyses of purified apatite may be suspect. Alteration of the OH-site of apatite implies that oxygen isotope analyses of bulk fossil tooth enamel may be systematically biased by $\pm 1\%$, and seasonal records of oxygen isotope composition may be spuriously shifted, enhanced, or diminished.

⁵³Mn–⁵³Cr Dating of Formation in the CV3 Chondrite Mokoia: Evidence for Asteroidal Alteration

Chondrites—which consist primarily of chondrules, Ca-Al-rich inclusions (CAIs), and matrix material—are a class of meteorites believed to represent remnants of primordial solid particles formed during the earliest epoch of solar system history; chondrites are the oldest rocks in the solar system.¹⁸

The chemical, isotopic, and petrologic properties of chondrites provide a key source of information on the chemical and physical processes operating in the solar nebula. Unfortunately, chondrites are not pristine relics, but were heated and altered during metamorphism after their primary constituents had accreted into asteroids.

Metamorphism may overprint the chemical and textural record of early solar system processes (distorting the historical record) and the studies initially focused on carbonaceous chondrites, because these meteorites appeared to have

escaped metamorphism and aqueous alteration. However, recent work suggests all meteorites were altered to some extent after they formed. The question as to where and when this metamorphism occurred—in the solar nebula before the chondrules, CAIs, and matrix material accreted, or on planetesimals (asteroids) following accretion—remains unresolved and highly contentious.¹⁹

The length of time over which nebular alteration processes may occur cannot exceed the lifetime of the solar nebula, while metamorphism and alteration in asteroids may continue long after the nebula has dissipated. Dating the time of formation of secondary minerals in chondrites—the focus of this study—thus offers a powerful approach to distinguish between nebular and asteroidal alteration.

Three short-lived and now extinct radionuclides—²⁶Al, ⁵³Mn and ¹²⁹I, with respective half-lives of 0.75 My, 3.7 My, and 15.7 My—have been applied to this problem, with mixed results. The ages of secondary minerals span a 15-My interval and suggest that alteration may have commenced early but continued for at least 20 My after CAI formation. This isotopic evidence for an extended time scale of secondary mineralization favors an asteroidal setting, but a nebular origin of some metamorphic features cannot be excluded.

Ian Hutcheon and Doug Phinney, in conjunction with colleagues at University of Hawaii (Alexander N. Krot, Klaus Keil, and Edward R. D. Scott), have dated the time of formation of four fayalite crystals in three chondrules in the carbonaceous chondrite Mokoia, using the LLNL ion microprobe to search for evidence of radiogenic ⁵³Cr produced by the *in-situ* decay of ⁵³Mn. All four Mokoia fayalites show well-resolved excesses of ⁵³Cr, correlated with the respective ⁵⁵Mn/⁵²Cr ratios (Fig. 6).

The linear correlation between the magnitudes of the ⁵³Cr excesses and the respective Mn/Cr ratios is characteristic of the *in-situ* decay of ⁵³Mn and demonstrates that these fayalite crystals formed while ⁵³Mn was still extant. The slope of the correlation line fitted to the data indicates the initial abundance of ⁵³Mn at the time the fayalites formed and cooled below the closure temperature for Cr diffusion, $(^{53}\text{Mn}/^{55}\text{Mn})_0 = (2.32 \pm 0.18) \times 10^{-6}$.

These data provide the first evidence for radiogenic ⁵³Cr in fayalite in a chondritic meteorite and allow us to determine the time of fayalite formation by comparing the abundance of ⁵³Mn found here with the solar system initial value, $^{53}\text{Mn}/^{55}\text{Mn} = 4.4 \times 10^{-5}$.²⁰

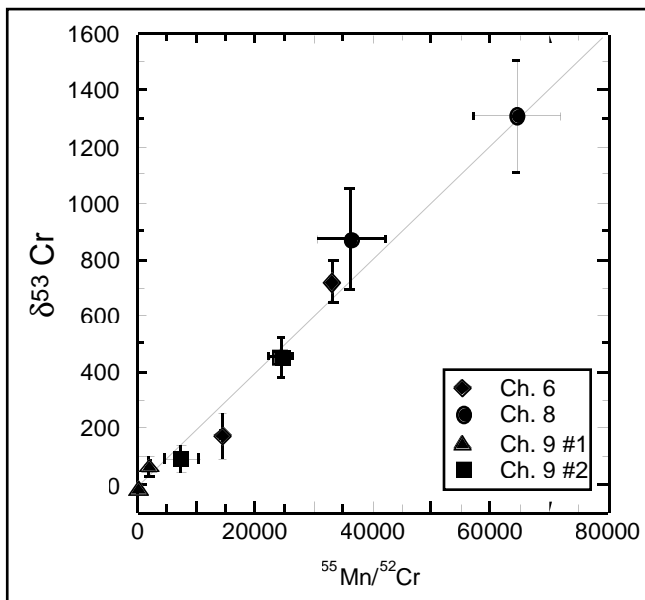


Figure 6. ⁵³Mn - ⁵³Cr evolution diagram for four fayalite grains in three olivine-pyroxene chondrules in the oxidized CV3 chondrite Mokoia. The slope of the line fitted to the data yields the initial ⁵³Mn abundance at the time of fayalite formation, $(^{53}\text{Mn}/^{55}\text{Mn})_0 = (2.32 \pm 0.18) \times 10^{-6}$. The data are plotted as $\delta^{53}\text{Cr}$, the permil deviation from the ⁵³Cr/⁵²Cr ratio measured in a fayalite standard; errors are $\pm 2\sigma_{\text{mean}}$.

If we assume the lower abundance of ^{53}Mn in fayalite is due to decay of ^{53}Mn prior to fayalite formation, we conclude the Mokoia fayalites formed between 14 and 17 My after Allende CAIs, the oldest objects in the solar system. This time scale is at least 4 My longer than the estimated lifetime of the solar nebula, leading to the conclusion that the Mokoia fayalites formed in an asteroid and not in the nebula.

The results of this study suggest that the aqueous activity that produced fayalite on the parent body of the CV chondrites was occurring simultaneously with the aqueous activity that produced carbonates on the parent bodies of the CI and CM chondrites, shortly after the parent bodies accreted.

This time scale is consistent with heating of asteroids by ^{26}Al decay, leading to the production of liquid water by melting of ice, and suggests water played an important role in the chemical evolution of primitive solar system bodies.

Cosmogenic Nuclides in Antarctic and Greenland Ice Cores: Implications for Solar History

Bob Finkel and Kuni Nishiizumi (UC Berkeley) are engaged in a program to measure and interpret a high-resolution time series of ^{10}Be and ^{36}Cl in ice cores from Greenland and the Antarctic in order to test the hypothesis that changes in solar activity have an influence on terrestrial climate.

Although it is clear that the Sun is the driving force of climate, it is less clear whether changes in solar output play a role in climate change. Reliable prediction of climate change requires an assessment of the possible effects of solar luminosity on climate. Direct measurement of solar output exists for only the last 20 years.

Although numerous publications have shown the plausibility of a connection between solar variability and climate change, the brevity of direct observations has hindered investigations into the role the Sun might play in controlling climate. By developing a time series of solar activity that extends beyond the era of instrumental measure-

ments, we propose to test this hypothesis in a quantitative way.

It is necessary to use a proxy of solar luminosity to determine solar irradiance before the era of instrumental observations. Our method follows. Satellite data show that both solar irradiance and the cosmic-ray flux at the Earth are correlated. This is not surprising because changes in solar luminosity and solar magnetic activity are related to underlying solar transport properties.

Solar magnetic intensity affects the ability of galactic cosmic rays to penetrate the solar system to the orbital distance of the Earth. Cosmogenic radionuclide concentrations in polar ice cores change with the cosmic-ray flux in the Earth's atmosphere, and therefore, through the magnetic field connection, with solar activity.

Nuclide concentrations can, therefore, be used as a proxy to extend the solar activity record to periods before recorded observations. In fact, earlier measurements in central Greenland have shown that during the Maunder Minimum (1645–12715 AD), a period of quiet Sun when there were almost no sunspots and of cold climate in Europe and North America, the ^{10}Be concentration was substantially higher than during other periods.

We are using ^{10}Be and ^{36}Cl in polar ice cores as well as published ^{14}C concentrations in tree rings to determine the history of solar irradiance throughout the Holocene. The comparison of ice core results with those from tree rings will help detect and eliminate perturbing factors other than solar luminosity, such as changes in atmospheric mixing or ocean circulation, which might also change atmospheric nuclide concentrations.

Our measurements at GISP2 in central Greenland have shown a good correlation between the main short-term variations of the ^{10}Be and ^{36}Cl record in ice and the ^{14}C record in tree rings between the end of the last glacial period and about 1000 years ago. Part of this record is shown in Figure 7. These data strongly support the explanation that solar modulation of the galactic cosmic-ray flux is primarily responsible for these fluctuations. We are currently measuring a higher-resolution record for the last 1000 years in both Greenland and the Antarctic in order to extend this comparison.

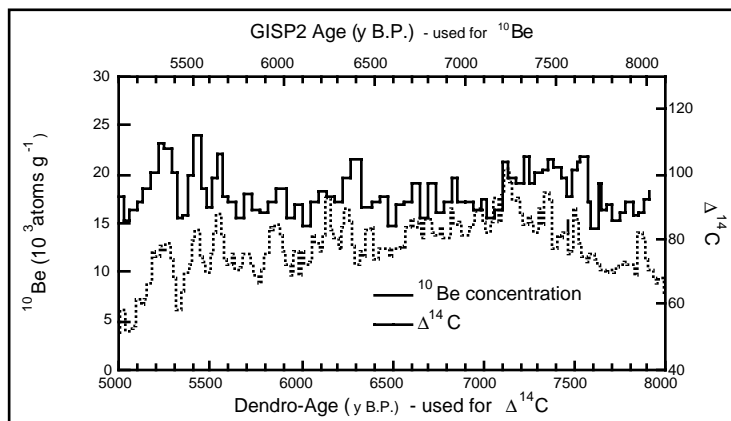


Figure 7. ^{10}Be measurements from GISP2 in central Greenland showing the good correlation between the main short-term variations of the ^{10}Be and the ^{14}C record in tree rings between the end of the last glacial period and about 1000 years ago.

The Geochemical Earth Reference Model – GERM

Understanding the global chemical dynamics of the Earth requires a simple but comprehensive set of data on chemical inventories of the major Earth reservoirs and the fluxes between them. Ideally, such a data set could be formulated in terms of a reference model consisting of direct measurements that represent a very close approximation to the actual compositions and exchange rates.

Unfortunately, such a model would be impossible to establish for the Earth because most of our planet is not accessible to direct observation. Nevertheless, even an imperfect chemical “reference” model for the Earth would be of enormous utility for Earth scientists.

This model would simply provide the current best consensus values for parameters, with estimates of uncertainties. Such a consensus would allow for coherent testing of global models, highlight gaps in our knowledge, trigger more focused work on improving existing estimates, and make geochemistry more transparent to non-specialists.

The need for a “Geochemical Earth Reference Model” (GERM) was identified as a major goal at the Mantle-Ocean/Atmosphere (MOC) conference in August 1994 in Amsterdam.²¹ Out of that realization grew a grass-roots initiative to establish a community consensus on a chemical charac-

terization of the Earth’s major reservoirs and the fluxes between them. The GERM initiative provides a forum for the review of available scientific constraints for

1. The composition of all major chemical reservoirs of the present-day Earth, from core to atmosphere.
2. Present-day fluxes between reservoirs.
3. The Earth’s chemical and isotopic evolution since accretion.
4. The chemical and isotopic evolution of seawater as a record of global tectonics and climate.

The development of the model began with an initial workshop in Lyon, France, in March 1996.²² Since then, the GERM effort has continued, fostered by workshops and special sessions at professional meetings. A second GERM workshop, sponsored in part by the UC San Diego branch of IGPP, was held in La Jolla, California, in March 1998, and a third workshop is being planned for the year 2000.

The actual model is being developed in an open community forum on the World Wide Web (<http://www.es.llnl.gov/germ/>), hosted at LLNL. The development is moderated by editors with responsibilities for different reservoirs, fluxes, databases, and other scientific or technical aspects. These editors have agreed to lay out an initial, strawman GERM for their respective sec-

tions and to moderate community discussions leading to a first, preliminary consensus. Overall coordination of the effort is provided by an 8-person steering committee, including IGPP-LLNL scientist Henry Shaw.

**Late Pleistocene Fluctuations in
Southern Tropical Alpine Glaciers:
 ^{10}Be and ^{26}Al Exposure Ages of Moraines
from the Cordillera Blanca, Perú**

High-resolution isotopic studies of ice cores have demonstrated that the last glacial period was a time of dramatic climate instability. The precise timing and global distribution of climate fluctuations can yield information about the dynamics of the ocean-atmosphere system,²³ and therefore, understanding global climatic change requires precise documentation of past climatic fluctuations.

Most climate records are derived from mid- to high-latitude regions; therefore, the nature of climate change in the tropics and the degree to which the climate of the tropics mirrors that of temperate regions remains the subject of debate.

Although glacial moraines record a detailed record of local climate change, obtaining accurate ages on depositional features like moraines is often difficult. Recently, *in-situ*-produced cosmogenic radionuclides have proven to be a powerful tool for precisely dating such deposits.²⁴ Here the *in-situ* production of ^{10}Be and ^{26}Al is used to date Pleistocene moraines of the Cordillera Blanca in Perú in order to develop a detailed chronology of alpine glacier fluctuations in the southern tropics during the LGM.

Because the low altitude limit of glaciers in this region is primarily a function of temperature,²⁵ past glacier extent recorded by moraines can serve as a sensitive indicator of paleotemperature fluctuations at this latitude. Glacial deposits are particularly sensitive indicators of paleoclimate, and central Perú's climate is strongly affected by changes in global atmospheric patterns; the Amazon basin immediately to the east is subject to the Southern Oscillation, while northern

Perú is affected by fluctuations of the Intertropical Convergence Zone.

Thus, the Pleistocene history of alpine glacier fluctuations in Perú can be used to address both global and regional climatic issues. Working with colleagues from UC Santa Cruz (Gregory S. Hancock, Robert S. Anderson, and Keith Pankow); California State University (Brendan McNulty); Dominguez Hills and the Instituto de Geológico Minero y Metalúrgico, Lima, Perú (Oscar Palacios and Hugo Rivera), Dan Farber and Bob Finkel have determined the time of glacial retreat by measuring the concentration of ^{10}Be and ^{26}Al in quartz extracted from the Laguna Baja, Rurec, and Cojup deposits. Samples were collected northeast of Huaraz in the Quebradas (valleys) of Llaca and Cojup (Fig. 8).²⁶ Figure 9 shows the data and model ages based on the production rates of Nishiizumi *et al.*²⁷ together with our estimate of the local ~15 ky time-integrated production rate. While these ages suggest two distinct LGM moraine groups (~25 ka and ~18 ka), they alone do not necessitate two separate advances (e.g., the group 1 moraines may simply mark the recession from the group 2 moraines). However, palynological, climatic, and regional studies lend support to the idea of two separate advances.^{28,29}

In addition, our timing for the LGM advances in the Cordillera Blanca matches (within error) Heinrich events 1 (~16.5 ka) and 2 (~23.0 ka), and is similar to the moraine chronologies in temperate North and South America,^{30,24} and to the timing of changes in isotopic compositions from marine records in the tropical Pacific and temperate Atlantic basins.^{31,32} Thus, our new data suggest that this multiple LGM was a rapid, global-scale climatic event, and support models of large, high-frequency climate instability at the end of the LGM.^{23,33}

Although glacial extent may reflect both precipitation and temperature, glacial levels in the Cordillera Blanca are sensitive primarily to temperature.²⁵ Therefore, paleo-snowlines can be used to estimate decreases in mean annual temperature. Based on the present atmospheric lapse rate

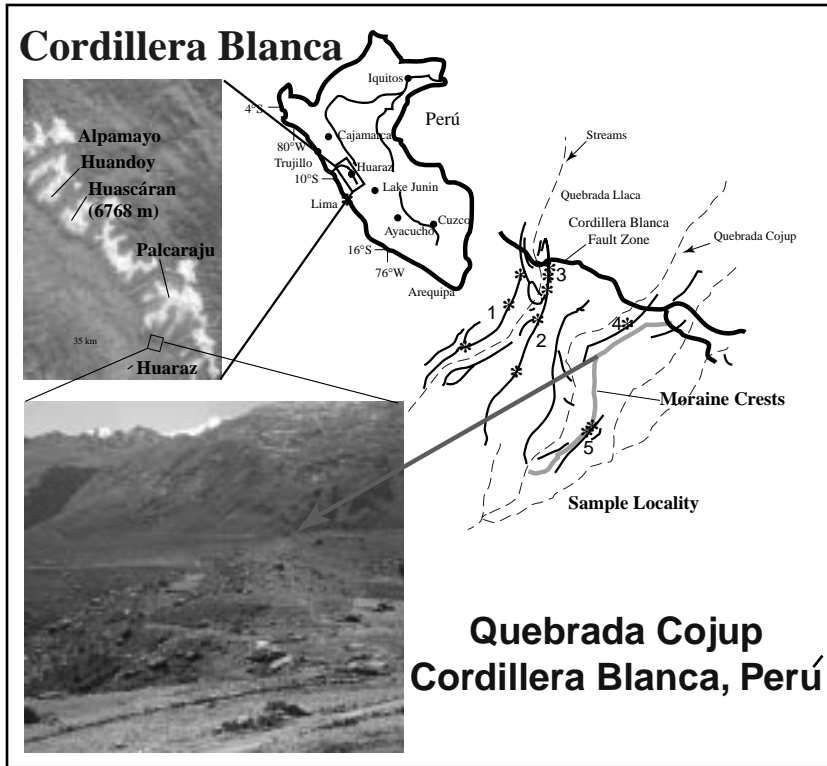


Figure 8. Map showing the location of the Cordillera Blanca in Perú. The satellite image shows the central portion of the range with the field area outlined. Insets show a detailed sketch of the moraines sampled (after Rodbell, 1993²⁶) and a photo of the Rurec moraine crest in Quebrada Cojup.

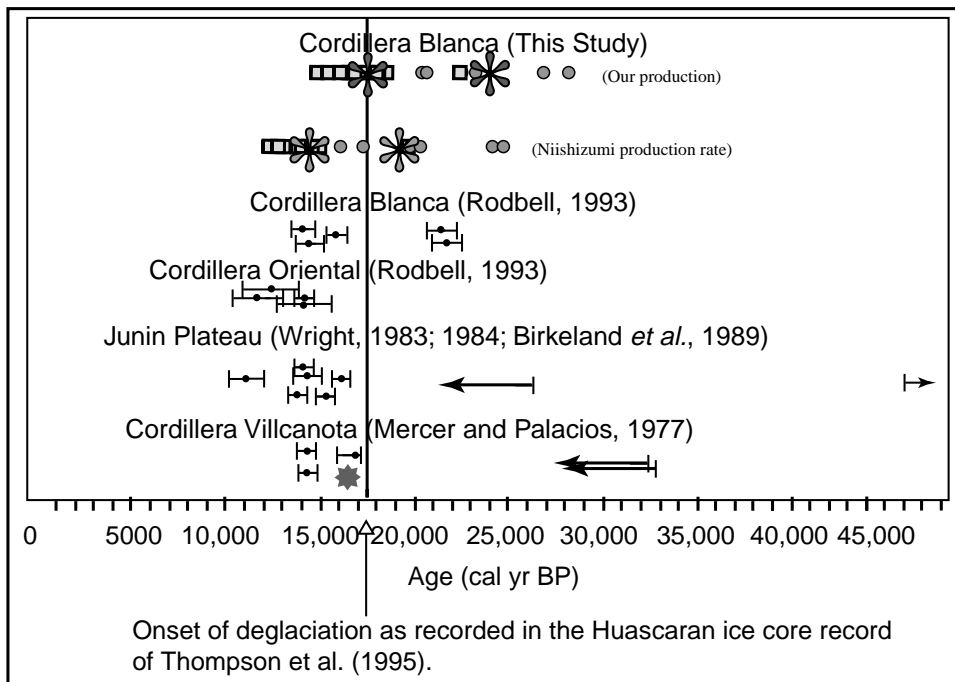


Figure 9. Summary diagram showing ^{10}Be and ^{26}Al model ages together with ^{14}C constraints from previous studies. ^{14}C data are all minimum limiting ages except where indicated by arrows (i.e., in the positive direction for minimum ages and vice versa). Data from the following studies were used in this compilation: Cordillera Blanca,²⁶ Cordillera Oriental,^{26,35,36} Junin Plateau,³⁷⁻³⁹ and Cordillera Villcanota.⁴⁰ The star in the data set for the Cordillera Villcanota is Mercer's⁴¹ estimate of the onset of deglaciation. For the ^{14}C data older than ~24 ka, we used the calibration of Kitagawa and van der Plicht.⁴² Our new ^{10}Be and ^{26}Al data are shown at the top of the figure. In the bottom row, the data are presented using the production rate of Nishiizumi *et al.*,²⁷ and in the top row, using our new production estimates. The group 1 moraines are shown with filled boxes, and the group 2 moraines are shown with filled circles.

of 7.5°C/km and the snowline depression recorded in the LGM moraine record (moraines at 1.2 km below present terminus), the authors estimate an ~9°C difference between present and LGM mean annual temperatures.

This estimate suggests significant cooling in the tropics during the last glacial and is consistent with estimates derived from geochemical,⁴³ isotopic,⁴⁴ glacial,⁴⁵ and palynological^{34,29} studies throughout the tropical Andes and the Amazon basin.

Our data clearly demonstrate the existence of older Andean glaciations that predate the last interglacial in the Cordillera Blanca. Our evidence for an extensive glacial advance at >200 ka, together with the existence of even older moraines (still undated) at lower elevations in the Cordillera Blanca, suggests that maximum alpine ice vol-

umes occurred during previous glacials and not at the close of the last glacial.

These measurements of ¹⁰Be and ²⁶Al demonstrate the applicability of cosmogenic nuclide surface exposure age dating to tropical moraines and strongly support the global nature of the climate instability at the end of the last glacial maximum.

The most likely interpretation of our results requires recalibration of the high-latitude, sea-level ¹⁰Be production rate to 4.79 at/g qtz yr at least in high elevation tropical settings. Confirmation of these results by future studies should lead to both a much clearer understanding of the history of tropical glaciers and icecaps, and the teleconnections of global climate, providing a firmer basis for assessing the magnitude and timing of future climate change.

REFERENCES

1. Van der Woerd, J., *et al.* "Holocene Left-Slip Rate Determined by Cosmogenic Surface Dating on the Xidatan Segment of the Kunlun Fault (Qinghai, China)," *Geology* **26**, 695; UCRL-JC-128338, Lawrence Livermore National Laboratory, Livermore, CA (1997).
2. Langmuir, C. H., J. F. Bender, A. E. Bence, and G. N. Hanson, "Petrogenesis of Basalts from the FAMOUS Area: Mid-Atlantic Ridge," *Earth Planet. Sci. Lett.* **36**, 133 (1977).
3. Hofmann, A. W., and W. M. White, "Mantle Plumes from Ancient Oceanic-Crust," *Earth Planet. Sci. Lett.* **57**, 421 (1982).
4. Hirschmann, M. M., and E. M. Stolper, "A Possible Role for Garnet Pyroxenite in the Origin of the 'Garnet Signature' in MORB," *Contrib. Mineral. Petrol.* **124**, 185 (1996).
5. Hauri, E. H., "Major-Element Variability in the Hawaiian Mantle Plume," *Nature* **382**, 415 (1996).
6. Okano, O., and M. Tatsumoto, "Petrogenesis of Ultramafic Xenoliths from Hawaii Inferred from Sr, Nd and Pb Isotopes," in *Earth Processes: Reading the Isotopic Code*, *Geophysical Mon. Ser.* **95**, S. Hart and A. Basu, eds., pp. 135–147, AGU, Washington, D.C. (1996).
7. Klein, E. M., and C. H. Langmuir, "Global Correlations of Ocean Ridge Basalt Chemistry with Axial Depth and Crustal Thickness," *J. Geophys. Res.* **92**, 8089(1987).
8. Kinzler, R. J., and T. L. Grove, "Primary Magmas of Mid-Ocean Ridge Basalts. 2. Applications," *J. Geophys. Res.* **97**, 6907 (1992).
9. Putirka, K., "Garnet + Liquid Equilibrium," *Contrib. Mineral. Petrol.* **131**, 273 (1998).
10. Salters, V. J. M., "The Generation of Mid-Ocean Ridge Basalts from the Hf and Nd Isotope Perspective," *Earth Planet. Sci. Lett.* **141**, 109 (1996).
11. Hofmann, A. W., K. P. Jochum, M. Seufert, and W. M. White, "Nb and Pb in Oceanic Basalts: New Constraints on Mantle Evolution," *Earth Planet. Sci. Lett.* **79**, 33 (1986).
12. Farber, D. L., Q. Williams, and F. J. Ryerson, "Diffusion in Mg₂SiO₄ Polymorphs and

- Chemical Heterogeneity in the Mantle Transition Zone,” *Nature* **371**, 693 (1994).
13. MELT Seismic Team, “Imaging the Deep Seismic Structure beneath a Mid-Ocean Ridge: The MELT Experiment,” *Science* **280**, 1215 (1998).
 14. Sleep, N. H., “Hotspots and Mantle Plumes: Some Phenomenology,” *J. Geophys. Res.* **95**, 6715 (1990).
 15. Romanowicz, B., “A Global Tomographic Model of Shear Attenuation in the Upper Mantle,” *J. Geophys. Res.* **100**, 12375 (1995).
 16. Hoffman, A. W., “Mantle Geochemistry: The Message from Oceanic Volcanism,” *Nature* **385**, 219 (1997).
 17. Kent, A. J. R., M. D. Norman, I. D. Hutcheon, and E. M. Stolper, “Sea Water Assimilation in an Oceanic Volcano: Evidence from Matrix Glasses and Glass Inclusions from Loihi Seamount, Hawaii,” UCRL-JC-130454, Lawrence Livermore National Laboratory, Livermore, California; *Chem. Geol.*, in prep. (1998).
 18. Kerridge, J. F., and M. S. Matthews, *Meteorites and the Early Solar System*, University of Arizona Press, Tucson, Arizona (1988).
 19. Zolensky, M. E., A. N. Krot, and E. R. D. Scott, eds., *Workshop on Parent Body and Nebular Modification of Chondritic Materials*, LPI Tech. Rpt. 97-02 (Lunar and Planetary Institute), Parts 1–2 (1997).
 20. Birck, J.-L., and C. J. Allègre, “Manganese Chromium Isotope Systematics and the Development of the Early Solar System,” *Nature* **331**, 579 (1988).
 21. Staudigel, H., F. Albarede, D. Hilton, and T. Elliott, Preface to the Special Issue The Mantle-Ocean Connection, *Chem. Geol.* **126**, iii-v (1995).
 22. Staudigel, H., F. Albarede, J. Blichert-Toft, J. Edmond, B. McDonough, S. B. Jacobsen, R. Keeling, C. H. Langmuir, R. L. Nielsen, T. Plank, R. Rudnick, H. F. Shaw, S. Shirey, J. Veizer, and W. White, “Geochemical Earth Reference Model (GERM): Description of the Initiative,” *Chem. Geol.* **145**, 153 (1998).
 23. Broecker, W. S., and G. H. Denton, “The Role of Ocean-Atmosphere Reorganizations in Glacial Cycles,” *Quaternary Sci. Rev.* **9**, 305 (1994).
 24. Phillips, F. M., M. G. Zreda, J. Gosse, E. B. Evenson, R. D. Hall, O. A. Chadwick, and P. Sharma, “Cosmogenic ^{36}Cl and ^{10}Be Ages of Quaternary Glacial and Fluvial Deposits of the Wind River Range, Wyoming,” *Geol. Soc. of Am. Bull.* **109**, 1453 (1997).
 25. Lilboutry, L., B. M. Arnao, and B. Scheider, “Glaciological Problems Set by the Control of Dangerous Lakes in the Cordillera Blanca, Perú. III. Study of Moraines and Mass Balances at Safuna,” *J. Glaciology* **18**, 275 (1977).
 26. Rodbell, D. T., “Subdivisions of Late Pleistocene Moraines in the Cordillera Blanca, Perú, Based on Rock-Weathering Features, Soils, and Radiocarbon Dates,” *J. Quaternary Res.* **39**, 133 (1993).
 27. Nishiizumi, K., E. L. Winterer, C. P. Koh., J. Klein, R. Middleton, D. Lal, and J. R. Arnold, “Cosmic Ray Production Rates of ^{10}Be and ^{26}Al in Quartz from Glacially Polished Rocks,” *J. Geophys. Res.* **94**, 17907 (1989).
 28. Clapperton, C. M., “Glacier Re-Advances in the Andes at 12,500–10,000 yr BB: Implications for Mechanism of Late-Glacial Climatic Change,” *J. Quaternary Sci.* **58**, 197 (1993).
 29. Thouret, J., T. V. d. Hammen, B. Salomons, and E. Juvigne, “Paleoenvironmental Changes and Glacial Stages of the Last 50,000 Years in the Cordillera Central, Columbia,” *J. Quaternary Res.* **46**, 1 (1996).
 30. Lowell, T. V., C. J. Heusser, B. G. Anderson, P. I. Moreno, A. Hauser, L. E. Heusser, C. Schlüchter, D. R. Marchant, and G. H. Denton, “Interhemispheric Correlation of Late

- Pleistocene Glacial Events,” *Science* **269**, 1541 (1995).
31. Bard, E., M. Arnold, P. Maurice, J. Duprat, J. Moyes, and J.-C. Duplessy, “Retreat Velocity of the North American Polar Front during the Last Deglaciation Determined by ^{14}C Accelerator Mass Spectrometry,” *Nature* **328**, 791 (1987).
 32. Linsley, B. K., “Oxygen-Isotope Record of Sea-Level and Climate Variations in the Sula Sea over the Past 150,000 Years,” *Nature* **380**, 234 (1996).
 33. Helmens, K. F., N. W. Rutter, and P. Kuhry, “Glacier Fluctuations in the Eastern Andes of Cumbio (South America) during the Last 45,000 Radiocarbon Years,” *Quaternary Internat’l.* **38/39**, 39 (1997).
 34. Colinvaux, P. A., P. E. Oliveira, J. E. Moreno, M. C. Miller, and M. B. Bush, “A Long Pollen Record from Lowland Amazonia: Forest and Cooling in Glacial Times,” *Science* **274**, 85 (1996).
 35. Hughen, K. A., J. T. Overpeck, L. C. Peterson, and S. Trumbore, “Rapid Climate Changes in the Tropical Atlantic Region during the Last Deglaciation,” *Nature* **380(6569)**, 51 (1996).
 36. Rodbell, D. T., “The Timing of the Last Deglaciation in Cordillera Oriental, Northern Peru. Based on Glacial Geology and Lake Sedimentology,” *Geolog. Soc. Am. Bull.* **105(7)**, 923 (1993).
 37. Birkeland, P. W., D. T. Rodbell, and S. K. Short, “Radiocarbon Dates on Deglaciation, Cordillera Central, Northern Peruvian Andes,” *Quaternary Res.* **32(1)**, 111 (1989).
 38. Wright, H. E., “Late-Pleistocene Glaciation and Climate around the Junin Plain, Central Peruvian Highlands,” *Geografiska Annaler Series A-Phys. Geog.* **65(1–2)**, 35 (1983).
 39. Wright, H. E., “Late Glacial and Late Holocene Moraines in the Cerros Cuchpanga, Central Peru,” *Quaternary Res.* **21(3)**, 275 (1984).
 40. Mercer, J. H., and M. O. Palacios, “Radiocarbon Dating of the Last Glaciation in Peru,” *Geology* **5**, 600 (1977).
 41. Mercer, J. H. “Cenozoic Glaciation in the Southern Hemisphere,” *Ann. Rev. Earth Planet. Sci.* **11**, 99 (1983).
 42. Kitagawa, H., and J. van der Plicht, “Atmospheric Radiocarbon Calibration to 45,000-yr BP: Late Glacial Fluctuations and Cosmogenic Isotope Production,” *Science* **279(5354)**, 1187 (1998).
 43. Stute, M., M. Forster, H. Frischkorn, A. Serejo, J. F. Clark, P. Schlosser, W. S. Broecker, and G. Bonani, “Cooling of Tropical Brazil (5-Degrees-C) during the Last Glacial Maximum,” *Science* **269(5222)**, 379 (1995).
 44. Thompson, L. G., E. Mosleythompson, M. E. Davis, P. N. Lin, K. A. Henderson, J. Coledai, J. F. Bolzan, and K. B. Liu, “Late-Glacial Stage and Holocene Tropical Ice Core Records from Huascarán, Peru,” *Science* **269(5220)**, 46 (1995).
 45. Rodbell, D. T., “Late Pleistocene Equilibrium-Line Reconstructions in the Northern Peruvian Andes,” *Boreas* **21(1)**, 43 (1992).

Section III. Research Summaries of Collaborative Projects

Astrophysics

A VLA Survey of the Sky at 1400 MHz (98-AP001)

Principal Investigator: Robert Becker (UC Davis)

LLNL Collaborator: Wil van Breugel

Postdoc: Sally Laurent-Muehleisen (UC Davis)

The FIRST Survey (Faint Images of the Radio Sky at Twenty centimeters) completed the analysis of the fifth season of observing, which has resulted in an expanded catalog of ~550,000 discrete radio sources for ~6000 square degrees of sky. Using the expanded catalog, research has continued on the FIRST bright QSO survey, on a search for distant clusters of galaxies, and on a search for extremely high-redshift radio galaxies. We have also initiated a search for gravitationally lensed quasars.

OBJECTIVES

The primary objective is the creation of an accurate, high-dynamic-range image of the radio sky at 1400 MHz. The survey will allow astronomers to identify rare objects to brightness levels several orders of magnitude fainter than previously possible. This, in turn, will allow us to explore the evolution of quasars, radio galaxies, and clusters of galaxies out to very high redshifts.

PROGRESS

A number of ongoing scientific programs based on the FIRST Survey are producing important results. Publications originating under this mini-grant are listed in the Bibliography (see Section V), as well as in this report's references. Many of these papers arise from the FIRST Bright Quasar Survey, which is an ongoing attempt to create a large, uniformly selected sample of bright quasars over the entire area of the FIRST Survey.^{1,2}

To date, over 500 quasars have been found, and the sample is expected to double in size over the next two years. In the most recent paper reporting the current status of the survey, we demon-

strate conclusively that there is no bimodality in the distribution of radio-loudness for quasars, refuting a claim that has been widely accepted in the astrophysical community for a decade. In addition, the survey has found several unusual quasars that warrant special attention. These include radio-loud broad absorption line quasars,³⁻⁶ binary quasars,⁷ and gravitationally lensed quasars.⁸ Figure 1 shows the discovery image of the binary quasar FBQ1643+3156 as seen by the tvguider on Keck II.

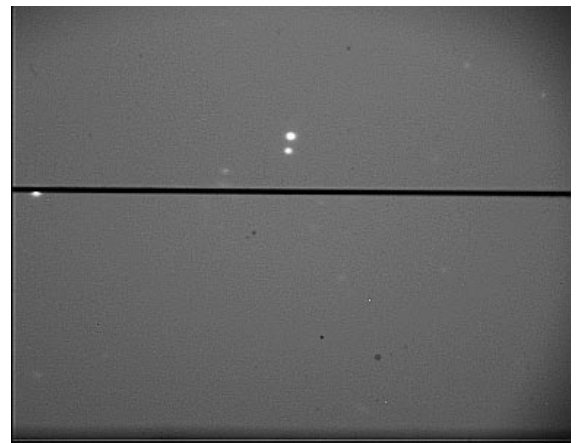


Figure 1. The discovery image of the binary quasar FBQ1643+3156 as observed by the Keck II telescope (Brotherton et al.).⁷

We have also been using the FIRST Survey to identify new examples of distant clusters of galaxies by studying the environment of bent-double radio sources. This unusual morphology is generally a good indicator that the radio source resides inside a cluster. Using Keck, we have identified ten such clusters.⁹

The FIRST Survey has also spawned a number of successful observing proposals for the use of the Hubble Space Telescope, the Advanced X-ray Astronomy Facility, the Very Large Array, and the Keck Observatory. These projects involve many IGPP postdoctoral researchers and graduate students.

REFERENCES

1. Gregg, M. D., R. H. Becker, R. L. White, D. J. Helfand, R. G. McMahon, and I. M. Hook, "The FIRST Bright QSO Survey," *Astron. J.* **112**, 407 (1996).
2. White, R. L., R. H. Becker, *et al.*, "The FIRST Bright Quasar Survey. II. 60 Nights and 1200 Spectra Later," *Astrophys. J. Suppl.*, submitted (1998).
3. Arav, N., R. H. Becker, S. A. Laurent-Muehleisen, M. D. Gregg, R. L. White, and M. de Kool, "What Determines the Depth of BALs? Keck HIRES Observations of BALQSO 1603+3002," *Astrophys. J.*, submitted (1998).
4. Becker, R. H., M. D. Gregg, I. M. Hook, R. G. McMahon, R. L. White, and D. J. Helfand, "The FIRST Radio-Loud Broad Absorption Line QSO and Evidence for a Hidden Population of Quasars," *Astrophys. J. Lett.* **479**, L93 (1996).
5. Brotherton, M. S., H. D. Tran, W. van Breugel, A. Dey, and R. Antonucci, "Spectropolarimetry of FIRST BAL QSOs," *Astrophys. J. Lett.* **487**, L113 (1997).
6. Brotherton, M. S., W. van Breugel, R. J. Smith, T. Shanks, S. M. Croom, L. Miller, and R. H. Becker, "Discovery of Radio-Loud Broad Absorption Line Quasars using Ultraviolet Excess and Deep Radio Selection," *Astrophys. J. Lett.* **505**, L10 (1998).
7. Brotherton, M. S., M. D. Gregg, R. H. Becker, S. A. Laurent-Muehleisen, R. L. White, and S. A. Stanford, "Discovery of a Radio-Loud/Radio-Quiet Binary Quasar," *Astrophys. J.*, in press (1998).
8. Schecter, P. L., M. D. Gregg, R. H. Becker, D. J. Helfand, and R. L. White, "The First FIRST Gravitationally Lensed Quasar: FBQ 0951+2635," *Astron. J.* **115**, 1371 (1997).
9. Blanton, E., M. Gregg, D. Helfand, R. Becker, and R. White, "Bent-Double Radio Sources: Tracers of High Redshift Clusters," *Astron. J.*, submitted (1998).

Speckle and Adaptive Optics Imaging of Planets and Satellites (98-AP011)

Principal Investigator: Imke de Pater (UC Berkeley)

LLNL Collaborators: Seran Gibbard, Don Gavel, Bruce Macintosh, and Claire Max

Student: Henry Roe (UC Berkeley)

SPECKLE IMAGING OF TITAN

We have obtained excellent images of Titan in speckle imaging mode with the 10-m Keck Telescope on Mauna Kea during the duration of this grant. Some examples are shown in Figure 1 at K- and H-bands; the resolution is close to the diffraction limit of the telescope (0.04"). At this point, we have good longitudinal coverage of the body. The images show clear bright and dark features, consistent with possible ice/rock "continents" and very.¹

In collaboration with researchers (C. McKay and E. Young) at NASA Ames, we have developed a simple atmospheric radiative transfer model that

we used to constrain atmospheric haze parameters and to separate the light contributions from atmosphere and surface. This has allowed us to recover the surface albedo (Fig. 1c and d), which shows a large contrast between very dark regions (albedo <0.05), especially on Titan's trailing hemisphere, and bright regions (albedo ~ 0.15) found on the leading hemisphere.

Two papers have been written on these results: a conference proceeding paper contrasting HST and Keck data,² and a detailed paper on the Titan 1996 images,³ including atmospheric modeling and a possible interpretation of the surface composition.

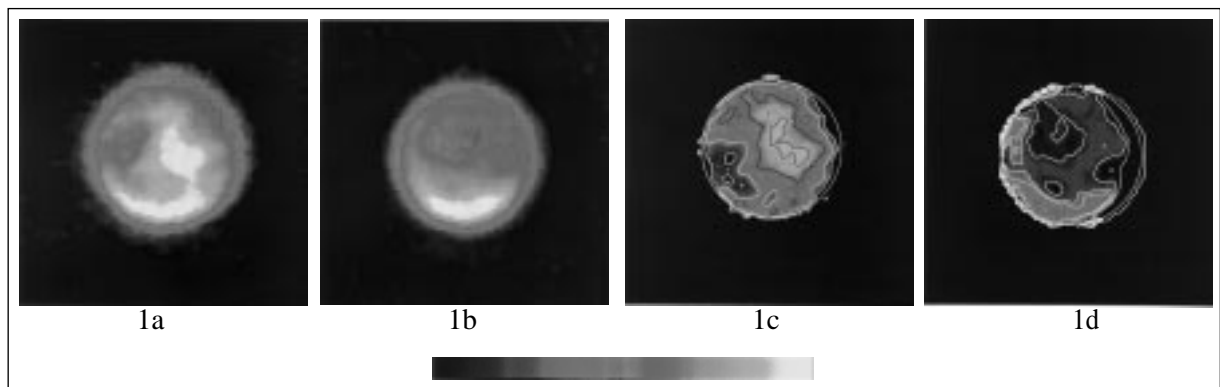


Figure 1. Speckle images of Titan taken at the Keck Telescope. 1a shows the leading hemisphere in September 1996; 1b is the trailing hemisphere taken in July 1998. These images include reflected light from both atmosphere and surface. 1c shows the surface albedo of the leading hemisphere (produced by subtraction of a model atmosphere); 1d is the surface albedo of the trailing hemisphere. Resolution on the order of 200 km is obtained. Brightening of the planet's southern hemisphere is due to an asymmetry in haze distribution in Titan's upper atmosphere. The scale is about 0.8 arcseconds across the disk.

SPECKLE IMAGING OF NEPTUNE

We have used the NIRC speckle system at Keck during the past few years to image Neptune at the diffraction limit of the telescope (0.04 arcseconds). Some of our resulting images over a 3-year span are shown in Figure 2.

We have completed a paper describing and analyzing the images from 1996 and 1997,⁴ using both the high resolution (0.04 arcsecond) broadband speckle imaging and conventional imaging with narrow-band filters (the latter were decon-

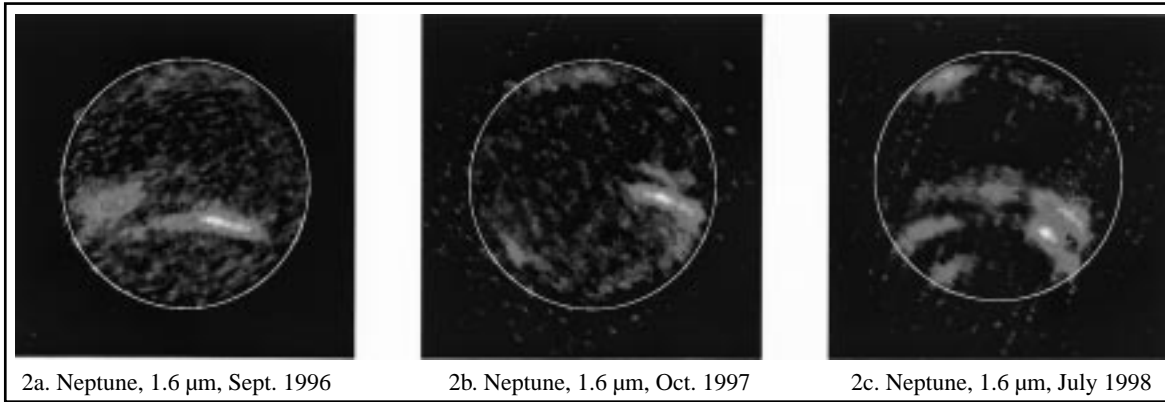


Figure 2. Speckle images of Neptune from the Keck Telescope, taken in (from left to right): September 1996, October 1997, and July 1998. The bright spots in the southern hemisphere may be associated with features similar to the “Great Dark Spot” seen by Voyager. Note also the northern limb brightening, probably due to a high-altitude haze layer. The scale is 2.33 arcseconds across the disk of Neptune.

volved using a Lucy-Richardson deconvolution technique; we also made some simulated images to test the validity of such algorithms in terms of precise photometry). The speckle data enables us to track the size and shape of infrared-bright features (‘storms’) as they move across the disk. We determined rotation periods for latitudes -30° and -45° , which agreed very closely with previous observations. We received a model atmosphere program from Kevin Baines (JPL), which student Henry Roe debugged and modified substantially. Roe used this model to estimate the stratospheric haze abundances both in storm-free regions and within the storms (Figure 3 shows an example of

the model in the form of a simulated spectrum of Neptune, with a hypothetical storm in the stratosphere).

We find that good fits to our storm-free data require a tropospheric methane haze particle column density that is about 6 times greater than previous estimates,⁵ and stratospheric haze that is about 20 times greater. These values are close to the maximum theoretical value derived by Romani *et al.* (1993).⁶ The storms appear to be produced by disturbances in the stratosphere rather than in the troposphere; they require the stratospheric haze column density to be increased by a factor of several thousands.

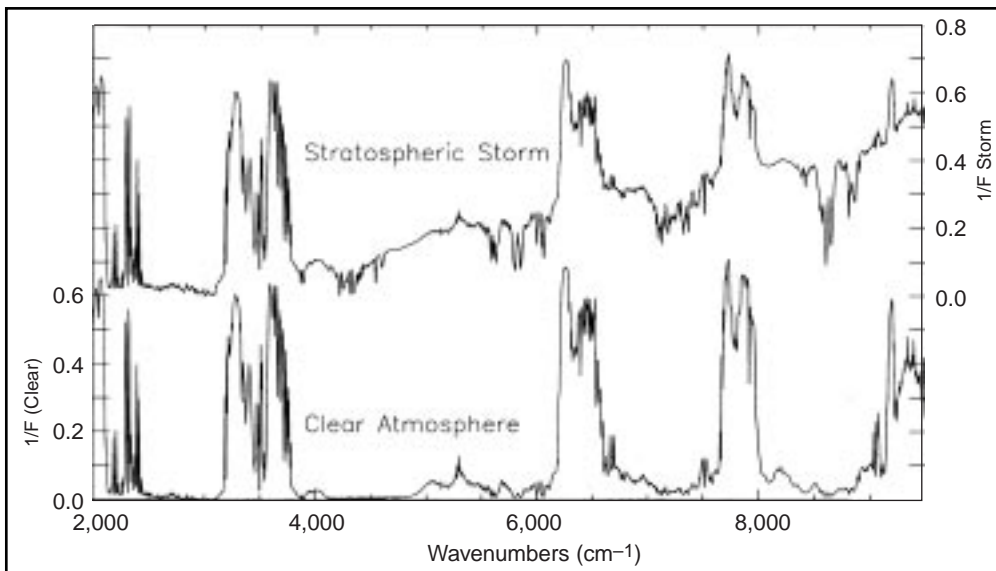


Figure 3. Simulated spectrum of Neptune with a hypothetical storm in the stratosphere.

SPECKLE IMAGING OF IO

Serendipitously, during our first speckle runs in 1996, Io was caught during a major volcanic outburst; speckle imaging observations of Io in later years have been even more successful. In the summer of 1998, we observed the satellite during three eclipses: July 12, July 28, and August 4. On July 12, we saw 17 hot spots at a resolution of 60 km/pixel (Fig. 4a), higher than can be obtained by the Galileo NIMS instrument, which is currently at Jupiter.

Many of our hot spots are clearly associated with albedo features on the surface of Io as seen by Voyager and Galileo (Fig. 4b). The volcanic

region Loki (number 2 in the image) was clearly visible during all three eclipses. On July 28, a very bright source to the left of Loki appeared, a transient event that faded quickly. The flux was 3.93 GW/ μm str on July 28, decreasing to 1.48 GW/ μm str on August 4. We registered the images with Io's disk based on the Galileo SSI position of the volcano Janus (labeled 0 in Fig. 4). Typical positional uncertainties are ≤ 0.5 pixels.

The images suggest that the position of Loki has changed as the July transient is fading away (2σ level).

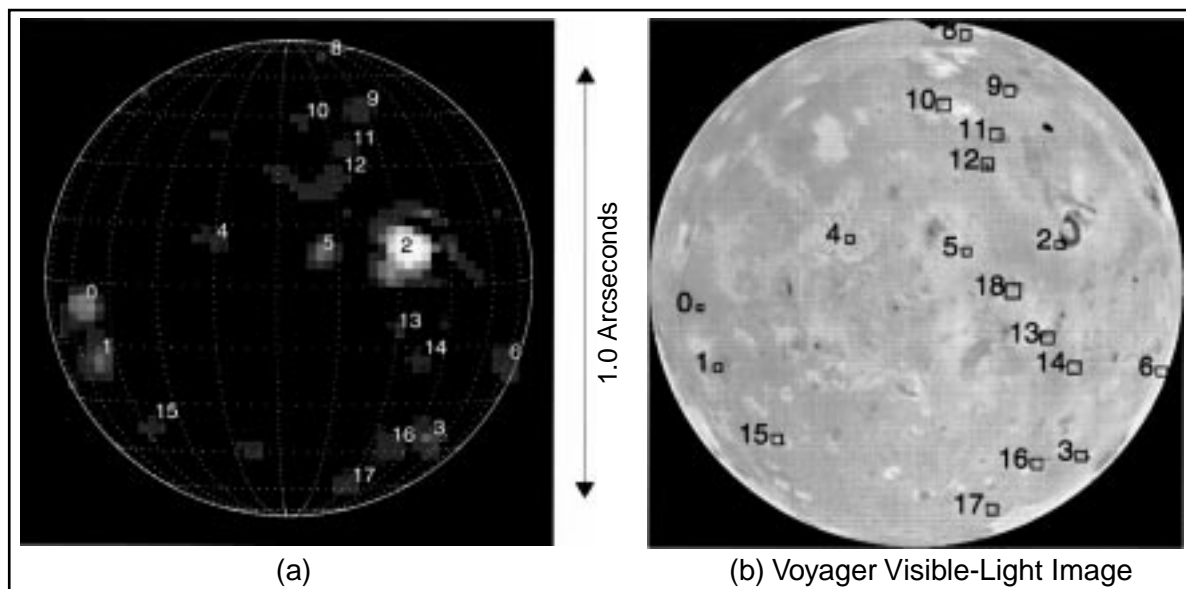


Figure 4: (a) Speckle image of Io in Jupiter's shadow, taken at 2.2 microns on July 12, 1998. Labeled features are volcanic hot spots. Spatial resolution is 0.04 arcseconds; the size of Io's disk is 1.1 arcseconds. (b) Voyager image of the same face of Io shown in (a); the location of our infrared hot spots is shown. Note correspondence of many hot spots with dark surface features (known volcanoes).

REFERENCES

1. Lunine, J. I., *Rev. Geophys. Space Phys.* **31**, 133 (1993).
2. de Pater, I., S. C. Gibbard, B. Macintosh, D. Gavel, C. E. Max, A. M. Ghez, E. F. Young, and C. P. McKay, "A Comparison of HST and Keck Data on Titan's Surface," WPAGU Conf. Proc., in press (1998).
3. Gibbard, S. G., B. Macintosh, D. Gavel., C. E. Max, I. de Pater, A. M. Ghez, E. F. Young, and C. P. McKay, "Titan: High Resolution Speckle Images from the Keck Telescope," *Icarus*, in press (1998).
4. Gibbard, S. G., I. de Pater, H. Roe, B. Macintosh, D. Gavel, C. E. Max, K. H. Baines, and A. Ghez, "High-Resolution Infrared Imaging of Neptune from the Keck Telescope," *Icarus*, submitted (1998).
5. Baines, K. H., and H. B. Hammel, "Clouds, Hazes and Stratospheric Methane Abundance Ratio in Neptune," *Icarus* **109**, 20–39 (1994).
6. Romani, P. N., J. Bishop, B. Bevard, and S. K. Atreya, "Methane Photochemistry on Neptune: Ethane and Acetylene Mixing Ratios and Haze Production," *Icarus* **106**, 442–463 (1993).

A Phonon-Mediated Particle Detector for Observational Cosmology and Gamma-Ray Astronomy (98-AP016)

Principal Investigator: Bernard Sadoulet (UC Berkeley)

LLNL Collaborators: Carl A. Mears, Simon Labov, and Matthias Frank

Student: Sunil Golwala (UC Berkeley)

The goal of our program of development of the hot-electron tunneling (HET) sensor is to produce a high mass, phonon-mediated particle detector useful for direct detection of WIMP dark matter and for gamma-ray astronomy. Over the past year, we have begun to measure the quasiparticle lifetime and diffusion length in aluminum films that we expect to use as phonon-to-quasiparticle transducers on the detector surface. Our measurements give a quasiparticle lifetime of about 3.5 μ s and a diffusion length of about 350 μ m.

OBJECTIVE

A number of cosmological and astrophysical measurements can be greatly improved by use of particle detectors with better energy resolution than those used now. The examples of interest to us are detection of WIMP dark matter and observation of gamma rays from high-energy astrophysical objects such as black holes and active galactic nuclei.

Germanium ionization detectors of the type used for many years have reached their limiting energy resolution. We aim to develop phonon-mediated detectors of comparable masses. Such detectors promise much better energy resolution with little dependence on detector size.

PROGRESS

Recall the basic architecture we have in mind for the final detector. The target material is a high-quality crystal. A particle interaction results in high-energy phonons that propagate ballistically through the crystal. A thin film of a superconductor is deposited on the crystal surfaces. Most of the athermal phonons have enough energy to break Cooper pairs in the superconducting film; this results in the creation of quasiparticles that may diffuse in the surface films.

At points along the edges of the superconducting films, HET sensors will be coupled to the superconducting film via their normal electrodes;

quasiparticle trapping results in the deposition of some fraction of the quasiparticles' energy in the HET sensor.

Quasiparticle trapping is a phenomenon in which a quasiparticle, when it reaches the boundary between a superconductor and a normal metal (or a superconductor of lower gap energy), falls into the normal metal and is trapped there due to the potential well it sees via the reduction of the gap energy.

Some part of the lost potential energy is thermalized among the electrons of the normal electrode of the HET sensor as the quasiparticle drops in; the heating of the electrons results in an increased tunneling current through the sensor (when voltage biased). Thus, a fraction of the energy deposited in athermal phonons is seen by the HET sensor; this fraction gives an estimate of the total energy deposited in the interaction.

Quasiparticles in a superconducting film suffer both from scattering processes, which slow their travel across a film, and from decay and recombination, which obviously results in a loss of energy back to the substrate. The length and time scales of these loss processes thus play a central role in the amount of energy received by the HET sensors, and thus on the signal size and energy resolution of the measurement as a whole. To gain an understanding of these loss processes in real films, we have embarked on a program to

study diffusion lengths and times in typical superconducting films. This work has been done in concert with Professor Blas Cabrera's group at Stanford University. We illuminate detectors of the following structure with low-energy X-rays (Fig. 1):

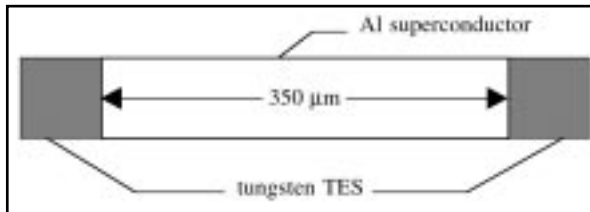


Figure 1. Device geometry.

Absorption of a single X-ray produces a large number of quasiparticles that then diffuse through the film. Sensors, which detect the quasiparticles, are placed at the ends of the film. In this simple system, one can make analytic calculations of the observed signal that depend only on the diffusion constant, lifetime, and trapping time of the quasiparticles. Thus, one can analyze the data to derive these important parameters.

In the experiments we have so far completed, the aluminum film has a thickness of 1500 Å and a length of 350 μm. The sensing elements are tungsten transition edge sensors (TES) that have been developed by Prof. Cabrera's group. The

TES's are important for this experiment because their energy response is easily calibrated due to their use of extreme negative electrothermal feedback, and hence the energy reaching the sensors is measured. The aluminum film is illuminated by 1.74 keV Si K_α X-rays. Figure 2 displays data measured from this device.

Figure 2a plots the energy received by sensor B against that received by sensor A. The hyperbolic locus of points are the 1.74 keV events (some fraction of the energy is lost to the substrate, so the events do not asymptote to 1.74 keV collected energy). The distribution traces the position of the events along the superconducting absorber: events that occur close to sensor A produce a large pulse in sensor A and a small pulse in sensor B, and vice versa for events near sensor B.

We can make two concrete conclusions from this data. First, we note that the distribution of events goes almost all the way to the two axes; that is, there are events for which one sensor sees almost all the energy and the other sees nearly none. This indicates that quasiparticle trapping is close to 100% efficient. From the hyperbolic shape, we make our second conclusion: the quasiparticle diffusion length (the distance that a quasiparticle diffuses in one decay lifetime):

$$l_{diff} = \sqrt{D\tau_{qp}}$$

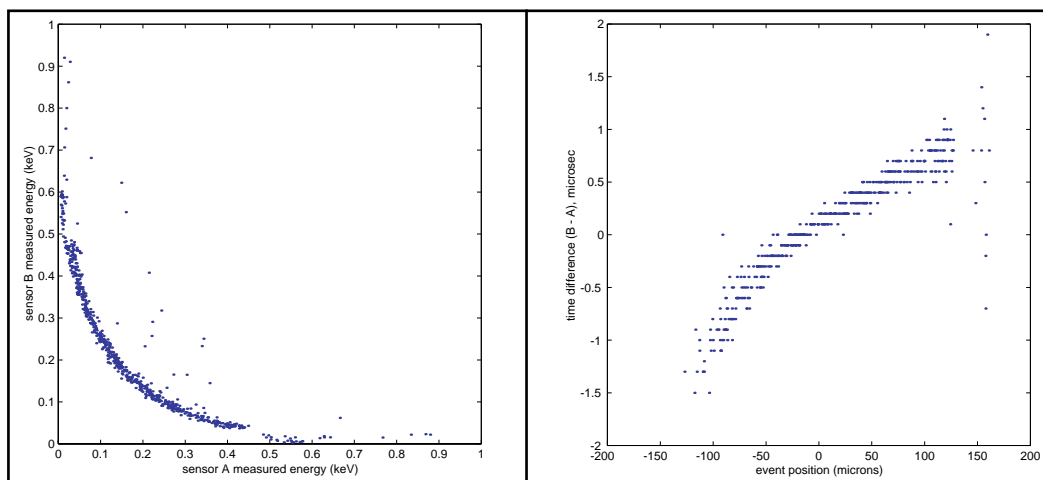


Figure 2a. Sensor-B collected energy vs. sensor-A collected energy for 1.74 keV X-ray absorption.

Figure 2b. Arrival time difference vs. event position for 1.74 keV X-ray absorption.

is of the same order of magnitude as the absorber length. If the diffusion length were much larger than $350\ \mu\text{m}$, there would be no dip for events with roughly equal energy in the two sensors (events near the center of the superconducting film) and we would see a straight line with slope -1 . If the diffusion length were much smaller than $350\ \mu\text{m}$, the hyperbola would approach the origin much more closely because very little energy would be collected for events in the center of the superconductor.

In fact, because of the simplicity of the system, a one-dimensional diffusion model fits the data quite well, and one can extract a diffusion length of about $140\ \mu\text{m}$. The model also allows one to determine, on an event-by-event basis, the position of the interaction to a resolution of roughly $30\ \mu\text{m}$ from the collected energies.

The diffusion length depends on both the diffusion constant D and the quasiparticle lifetime τ_{qp} , but the collected energy measurement does not allow one to separate the two. However, the active elements are fast enough to resolve the arrival of the diffusion wave of quasiparticles.

By comparing the arrival times at the two sensors, we can measure D independent of τ_{qp} . This is displayed in Figure 2b: We plot the time difference of the pulse onset in the two sensors vs. the event position (determined from the collected energies). A correlation is clear—by solving the diffusion equation, one finds that the timing is determined by the time constant of the slowest mode, which is $\tau_{rise} = \tau_{diff}/(\pi^2 D)$. The rise time of the observed pulses is roughly $1\ \mu\text{s}$, giving

$D = 0.01\ \text{m}^2/\text{s}$. From D and τ_{diff} , one can determine τ_{qp} ; this gives $3.5\ \mu\text{s}$ (a reasonable value).

However, the measured diffusion constant is a factor of 10 slower than expected from a calculation based on the observed residual resistance ratio and room temperature resistance.

Other groups (Yale, Munich, Harvard) also see such large discrepancies. One explanation we are considering is that the superconducting film's gap energy is somewhat non-uniform, with localized depressions. These "microtraps" trap and confine quasiparticles until phonons interact with and liberate them. The result is significantly slowed diffusion. Unfortunately, a cause of the microtraps is not forthcoming.

We have cycled the devices to remove trapped flux, to no effect. Impurities also do not seem to fit the bill: The measured diffusion constants appear anticorrelated with standard film quality measures. The diffusion constant becomes worse as the film quality improves!

There are obvious next steps. First, it would be good to confirm this data by measuring devices with different absorber lengths. Second, one should address the short diffusion length (though the standard culprits, such as flux trapping and impurities, do not appear likely).

Finally, independent of any improvements to the diffusion length, these measurements allow one to design the distribution of aluminum phonon absorber on the crystal surface to optimize pulse height, pulse speed, or some combination thereof and thereby build a full-size detector with some idea of the expected performance.

A Search for Red Quasars: The Radio-Loud Quasar Population at $z \geq 3$ (98-AP017)

Principal Investigator: Hyron Spinrad (UC Berkeley)

LLNL Collaborator: Wil van Breugel

Student: Daniel Stern (UC Berkeley)

With support from IGPP-LLNL, we have pursued a systematic search for high-redshift, radio-loud quasars. The quasars are selected using the 1.4 GHz VLA FIRST Survey (Faint Images of the Radio Sky at Twenty centimeters¹), in conjunction with the (second generation) digitized Palomar Observatory Sky Survey.² Considering optical counterparts to FIRST radio sources, we select unresolved optical identifications with colors consistent with distant quasars. High-redshift quasars provide some of the earliest glimpses we have of the Universe, constrain models of structure formation, and are valuable probes of the intervening intergalactic medium.

Our technique is successful. To date, we have discovered five quasars at redshift $z > 3.8$, including three at $z > 4$. These are the most distant sources identified from the FIRST Survey thus far. Only six radio-loud quasars at $z > 4$ are in the published literature thus far; our work represents a significant contribution. Our most distant source, VLA 1410+2409 at $z = 4.35$, is the third most distant radio-loud quasar currently known.

OBJECTIVES

The primary objective is to create a census of the high-redshift, radio-loud quasars. Previous studies³ focused on flat-spectrum sources with flux densities 1–3 orders of magnitude greater than the FIRST Survey limit and confirmed the decrease in the space density of radio-loud quasars at high redshift.⁴

Our sample probes a new regime of parameter space: low radio flux density, high-redshift quasars regardless of radio spectral index. This last point is by necessity since no large-area radio survey of comparable depth exists at a frequency different from FIRST.

This work will be valuable for constraining the faint end of the radio quasar luminosity function at high redshift, and will provide a useful sample of and to the distant Universe. Possible obscuration and absorption processes in quasars imply that radio is all ideal search wavelength for quasars, less prone to selection effects than optical (grism) surveys.

PROGRESS

Our technique is efficient at identifying high-redshift, radio-loud quasars. To date, we have discovered five quasars at $z > 3.8$, including three at $z > 4$ (Fig. 1). These are the most distant sources identified from the FIRST Survey thus far.

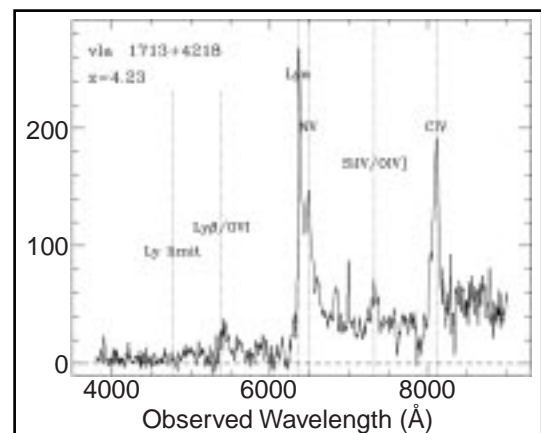


Figure 1. Spectrum one of our high-redshift quasars. The spectrum was obtained during twilight at the Keck II Telescope, confirming an ambiguous Lick spectrum of an unusual quasar.

Our work thus far has emphasized developing techniques and code to efficiently select spectroscopic candidates from the immense catalogs being considered. Stern has headed these efforts, which has necessitated close collaboration with the DPOSS working team (Steve Odewahn, Roy Gal, and S. G. Djorgovski). We now have software that is effective at selecting high-redshift candidates. Spectroscopy of the sample are being

obtained at the 3-m Shane Telescope at Lick Observatory. Preliminary results were presented at the Summer 1998 AAS meeting in San Diego,⁵ and a detailed paper is in preparation.⁶ This work, which we anticipate completing this year, should uncover several more high-redshift radio sources. The project will comprise the major portion of Stern's thesis at UC Berkeley.

REFERENCES

1. Becker, R. H., R. L. White, and D. J. Helfand, "The FIRST Survey: Faint Images of the Radio Sky at Twenty centimeters," *Astrophys. J.* **450**, 559 (1995).
2. Djorgovski, S. G., R. R. de Carvalho, R. R. Gal, M. A. Pahre, R. Scaramella, and G. Longo, "Cataloging of the Digitized POSS-11, and Some Initial Scientific Results from It," astro-ph/9612108 (1996).
3. Hook, I. M., and R. G. McMahon, "Discovery of Radio-Loud Quasars at $z = 4.72$ and $z = 4.010$," *Mon. Not. Royal Astron. Soc.* **294**, 7 (1998).
4. Shaver, P. A., I. M. Hook, C. A. Jackson, J. V. Wall, and K. I. Kellerman, "The Redshift Cutoff and the Quasar Epoch," astro-ph/9801211 (1998).
5. Stern, D., H. Spinrad, W. van Breugel, S. G. Djorgovski, S. Odewahn, R. Gal, and R. de Carvalho, "Correlating FIRST with DPOSS: A Search for Radio-Loud Quasars at $z \sim 4$," *Bull. Am. Astron. Soc.* **192**, #55.20, AAS Meeting, San Diego, California (1998).
6. Stern, D., H. Spinrad, W. van Breugel, S. G. Djorgovski, S. Odewahn, R. Gal, and R. de Carvalho, "Correlating FIRST with DPOSS: A Search for Radio-Loud Quasars at $z \sim 4$," in prep. (1998).

Numerical Studies of Fragmentation in Star-Forming Regions (98-AP024)

Principal Investigator: Christopher F. McKee (UC Berkeley)

LLNL Collaborator: Richard I. Klein

Student: Robert T. Fisher (UC Berkeley)

We are working on understanding the initial phases of star formation beginning with the collapse and fragmentation of low-mass molecular cloud cores. With support from IGPP-LLNL, we have developed and applied a new code ideally suited for simulation of self-gravitational hydrodynamics. This three-dimensional (3-D) code employs adaptive mesh refinement (AMR), a technique whereby the computational volume is evolved on a hierarchy of recursively finer grids. Multiple grids at multiple levels of resolution are dynamically inserted, positioned, and removed as dictated by the changing requirements of the simulated flow. With these recent technological advancements, we hope to address several outstanding problems of star formation.

OBJECTIVES

A key step in the star formation process is fragmentation, whereby molecular clouds or clumps within more massive clouds gravitationally collapse and break up into substantially less massive components that can in turn condense into stars.

Answers to basic questions concerning this process remain elusive. What is the qualitative nature of the fragmentation process: hierarchical, single-step, or some hybrid? What determines the fraction of an unstable cloud that will fragment into protostellar objects? What influences the distribution of fragment masses, and therefore the initial stellar mass function? What determines the pattern of stellar clustering into binaries and multiple systems?

Our work seeks to address these questions through direct numerical simulation.

PROGRESS

In the last year, we have conducted a series of calculations to determine the essentials of the fragmentation process in the non-isothermal regime. As a first approximation, we have utilized a two-component barotropic equation of state, which makes the transition from an isothermal equation in the optically thin regime, to a poly-

tropic equation of state in the optically thick regime in a smooth fashion. We have fixed the equation of state by comparison with detailed 1-D radiative hydrodynamics calculations of the formation of the first core.¹ For parameters typical of nearby star-forming molecular clouds, the transition is made at a density of about 10^{-13} gm/cm³.

We will describe the results we have obtained for one particular model—a gravitationally unstable, initially isothermal constant density cloud rigidly rotating near virial stability.²

The calculation begins with the overall collapse of the rotating cloud into an isothermal disk. Since specific angular momentum is conserved in the absence of viscous effects and gravitational torques, most parcels are prevented from reaching the center of the cloud by their centrifugal barrier, thereby leading to the formation of the disk. A strong isothermal shock above the plane of the disk is soon established, through which the infalling material is brought to the disk plane.

The cold isothermal disk is unstable to further fragmentation. As previous authors show,^{3,4} the fragmentation of cold isothermal sheets typically results in elongated filamentary structures, which are in turn unstable to further gravitational collapse. We find that the imposed density perturba-

tion results in the formation of a gravitationally unstable filamentary barlike structure. Shortly after the bar reaches the density at which the gas becomes optically thick, the collapse is arrested and the bar fragments into binary spherical cores, which correspond to the molecular first cores formed in 1-D calculations.^{1,5,6}

The material in the central bar has very low specific angular momentum. This is simply due to the fact that each parcel of gas entering the central region of the bar encounters an oppositely moving parcel; their collision shocks the gas to a near standstill.

The presence of shocks in barred potentials is a long understood and widely recognized phenomenon in galactic dynamics, and may play an important role in feeding the accretion of central sources in active galactic nuclei. Similarly, in our

case, the shocked gas tends to be accreted directly onto the cores due to its low centrifugal barrier.

The next step (the depletion of the central bar) is a key stage in forming a binary system. Since the length of the bar much exceeds its width, which is of order the Jeans length of the bar, the bar material is Jeans unstable, and so must either accrete onto the disks and cores or further fragment, thereby producing a multiple system.

Later, the binary cores, now surrounded by well-formed disks, form a morphologically distinct binary system. The disks exhibit a wealth of physical processes, including both an inner gap and spiral density waves excited by interactions with the surrounding material. The scale of the disks, of order 100 AU, is consistent with observations of gaseous disks surrounding single T-Tauri stars and debris disks surrounding systems such as Beta Pictoris.

REFERENCES

1. Masunaga *et al.*, *Astrophys. J.*, submitted (1998).
2. Klein, R., R. Fisher, C. McKee, and J. True-love, NAP98 Proceedings (1998).
3. Kiguchi, M., S. Narita, S. Miyama, and C. Hayashi, *Prog. Theor. Phys. Suppl.* **96**, 50 (1998).
4. Narita, S., S. Miyama, M. Kiguchi, and C. Hayashi, *Prog. Theor. Phys. Suppl.* **96**, 63 (1998).
5. Stahler, S., F. Shu, and R. Taam, *Astrophys. J.* **241**, 637.
6. Winkler, K., and M. Newman, *Astrophys. J.* **236**, 201 (1980).

Geologic Constraints on the Magnitude, Age, and Rate of Slip along the Cenozoic Karakorum Fault System in Western Tibet (98-GS002)

Principal Investigators: A. Yin and T. M. Harrison (UC Los Angeles)

LLNL Collaborator: F. J. Ryerson

Student: M. A. Murphy (UC Los Angeles)

In order to evaluate the role of extrusion tectonics during the Indo-Asian collision, an integrated field mapping and thermochronological analysis was conducted to constrain the timing and magnitude of displacement along the right-slip Karakorum Fault in western Tibet.

The results of this investigation suggest that extrusion tectonics via the Karakorum Fault system is rather limited, as indicated by both a relatively small magnitude of slip (tens of kilometers instead of hundreds of kilometers) and a slow average slip rate (several mm per year instead of several cm per year).

Fast slip rates of 2–3 cm/yr inferred from offset fans along the Karakorum Fault in the region immediately west of our study area imply either that motion on the Karakorum Fault has been dramatically accelerated in the Quaternary or that the fault has been activated periodically through the course of its evolution.

OBJECTIVE

The western Tibetan plateau is extruding eastward along the active right-slip Karakorum and left-slip Altyn Tagh Faults. Because the timing and magnitude of the two faults are uncertain, the importance of extrusion tectonics remains poorly constrained. We conducted 2-month field work in the summer of 1998 along Gar Valley near Mt. Kailas in western Tibet. The purpose of this study was to investigate the geologic evolution of the Karakorum Fault.

PROGRESS

The results of our field mapping suggest that this fault separates a Quaternary basin that is defined by Gar Valley to the north and a high-grade metamorphic gneiss complex (the Aiyi Shan gneiss) and Cretaceous plutons to the south (Fig. 1).

The active trace of the Karakorum Fault is marked by numerous fault scarps, which are associated with both right-lateral and normal offsets of alluvial fans, glacial deposits, and drainage networks, depending on the local strike of the fault system. The gneissic complex along the Karakorum Fault consists of both meta-igneous and meta-sedimentary rocks; all are overprinted by mylonitic fabrics. Detailed structural analysis indicates that the mylonitic gneisses were developed along two major releasing bends of the overall right-slip Karakorum Fault. They were uplifted to the surface by transtensional structures during the evolution of the Karakorum Fault system.

Magnitude of Slip

The magnitude of slip along the Karakorum Fault is constrained by two important geologic relationships. First, we were able to establish a piercing point across the active trace of the

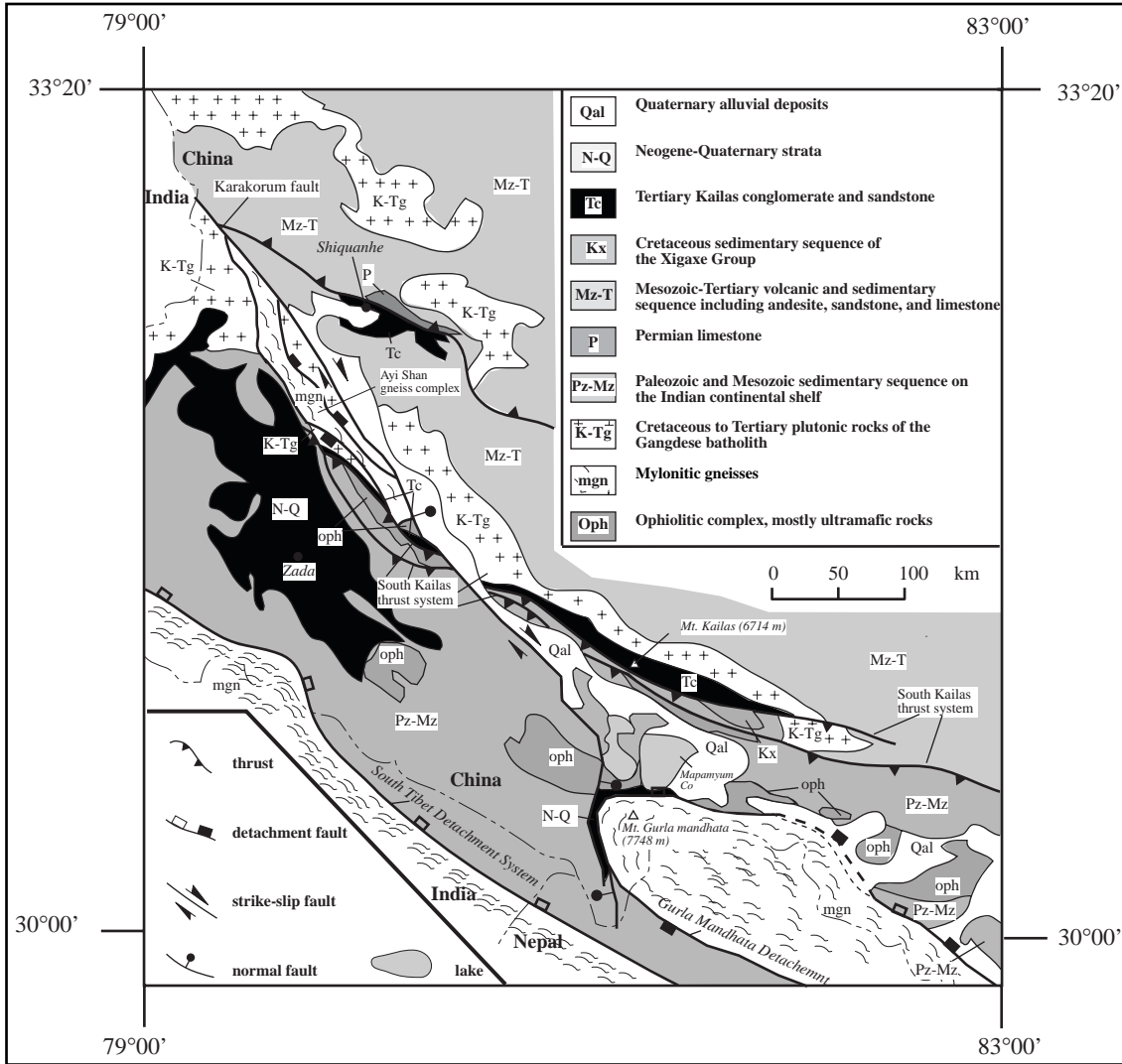


Figure 1. The Karakoram Fault separates a Quaternary basin to the north and a high-grade metamorphic gneiss complex and Cretaceous plutons to the south.

Karakoram Fault. This offset marker is defined by a distinctive thrust system (the Kailas thrust system) that juxtaposes an ophiolitic complex and a Mesozoic sequence over the Tertiary Kailas conglomerate (Fig. 1). The conglomerate unit is in a depositional contact on top of a Cretaceous granite, which is part of the Gangdese batholith belt in south Tibet. The unconformity and the thrust surface forms an intersection line, which we use as the piercing line. This line is constructed by using orthographic projection to be truncated and offset right laterally by the Karakoram Fault. The offset of the piercing line constrains the magnitude of right slip along the fault to be 50 ± 10 km.

The second constraint on the magnitude of slip along the Karakoram Fault comes from its relation to the N-S striking Gurla Mandhata-Purang extension system. Our mapping suggests that the NW-striking Karakoram Fault terminates at this ~80-km-wide system, which is defined by two structural elements: (1) the Gurla Mandhata detachment in the east that juxtaposes Tertiary sedimentary strata and a Paleozoic sequence in its hanging wall over meta-sedimentary sequences and mylonitic gneisses and schists in its footwall; and (2) the Purang rift in the west, which is bounded by both E- and W-dipping normal faults.

Analysis of kinematic indicators in the fault zones of the Karakorum Fault, the Purang rift, and the Gurla Mandhata detachment suggests that these fault systems have compatible transportation directions. The amount of extension across the N-S trending termination system is at least 28 ± 8 km based on restoring the mylonitic footwall rocks to the depth of the brittle-ductile transition at ~ 10 – 15 km along a low-angle normal fault dipping at 20° . This estimate provides a lower bound for the minimum amount of slip along the Karakorum Fault, which is broadly consistent with the estimated right slip of 50 ± 10 km by the piercing point argument.

Age and Slip Rate

Because the Karakorum Fault cuts the Kailas thrust system, its age postdates the thrust. The footwall of the thrust system cools rapidly at about 11 Ma, as dated by $^{40}\text{Ar}/^{39}\text{Ar}$ thermochronological analysis of K-feldspar from volcanic cobbles in the footwall. The cooling is interpreted as caused by emplacement of the thrust sheet along the Kailas thrust. Thus, the cooling age is syn-thrusting.

This age, together with the geologic relationship between the Kailas and Karakorum Fault systems, suggests that the initiation of the Karakorum Fault must be younger than 11 Ma. The age of the Karakorum Fault can also be constrained by dating the age of the kinematically lined Gurla Mandhata detachment fault.

We suggest, based on $^{40}\text{Ar}/^{39}\text{Ar}$ thermochronologic analysis of biotites and K-feldspars col-

lected from the mylonitic gneisses in the footwall, that the fault was active between 9 and 3 Ma. In particular, we detect a systematic younging of biotite ages from the interior of the footwall to the region directly below the detachment fault between 9 and 6 Ma, suggesting that the footwall rocks experienced progressive unroofing during this time interval.

The detachment fault remains active at 3.5 Ma, as indicated by $^{40}\text{Ar}/^{39}\text{Ar}$ analysis of K-feldspars. As normal faults in the Purang rift cut Quaternary deposits, extension in the termination system is active. Using 60 km as the maximum amount of slip along the Karakorum Fault and 10 Ma as its duration of motion, the average slip rate along the Karakorum Fault in western Tibet is about 6 mm/yr.

Summary

The results of this study suggest that extrusion tectonics via the Karakorum Fault system is rather limited in western Tibet, as indicated by both relatively small magnitude of slip (tens of kilometers instead of hundreds of kilometers) and slow average slip rate (several mm/yr instead of several cm/yr). Fast slip rates of 2–3 cm/yr inferred from offset fans along the Karakorum Fault in the regions directly west of our study area imply that motion on the Karakorum Fault has been either dramatically accelerated in the Quaternary or the fault has been activated periodically through its course of evolution.

Molten Crust Beneath Tibet? (98-GS003)

Principal Investigators: T. Mark Harrison and An Yin (UC Los Angeles)

LLNL Collaborator: F. J. Ryerson

Student: Paul Kapp (UC Los Angeles)

The two parallel belts of Miocene granite that extend across much of the Himalaya differ in age, petrogenesis, and emplacement style.¹ Although their origin has been actively debated over the past two decades, the recent discovery that anatexis and inverted metamorphism are not temporally related² has relegated most models to the geodynamic ashbin. However, two recently proposed models appear to have promise. One model² attributes melting to shear heating on the continuously active Main Central Thrust (MCT) decollement.

The MCT cuts through previously metamorphosed Indian supracrustal rocks that were transformed into basement during the initial stages of the Indo-Asian collision. Using the present fault geometry and convergence rate across the Himalaya, numerical simulations assuming a shear stress of ~30 MPa indicate that initiation of slip on the Himalayan thrust at 25 Ma could trigger discontinuous melting reactions leading to formation of the High Himalayan leucogranite (HHL) chain between 24–20 Ma and the North Himalayan granite (NHG) belt from 18–12 Ma, consistent with observation.

An alternate model³ views the middle Tibetan crust as being partially molten today, and the region between the MCT and South Tibetan Detachment System as an earlier extruded equivalent. The HHL and the NHG represent progressively younger time slices of the partially molten Tibetan crust and initiation of the MCT due to melting rather than being a consequence of it. A test of these two models is offered by the presence of an obliquely exposed crustal section in the Nyainqentanglha massif, southern Tibet.⁴

We have dated S- and I-type granitoids from this section using the U-Pb zircon and Th-Pb monazite ion microprobe methods. These results⁵ indicate that the cross-cutting intrusions were emplaced between 20–8 Ma; there is little evidence to support the notion that the Tibetan crust was partially molten during this period.

OBJECTIVES

Quite independent from which of the above hypotheses is preferred by the present data, there is an obvious need to obtain much improved age control on the two granite belts. For example, only two of the ~16 NHG have been securely dated. We targeted five previously undocumented plutons for ²⁰⁸Pb-²³²Th monazite dating: Gurlha Mandhata, Xungru, Peiku Tso, and Guizo. Measurements are currently underway.

Th-Pb monazite and U-Pb zircon dating of numerous samples of host rock, biotite granite,

and two-mica granite from the Nyainqentanglha crustal section will provide detailed insight into the thermal and physical state of the mid-Tibetan crust. Our goal in this research is to assess whether the resulting pattern of ages is consistent with steady-state partial melting of the mid-Tibetan crust or episodic anatexis. The answer to this question is central to understanding the timing of thrust development in southern Tibet and the Himalaya as well as to the mechanical coupling/decoupling of the crust and underlying mantle implicit in a pervasively partially molten lower crust.

PROGRESS

Granitoids and orthogneisses exhumed by the Nyainqentanglha shear zone (NSZ) in southern Tibet, about 100 km north of the Indus Tsangpo suture, provide an excellent opportunity to study the geologic and thermal evolution of the Lhasa block middle crust. The Nyainqentanglha massif bounds the central segment of the Yadong-Gulu rift, the most prominent of the north-trending Neogene graben that characterize the Tibetan plateau.

The eastern margin of the Nyainqentanglha range is bounded by a low-angle ($\sim 25^\circ$) detachment fault that involved mylonitic shearing under lower amphibolite grade conditions.⁶ The footwall of the NSZ consists of biotite-muscovite granite, granodiorite, orthogneiss, and various metasedimentary assemblages.

In general, the orthogneisses yield Late Cretaceous to Early Tertiary U-Pb crystallization ages, although one granite gneiss was found to be <13 Ma.⁷ Harrison *et al.*⁴ interpret thermochronological results from the footwall rocks of the NSZ as indicating that normal slip initiated at 8 ± 1 Ma and continued at ~ 4 mm/a until ~ 3 Ma.

Tracer isotope data of Nyainqentanglha granitoids^{5,8} are suggestive of mixing between Proterozoic crust, similar to the Greater Himalayan Crystallines, and the Gangdese batholith. Seismic evidence^{9,10} indicates that the Indian lithospheric mantle underthrusts the Lhasa block at a shallow angle to at least 32°N ; therefore, it is not surprising that isotopic signatures characteristic of the Indian craton and the Gangdese magmatic arc are both represented in the basement rocks of the Nyainqentanglha.

We have undertaken ion microprobe studies of both zircon and monazite from several granitoids in the footwall of the NSZ to better constrain crystallization ages of both metaluminous and peraluminous granitoids and orthogneisses.⁵

Samples were collected from the Goring La and Balum Chun, two hanging valleys deeply incised into the footwall of the central Nyainqentanglha range. Th-Pb ages of monazites and U-Pb

ages of zircons from undeformed, two-mica leucogranites indicate interpreted emplacement ages of 8, 9, and 12 Ma.

Zircon from variably deformed, deeper-level granitoids collected closer to the shear zone yield crystallization ages of ~ 20 Ma with significant zircon inheritance. The inheritance represents ages characteristic of both the Gangdese arc (~ 50 Ma and ~ 120 Ma) and Pan African basement (~ 500 Ma). The origin of the ~ 20 Ma granitoids remains unclear but they appear to have affinity with the Gangdese batholith, suggesting that fluid and/or temperature conditions remained sufficient for calc-alkaline magmatism ~ 30 m.y. after subduction of oceanic lithosphere ceased.

Monazites from the deeper-level granitoids yield a spectrum of Th-Pb ages from ~ 22 Ma to ~ 12 Ma, indicating that monazite was losing radiogenic Pb until ≤ 12 Ma. This is consistent with the higher ambient temperatures indicated by thermochronometry⁴ for the granitoids exposed adjacent to the NSZ. Quantifying the magnitude and spatial distribution of Pb loss should permit us further insights into the T-t evolution of the massif.

Observations during reconnaissance sampling suggest that widespread partial melting was not present in the middle crust immediately prior to initiation of detachment faulting around 8–9 Ma.^{4,6}

The two-mica granites of the Nyainqentanglha are the youngest in a series of leucogranites, the oldest of which are the HHL, an E-W belt of ca. 23 Ma plutons ~ 300 km south of Goring La. Hypotheses to explain the origin of crustally-derived magmas, and their progressive younging to the north, include (1) shear heating resulting from continuous slip on the Main Himalayan thrust (MHT) induces partial melting of lower crustal rocks,² and (2) existence of a partially molten middle Tibetan crust over at least the past 20 Ma.³

In the latter view, thrusting within the Himalaya is caused by melting rather than being a consequence of it, with the age variation of exhumed Himalayan granites representing progressively

younger ‘snapshots’ of the anatectic layer. Our results permit further testing of, and discrimination between, these hypotheses.

In model (1), the lag between magmatism appearing in the HHL and Nyainqentanglha is dictated by the slip rate along the MHT. The HHL are the earliest crustal melts associated with slip on the MCT. The two-mica leucogranites of the Nyainqentanglha appear to be emplaced at ca. 9 Ma. An age contrast of ~14 m.y. over a distance of ~300 km translates into a slip rate of ~20 mm/yr, consistent with the present convergence rate across the Himalaya.¹¹ At this rate, the

Indian craton would today have reached the Banggong suture, as proposed by Owens and Zandt.⁹ This model also appears to be consistent with isotope tracer results, which indicate the presence of an Early Proterozoic component in the crustal melts.

In contrast, model (2) predicts that the isotopic systematics of the granitoids should reflect the Lhasa Block composition. The lack of widespread migmatization within the Nyainqentanglha massif would appear inconsistent with widespread *in-situ* partial melting within this obliquely exposed, mid-crustal section.

REFERENCES

1. Harrison, T. M., O. M. Lovera, and M. Grove, “New Insights into the Origin of Two Contrasting Himalayan Granite Belts,” *Geology* **25**, 899 (1997).
2. Harrison, T. M., M. Grove, O. M. Lovera, and E. J. Catlos, “A Model for the Origin of Himalayan Anatexis and Inverted Metamorphism,” *J. Geophys. Res.* **103(B11)**, 27,017 (1998).
3. Nelson, K. D., and 27 others, “Partially Molten Middle Crust beneath Southern Tibet: Synthesis of Project INDEPTH Results,” *Science* **274**, 1684 (1996).
4. Harrison, T. M., P. Copeland, W. S. F. Kidd, and O. M. Lovera, “Activation of the Nyainqentanglha Shear Zone: Implications for Uplift of the Southern Tibetan Plateau,” *Tectonics* **14(3)**, 658 (1995).
5. D’Andrea, J., T. M. Harrison, and M. Grove, “The Thermal and Physical State of the South Tibetan Middle Crust between 20–8 Ma: U-Th-Pb and Nd Isotopic Evidence from the Nyainqentanglha Massif,” 14th Himalaya-Karakorum-Tibet International Workshop Abstract volume, Kloster Ettal, Germany, in prep. (1998).
6. Pan, Y., and W. S. F. Kidd, “Nyainqentanglha Shear Zone: A Late Miocene Extensional Detachment in the Southern Tibetan Plateau,” *Geology* **20**, 775 (1992).
7. Xu, R.-H., U. Scharer, and C. J. Allegre, “Magmatism and Metamorphism in the Lhasa Block (Tibet): A Geochronological Study,” *J. Geol.* **93**, 41 (1985).
8. Harris, N. B. W., T. B. J. Holland, and A. G. Tindle, “Metamorphic Rocks of the 1985 Tibet Geotraverse, Lhasa to Golmud,” *Phil. Trans. R. Soc. London* **A327**, 203 (1988).
9. Owens, T. J., and G. Zandt, “Implications of Crustal Property Variations for Models of Tibetan Plateau Evolution,” *Nature* **387**, 37 (1997).
10. Hauck, M. L., K. D. Nelson, L. D. Brown, W. Zhao, and A. R. Ross, “Crustal Structure of the Himalayan Orogen at ~90° East Longitude from Project INDEPTH Deep Reflection Profiles,” *Tectonics* **17(4)**, 481 (1998).
11. Bilham, K., S. Larson, J. Freymueller, and Project Idylhim members, “GPS Measurements of Present-Day Convergence across the Nepal Himalaya,” *Nature* **386**, 61 (1997).

Application of the UC-LLNL Regional Climate System Model to the Malibu Creek Watershed (98-GS005)

Principal Investigator: John A. Dracup (UC Los Angeles)

LLNL Collaborator: Norman L. Miller (currently at Lawrence Berkeley National Laboratory)

Postdoc: Thomas C. Piechota (UC Los Angeles)

This collaborative research project has applied the Regional Climate System Model (RCSM), originally developed by the LLNL collaborator, to the Malibu Creek watershed in Southern California. During FY 1997–1998, the hydrologic model was calibrated and verified on the wet season flows (November through May) from 1988, 1992, 1994, 1995, 1997, and 1998. Calibration and verification was performed using two procedures: (1) split-sample, and (2) Generalized Likelihood Uncertainty Estimation (GLUE).

The results of the simulation of 1997 and 1998 wet seasons flows are encouraging. For many of the rainfall events, the observed streamflow falls between the 10% and 90% confidence limits of the model predictions. The RCSM is now properly calibrated for the Malibu Creek watershed, and the PI's are currently running real-time simulations that use atmospheric model output from the RCSM to predict the runoff for the winter and spring of 1998–99. These results will be compared with other simulations that are being made with the RCSM in other California watersheds.

OBJECTIVES

The scientific objective of this research was to apply the Regional Climate System Model (RCSM), developed by the LLNL PI, to a watershed in the Southern California area where the UCLA PI has been performing hydrologic modeling. The RCSM has been applied in several countries (Korea, China, Australia, United States) to better understand water resources of developing regions and to gain insight to processes that occur at regional and local scales.¹

The scientific product is a physically-based hydrologic model that is coupled with atmospheric, land, and coastal ocean components. Such a coupled system provides a means for investigating the long-term changes in the watershed environment due to changes in the regional setting. The scientific motivation for this research is a better understanding of the flow regimes in the South Coast region of California due to land use changes and climate variations.

PROGRESS

The progress made during the period October 1997 to September 1998 focused on the application of the RCSM to the Malibu Creek watershed, one of the largest watersheds in the Los Angeles area. The Malibu Lagoon, at its terminus, provides unique and valuable coastal resources. The RCSM has been under development since 1991 and is a modeling system that includes interactions among atmospheric, land surface, and subsurface processes.^{2,3} The developers of the RCSM are currently at Lawrence Berkeley National Laboratory.

The hydrologic model used in this project (TOPMODEL⁴) was integrated into the RCSM and was calibrated and verified for the Malibu Creek watershed. TOPMODEL is a physically based semi-distributed model that uses topography, soils types, and contributing drainage areas to calculate the runoff from subwatersheds.

TOPMODEL was calibrated and verified using two procedures and using only the wet season flows (November through May). The first

analysis used a standard split-sample procedure where the wet season flows in 1988, 1992, 1994, and 1995 were used for calibration, and the wet season flows in 1997 and 1998 were used for verification.

Figure 1(a) presents the model simulations for rainfall events in February and March 1998. The model simulations compare well with the observed streamflow during rainfall events; however, prior to and after the events, the model does not perform as well. This is due to the poor representation of baseflow in the model structure. A better representation of the baseflow process is an area of continued research.

The other calibration analysis uses the concept of Generalized Likelihood Uncertainty Estimation (GLUE) whereby the calibration of the

model generates a set of uncertainty bounds (i.e., confidence limits) on the range of expected model responses. Figure 1(b) demonstrates the use of GLUE on the 1997 and 1998 wet season flows. It is encouraging that for many of the rainfall events in Figure 1(b), the observed streamflow falls between the 10% and 90% confidence limits.

The RCSM is now properly calibrated for the Malibu Creek watershed, and the PI's are currently running real-time simulations using the atmospheric model output from the RCSM as input to the hydrologic model. These simulations are being made for the winter and spring of 1999. These results will be compared with other simulations in other California watersheds that are being made using the atmospheric model output from the RCSM as input to the hydrologic model.

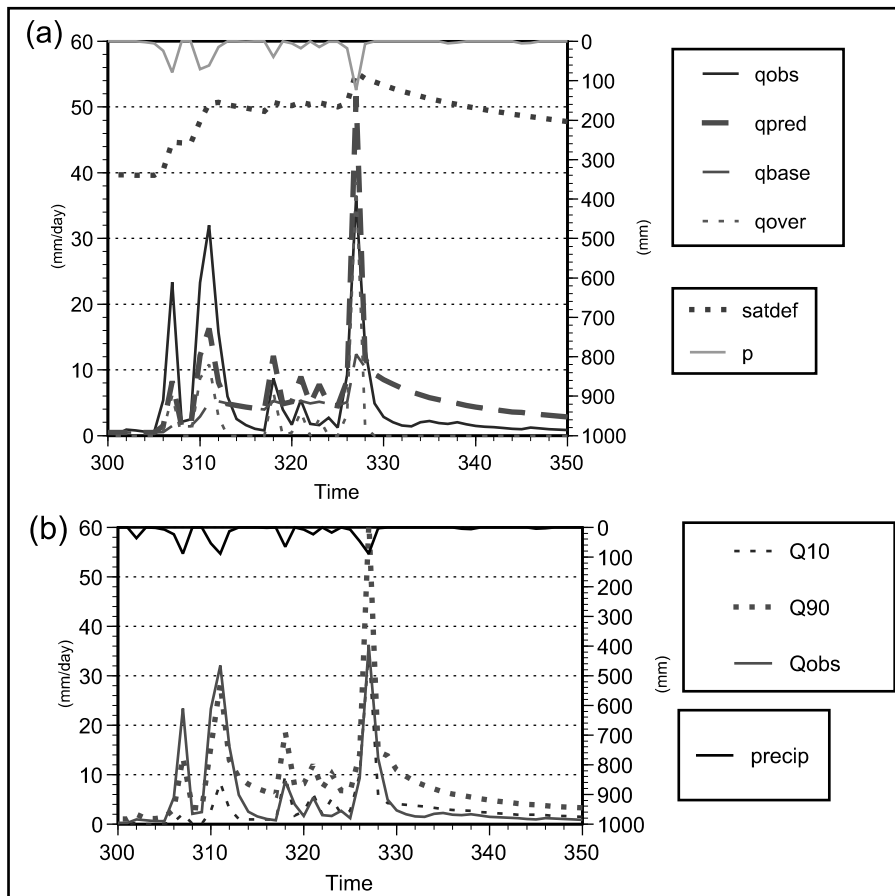


Figure 1. Observed versus simulated flows for 1997 and 1998 wet season (November–May) flows. The events shown here are for February ($x = 296$ to 327) and March ($x = 328$ to 358) 1998. The different flow processes are shown in (a); and the 10% and 90% confidence limits, as determined from the GLUE procedure, are plotted with the observed flows in (b).

REFERENCES

1. Kim, J., N. L. Miller, A. Guetter, and K. Georgakokas, "River Flow Response to Precipitation and Snow Budget in California during 1994–1995 Winter," *J. Clim.* **11(9)**, 2376 (1998).
2. Miller, N. L., and J. Kim, "Numerical Prediction of Precipitation and River Flow over the Russian River Watershed during the January 1995 California Storms," *Bull. Am. Meteor. Soc.* **77(1)**, 101 (1996).
3. Miller, N. L., and J. Kim, "The UC-LLNL Regional Climate System Model: Southwestern United States and Eastern Asia Studies," in *Research Activities in Atmospheric and Oceanic Modeling*, WMO/CAS/JSC Report (1997).
4. Beven, K. J., and M. J. Kirkby, "A Physically Based Variable Contributing Area Model of Basin Hydrology," *Hydrological Sci. Bull.* **24(1)**, 43 (1979).

Noble Gases Dissolved in Groundwater from the Northern United States: Tracers for Paleoclimate and Groundwater Flow (98-GS006)

Principal Investigator: Jordan F. Clark (UC Santa Barbara)

LLNL Collaborators: G. Bryant Hudson and Mark Caffee

Student: Laura K. Rademacher (UC Santa Barbara)

The mean annual air temperature at the time of recharge can be inferred from noble gases dissolved in groundwater. By collecting and dating samples from a number of wells within an aquifer system, temperature records can be determined. This technique provides quantitative information and has become a powerful paleoclimate tool.

Dissolved noble gases are also a powerful hydrologic tool for evaluating the interaction between local and regional groundwater flow systems, which have groundwater residence times of 10^{2-3} /yr and 10^{3-4} /yr, respectively. This geochemical technique works because noble gas recharge temperatures can be used to separate groundwater that recharged during the warm climate of the Holocene (age <10,000 yr) and the cold climate of the last glacial period (age >15,000 yr).

PROGRESS

We collected 25 groundwater samples along flow paths in the Cambrian-Ordovician aquifer, Iowa, for analysis of noble gases, radiocarbon, stable isotopes of water, and major ion chemistry. A comparison of the sample's major ion chemistry with existing analyses suggests that the flow system has not been significantly altered by pumping during the last two decades. We will be able to construct a 30,000-yr paleotemperature record for

Iowa, indicated by ^{14}C content and $\delta^{18}\text{O}$ values ranging between 100 pmc to 0.4 pmc and -7.5‰ to -12.2‰ , respectively. Unfortunately, we have been unable to analyze the samples for noble gas concentrations (the primary objective of this work) because of an analytical problem. We hope that this problem will be solved shortly and that we will be able to complete these measurements during the next year.

Schumann Resonance Measurements and Climate Models (98-GS007)

Principal Investigator: Steven Constable (UC San Diego)

LLNL Collaborator: Benjamin Santer

Other Collaborator: Martin Fullekrug (University of Frankfurt, Germany)

Tropical lightning increases nonlinearly with temperature, so the observation of global lightning activity can be used as an independent estimation of global temperature. Lightning discharges also produce nitrogen oxide compounds, which are an important component of atmospheric chemistry. A detailed estimation of global lightning activity in time and space can be achieved by the analysis of electromagnetic (EM) radiation in the lower ELF range, and the Earth-ionosphere cavity resonances (Schumann resonances) in particular.

Systematic lightning mapping using ELF data had never been carried out, mainly because of the limitations of data logging equipment and computational facilities. These limitations have disappeared with the recent development of fast, high-quality digital acquisition equipment, accurate timing available from the Global Positioning System, and the ability to collect, store, and process very large time-series datasets.

During April 1998, we installed portable EM observatories in Germany and Australia, and used data from an existing observatory in California, to triangulate 52,510 individual lightning flashes. The positive polarity of most of these events shows that they are likely to be associated with emissions in the mesosphere above thunderstorms, called sprites.

From the data, we can track the spatial and temporal evolution of individual storm systems and deduce their integrated planetary source current, which is of positive polarity, rather than the negative polarity previously assumed for ELF measurements of lightning.

OBJECTIVES

Because the amount of tropical lightning activity is observed to vary nonlinearly with wet-bulb temperature, Williams¹ suggested that observations of electromagnetic radiation at the Schumann resonances could be used to study temporal variations in atmospheric temperature, and he presented observations over a 6-year period to support this claim. This idea has recently been reinforced by a study of the annual variability of temperature and lightning.²

Current knowledge on global lightning activity relies mainly on observations of audible

thunder at land-based meteorological observatories. A more detailed temporal and spatial resolution of global lightning activity can be achieved from space with lightning sensors on orbiting satellites, but these have a footprint of only ~1300 km² and also spend much of their time over oceans or other areas devoid of thunderstorm activity.

Another approach to observing lightning flashes in thunderstorms is to record their electromagnetic radiation. In the frequency range from 6–60 Hz, the wavelength of electromagnetic radiation in the atmosphere is on the order of the circumference of the Earth, and constructive interference yields the Earth-ionosphere cavity

resonances.³ Fullekrug and Reising⁴ showed how individual lightning events could be located using EM measurements. The purpose of this project was to demonstrate the capability of global triangulation using a sparse network of observatories, based initially on portable, high-capacity data loggers.

PROGRESS

During April 1998, we installed a portable data logger near Lameroo, Australia, equipped with two horizontal magnetic field sensors. The logger was of a type originally designed for sea-floor use and was capable of recording two-channel, 50-Hz data for a month or more unattended. A temporary, manned, observatory sampling at 4 kHz was installed near Silberborn, Germany. Data from the two temporary installations was supplemented by 40-Hz EM data collected at a seismic observatory near Hollister, California, operated by UC Berkeley.

From these data, a total of 52,510 individual lightning flashes were located in space and time, using the orientation of the Poynting vector for triangulation. Verification and calibration was achieved by using local data from VLF arrays operated by the British Meteorological Office. Figure 1 shows one such event recorded at the three stations. Figure 2 shows a snapshot of lightning for April 28, 1998.

A Quicktime movie of the entire dataset at 1-hour resolution can be viewed at <http://mahi.edu/Steve/Schumann/light.html>.

An animated GIF of a 1-week segment at 15-minute resolution can be viewed at <http://www.geophysik.uni-frankfurt.de/~fuellekr/glas.html>.

These movies allow the spatial migration and temporal evolution of individual storm systems to be studied in detail.

About 64% of our observed flashes are of positive polarity, and the integrated global electric current can be calculated by summing the product of polarity and magnitude for all the events.

It is known that the atmospheric fair-weather electric field over the oceans exhibits a diurnal variation in universal time (the Carnegie curve; Fig. 3) and is also of positive polarity. The Carnegie curve and our data are highly anti-correlated,

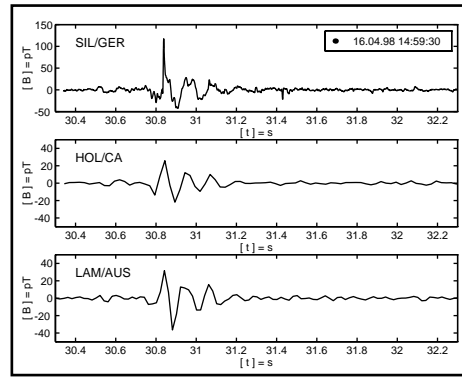


Figure 1. A lightning event simultaneously recorded in Germany (SIL/GER), California (HOL/CA), and Australia (LAM/AUS).

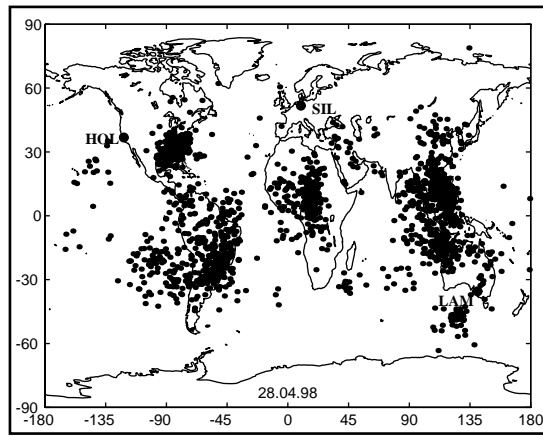


Figure 2. Lightning flash locations recorded on April 28, 1998, triangulated from our three observing stations (SIL, HOL, and LAM).

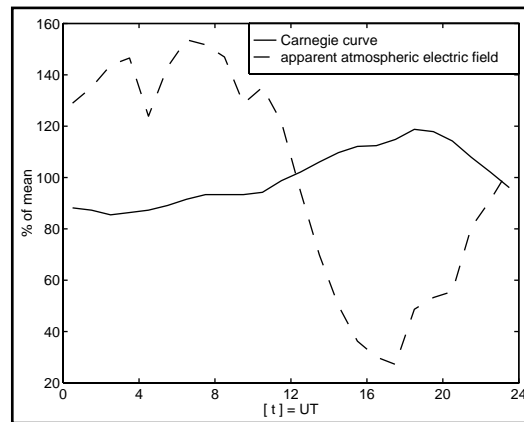


Figure 3. Relative mean diurnal variation of the atmospheric electric field over the oceans and polar regions (the Carnegie curve) compared with the atmospheric electric field deduced from our electromagnetic recordings.

showing that they are both associated with global lightning activity but that the atmospheric electric field is maintained by negative lightning, while our magnetic field measurements are associated with positive flashes.

A wealth of information has been gained from this highly successful demonstration project, which lasted only one month.⁵ Using the results of

this experiment, the PI's are trying to attract support for the installation of four to six permanent world-wide observatories of this type, which will allow us to extend our results to seasonal and long-term variations in lightning activity (a proxy for temperature and NO_x production). A real-time capability of this kind would even allow the re-routing of air traffic around storm systems.

REFERENCES

1. Williams, E. R., "The Schumann Resonance: A Global Tropical Thermometer," *Science* **256**, 1184 (1992).
2. Fullekrug, M., and A. C. Fraser-Smith, "Global Lightning and Climate Variability Inferred from ELF Magnetic Field Measurements," *Geophys. Res. Lett.* **24**, 2411 (1997).
3. Schumann, W. O., "Über die strahlungslosen Eigenschwingungen einer leitenden Kugel, die von einer Luftschicht und einer Ionosphärenhülle umgeben ist," *Zeitschrift für Naturforschung* **B**, 149 (1952).
4. Fullekrug, M., and S. C. Reising, "Excitation of Earth-Ionosphere Cavity Resonances by Sprite-Associated Lightning Flashes," *Geophys. Res. Lett.* **25**, 4145 (1998).
5. Fullekrug, M., and S. Constable, "Sprites Shed New Light on the Global Circuit," *Nature*, in prep. (1998).

Integrating Postseismic Relaxation into Crustal Stress Evolution Models (98-GS008)

Principal Investigator: Louise Kellogg (UC Davis)

LLNL Collaborator: William Foxall

Postdoc: Fred Pollitz (UC Davis)

Earthquake generation in California is governed to a large extent by a crustal deformation cycle consisting of interseismic strain accumulation around major fault zones, coseismic stress release, and postseismic relaxation of the ductile lower lithosphere following earthquakes. Postseismic relaxation is an important component in this cycle, but has been traditionally difficult to incorporate into crustal stress evolution models. We have estimated its possible impact by performing research on several fronts:

1. *Estimating the first-order viscoelastic stratification beneath northern California using geodetic data collected after the 1989 Loma Prieta earthquake.*
2. *Accounting explicitly for postseismic relaxation effects following the 1906 San Francisco earthquake using this viscoelastic model.*
3. *Estimating the viscoelastic stratification beneath the central Mojave Desert using geodetic data collected after the 1992 Landers earthquake.*

We find that there are differences in viscoelastic structure between San Francisco Bay and Mojave Desert regions, leading to quite different transient response of these regions following earthquakes. The effect of post-1906 relaxation has been mainly to accelerate emergence of the San Andreas Fault, and to slightly retard emergence of the Hayward-Calaveras branches, from the stress shadow created by the 1906 earthquake.

OBJECTIVES

Secular strain accumulation is documented ubiquitously in California, though precise mechanisms producing it (i.e., slip-at-depth versus side-loading of a finite-width shear zone) are the subject of current debate. Stress release associated with major earthquakes creates stress shadows, which tend to suppress regional seismicity for decades following these events.¹⁻³

Very long-term postseismic transients following such earthquakes are best attributed to viscoelastic relaxation of the lower crust and upper mantle. Prediction of regional stress evolution requires integration of the above processes into a self-consistent modeling framework. This need is highlighted by the fact that the physical mechanism most commonly invoked for interseismic

strain accumulation, slip-at-depth beneath the seismogenic layer, is incompatible with the mechanism most commonly invoked for the postseismic evolution, i.e., Maxwell viscoelastic behavior beneath the seismogenic layer.

A further challenge is to be able to utilize good estimates of the mechanical properties of the lower crust and upper mantle. Our study naturally came to focus on formulating a self-consistent framework for including interseismic and postseismic processes as well as obtaining estimates of regional viscoelastic stratification.

PROGRESS

Our simple physical model consists of a spherically stratified elastic-viscoelastic system, which is constantly loaded beneath the upper seis-

mogenic layer, undergoes an earthquake, and subsequently relaxes. The stratification for the San Francisco Bay area consists of a purely elastic upper crust, a viscoelastic lower crust behaving as a standard linear solid,⁴ a strong viscoelastic mantle lid, and a weaker viscoelastic upper mantle beneath 50-km depth. Interpretation of geodetic data in the 5 years following the 1989 Loma Prieta earthquake⁵ provides us with a viscoelastic model characterized by a lower crust with viscosity of about 1.4×10^{19} Pa s.

By virtue of the lower crustal rheology chosen, this mechanical model is capable of both transmitting relative plate motion to the seismogenic layer during interseismic periods and relaxing after earthquakes. In order to do the most complete job possible with the interseismic component, we have modeled it in terms of the components shown in Figure 1. These involve slip-at-depth (resolved both parallel and normal to the respective fault traces) along either vertical (A–C) or shallowly dipping planes (D) with prescribed rates.

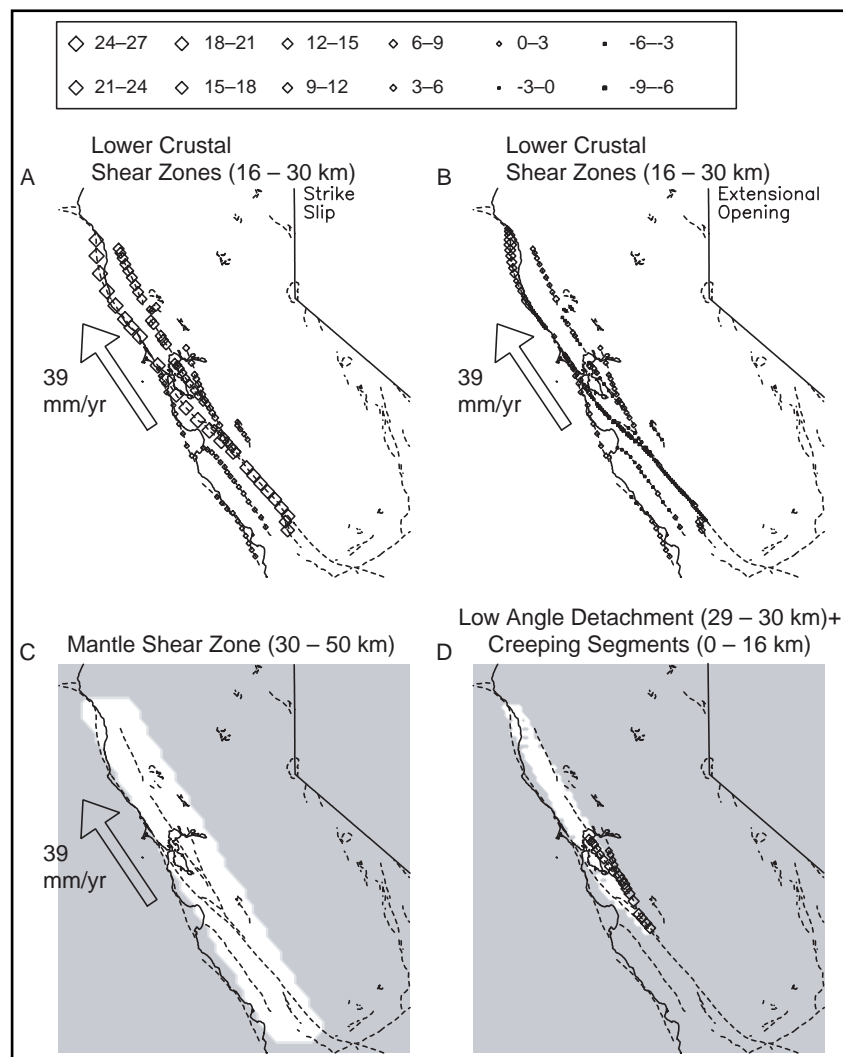


Figure 1. Geometry of interseismic loading as defined by vertical shear zones in lower crust with prescribed (A) right-lateral slip and (B) normal slip distributions; (C) a 70-km-wide vertical shear zone in the upper mantle with prescribed right-lateral slip velocity distribution; and (D) low-angle detachment fault at the base of the crust. Symbols give rates in mm/yr.

This geometry is fairly complicated but is still only a rough approximation to the real architecture of faulting with depth. It includes prescribed creeping rates in the upper crust along the Hayward, Calaveras, and San Andreas Faults north of Parkfield.

Figure 2 shows the change in Coulomb failure stress⁶ on potentially failing N35°W-trending right-lateral strike-slip faults at 8-km depth at several times after the 1906 earthquake.

We assume an effective coefficient of friction of 0.4 and include the effects of 1906 coseismic offsets, interseismic strain accumulation (Fig. 1), and postseismic relaxation following the 1906 earthquake. Correlation of high Coulomb failure stress with regional seismicity is very good, the only notable exception being the sequence of events near Coalinga, which are generally not right-lateral strike-slip events.

The 1906 earthquake resulted in a stress shadow roughly symmetric with respect to the San Andreas Fault. The geometry of loading within the mantle shear zones, however, is asymmetric (Fig. 1C), leading to preferential erosion of

the stress shadow on the east side of the San Andreas Fault. This pattern, combined with the added contribution of post-1906 relaxation, may have eroded the stress shadow in the San Francisco Bay area enough to help trigger the many $M > 5$ earthquakes that occurred there from 1979 to 1989.

Postseismic relaxation in our model leads to an increase in Coulomb failure stress along the northern San Andreas Fault of about 10 bars from 1906 to 1970, as well as a decrease of 0.3–1.0 bars along the Hayward-Calaveras fault system during the same time period.

Another factor contributing to that 10-year elevation in seismicity may have been a 5% transient increase in Pacific-North America relative plate motion. This external perturbation resulted from propagation of a stress pulse through Pacific oceanic lithosphere following several large earthquakes in the N/NW Pacific in 1952–1965.⁷ We intend to use the loading geometry of Figure 1 to test this idea, i.e., to test how the fault system would respond to a transient change in the velocity boundary conditions.

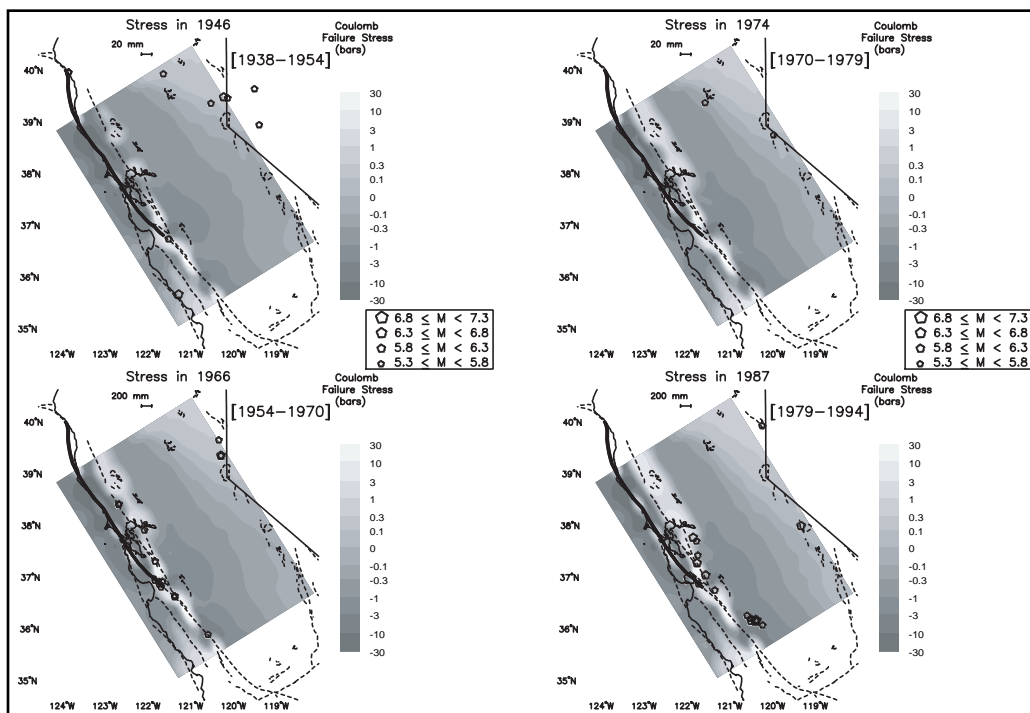


Figure 2. Cumulative change in Coulomb failure stress at 8-km depth at various times. Epicenters of $M \geq 5$ earthquakes at indicated times are superimposed.

We have analyzed postseismic relaxation around the $M_w = 7.3$ Landers earthquake as defined by InSAR and GPS data collected over the period late 1992 to late 1995.⁸ The strong signal and complementary information provided by this joint dataset has effectively allowed us to pene-

trate the crust and robustly estimate the mechanical properties of the uppermost mantle. We infer an uppermost mantle viscosity of 3.5×10^{18} Pa s beneath the central Mojave Desert, making it much weaker than its counterpart in the San Francisco Bay area.

REFERENCES

1. Jaume, S. C., and L. R. Sykes, "Evolution of Moderate Seismicity in the San Francisco Bay Region, 1850 to 1993: Seismicity Changes Related to the Occurrence of Large and Great Earthquakes," *J. Geophys. Res.* **101**, 765 (1996).
2. Harris, R. A., and R. W. Simpson, "In the Shadow of 1857—The Effect of the Great Ft. Tejon Earthquake on Subsequent Earthquakes in Southern California," *Geophys. Res. Lett.* **23**, 229 (1996).
3. Deng, J., and L. R. Sykes, "Stress Evolution in Southern California and Triggering of Moderate-, Small-, and Micro-Size Earthquakes," *J. Geophys. Res.* **102**, 24411 (1997).
4. Cohen, S. C., "A Multi-Layer Model of Time-Dependent Deformation Following an Earthquake on a Strike-Slip Fault," *J. Geophys. Res.* **87**, 5409 (1982).
5. Pollitz, F. F., R. Burgmann, and P. Segall, "Joint Estimation of Afterslip Rate and Postseismic Relaxation Following the 1989 Loma Prieta Earthquake," *J. Geophys. Res.* **103**, 26975 (1998).
6. Reasenber, P. A., and R. W. Simpson, "Response of Regional Seismicity to the Static Stress Change Produced by the Loma Prieta Earthquake," *Science* **255**, 1687 (1992).
7. Pollitz, F. F., R. Burgmann, and B. Romanowicz, "Viscosity of Oceanic Asthenosphere Inferred from Remote Triggering of Earthquakes," *Science* **280**, 1245 (1998).
8. Pollitz, F. F., G. Peltzer, and R. Burgmann, "Mobility of Continental Mantle: Evidence from Postseismic Geodetic Observations Following the 1992 Landers Earthquake," *Science*, in prep. (1998).

Dynamic Earthquake Rupture Simulation on Dipping Faults (98-GS012)

Principle Investigator: Ralph J. Archuleta (UC Santa Barbara)

LLNL Collaborators: William Foxall and Larry J. Hutchings

Other Collaborators: Stefan B. Nielsen (UC Santa Barbara) and Edward Zywickz (LLNL)

Student: David D. Oglesby (UC Santa Barbara)

We have used the two-dimensional finite element method to simulate the dynamics of dip-slip faulting on non-vertical faults. These simulations show asymmetric near-source ground motion due to the asymmetric geometry of such faults. The ground motion from a thrust/reverse fault is larger than that of a normal fault by a factor of two or more, given identical initial stress magnitudes. The motion of the hanging wall is larger than that of the footwall in both thrust/reverse and normal earthquakes. The asymmetry between normal and thrust/reverse faults results from time-dependent normal stress caused by the reflected waves from the Earth's free surface. The asymmetry between hanging wall and footwall results from the asymmetric mass and geometry on the two sides of the fault.

OBJECTIVES

Our main goal in this project was to investigate the dynamics of dip-slip faulting, and specifically to characterize the effect of asymmetric geometry on the rupture propagation, fault slip, and resultant ground motion.

For compressive tectonic regimes such as the Los Angeles area, Japan, and Central and South America, and in extensional regimes such as the Mediterranean and the Great Basin of Nevada, Utah, and Idaho, most seismic hazard lies in such non-vertical (dipping) faults.

A general goal was to show that an important difference between a vertical and a non-vertical fault is the breakdown of symmetry with respect to the free surface (Fig. 1).

Because of this geometrical asymmetry in the non-vertical case, seismic waves radiated by an earthquake rupture can bounce off the free surface and hit the fault again, and thus modify the stress field on the fault. This interaction causes variations in the normal stress on the fault, which could

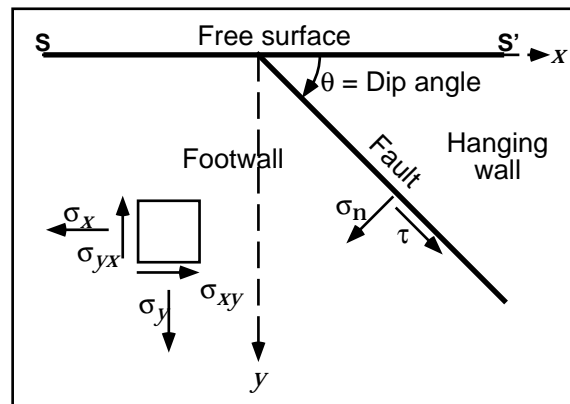


Figure 1. Schematic diagram of the geometry and coordinate system of the fault models. For a non-vertical (dipping) fault such as this case, the symmetry between the two sides of the fault and the free surface is broken.

affect the friction and hence the rupture and slip dynamics of the earthquake.

The net result is that the time-dependent normal stress produces asymmetric ground motion in the proximity of the fault. Using a numerical simulation technique, we sought to document this effect and explain its physical origin.

PROGRESS

Using a 2-D finite element method (developed at LLNL¹ and modified at UCSB), we simulated the dynamics of thrust and normal faults. The simulations included all elastic waves, and unlike most previous dynamic earthquake simulations,² the models also included the time-dependent normal stress on the fault that results from the asymmetric geometry.

We simulated thrust and normal faults with dip angles of 30°, 45°, and 60°. For any given dip angle, the initial stresses, friction laws, and nucleation were the same for the thrust and normal faulting cases, with the exception of the sign of the shear stress.

The asymmetry of the fault with respect to the free surface manifests itself chiefly by causing the normal stress on the fault to change with time. Ahead of the crack tip, due to the shear stress increase, the normal stress change is tensional for a normal fault and compressional for a thrust fault.

Behind the crack tip, in the slipping region of the fault, the stress changes are of opposite sign due to the drop from static to sliding friction on the fault. Therefore, the effect of the free surface on normal stress also changes sign: In the slipping region near the free surface, the normal stress on a normal fault is increased, while it is decreased for a thrust fault.

After starting to slip, a normal fault will have a stronger frictional force holding it back, and will

have decreased particle motion. Conversely, a thrust fault will have lower friction, a greater stress drop, and increased particle motion.

Additionally, for both thrust and normal faults, the hanging wall has higher ground motion than the footwall, because the hanging wall has less volume and thus less mass than the footwall near the free surface.

The results of our simulations show that, in all cases, the thrust fault produces higher ground motion than the normal fault on the free surface above the fault, and there is a large discontinuity in particle velocity and displacement as one crosses from the footwall to the hanging wall (Fig. 2, pg. 60).

The consistently higher ground motion for the thrust faults is caused by the larger displacement on the fault in the thrust case and the resultant higher seismic moment for the same initial stress. However, correcting for the different moments slightly reduces but does not remove the difference between thrust and normal fault motion.

The results of our simulations may explain some observations in the vicinity of non-vertical dip-slip faults, such as increased ground motion in the hanging wall³ and the observation that thrust faults produce greater ground motion than normal faults.⁴

REFERENCES

- Whirley, R. G., B. E. Engelmann, and J. O. Hallquist, *DYNA2D: A Nonlinear, Explicit, Two-Dimensional Finite Element Code for Solid Mechanics—User Manual*, UCRL-MA-110630, Lawrence Livermore National Laboratory, Livermore, CA (1992).
- Andrews, D., *J. Geophys. Res.* **81**, 3575 (1976); D. Andrews, *ibid.*, 5679 (1976); R. Archuleta, Ph.D. Thesis, University of California, San Diego (1976); R. Archuleta and P. Frazier, *Bull. Seis. Soc. Am.* **68**, 541 (1978); S. Day, *ibid.*, **72**, 705 (1982); S. Day, *ibid.*, 1881 (1982); A. Ruina, *J. Geophys. Res.* **88**, 10359 (1983); T. Mikumo and T. Miyatake, *Geophys. J. Int.* **112**, 481 (1993); R. Madariaga and A. Cochard, *Proc. Natl. Acad. Sci. USA* **93**, 3819 (1996).
- Abrahamson, N., and P. Somerville, *Bull. Seis. Soc. Am.* **86**, S93 (1996).
- McGarr, A., *J. Geophys. Res.* **89**, 6969 (1984); N. Abrahamson and K. Shedlock, *Seis. Rev. Lett.* **68**, 9 (1997).

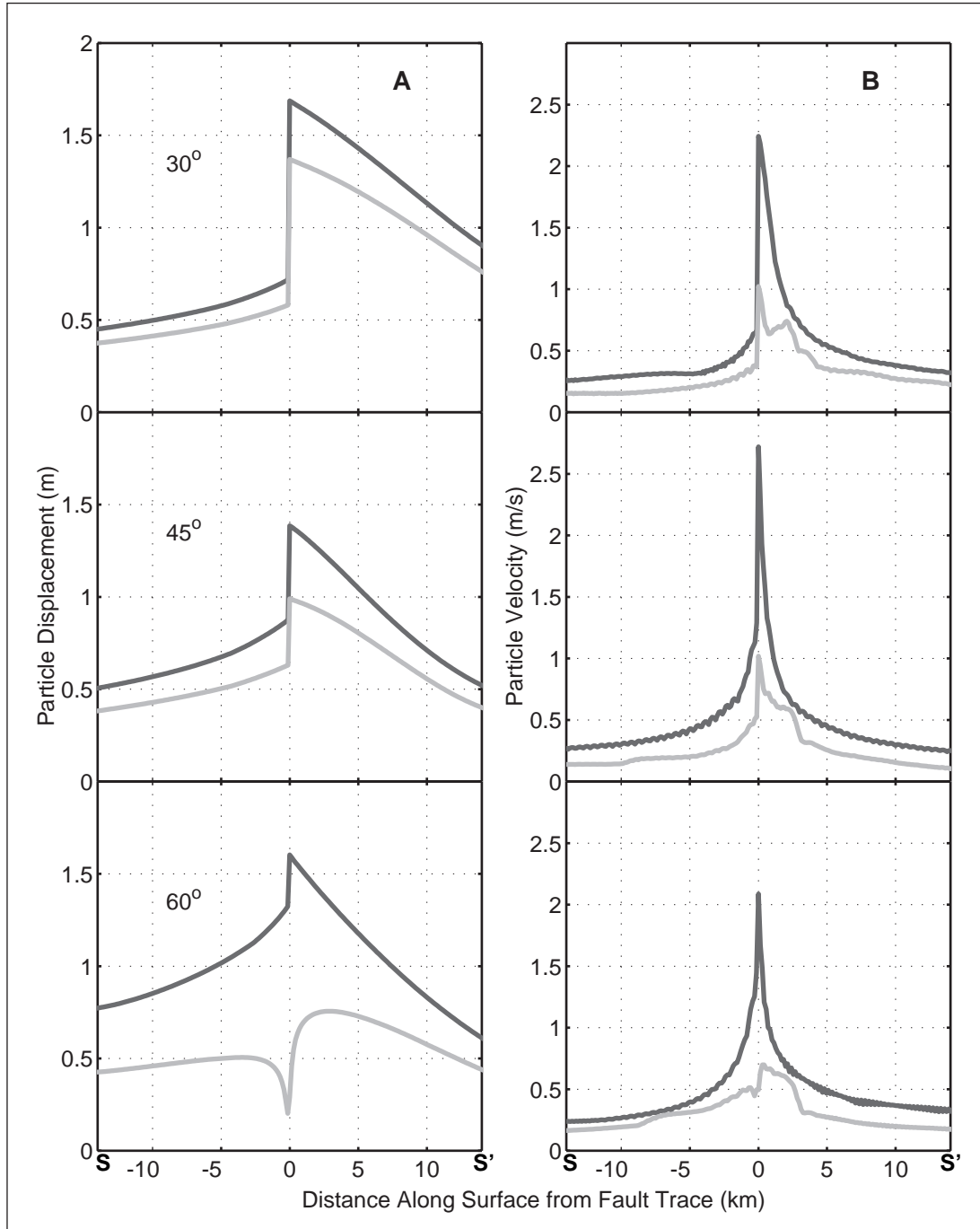


Figure 2. Peak particle displacements (A) and velocities (B) on the surface near 30°, 45°, and 60° dipping faults. S and S' correspond to the points on the surface in Figure 1, so that negative distances are above the footwall, zero distance is on the fault trace, and positive distances are on the hanging wall. Dark curves denote thrust faults, and light curves denote normal faults.

3-D Modeling of Structure in D" (98-GS014)

Principal Investigators: Barbara Romanowicz and Doug Dreger (UC Berkeley)

LLNL Collaborator: Shawn Larsen

Student: Ludovic Bréger (UC Berkeley)

We have carried the forward modeling of differential travel times of phases sensitive to the lowermost mantle beneath the Central Pacific, and have shown the existence of strong lateral heterogeneity in this region of D", with an amplitude that is significantly higher than predicted by existing tomographic models. Two main features were present in the region of D" sampled by our data:

1. *A zone of very low S-velocity (−4% with respect to standard models) likely related to the base of a thermal “plume.” This zone appears to narrow and deflect as it extends ~1000 km above the core-mantle boundary.*
2. *A spatially limited region of very fast S-velocity (+5%) to the east of this zone, which implies the presence of chemical heterogeneity. The location of this zone away from the trace of paleo-subduction zones precludes an interpretation in terms of remnant slab material, but rather suggests the existence of a chemically distinct assemblage.*

In light of these results, we have started to investigate the potential effects of D" strong heterogeneity structure on PKP(AB-DF) differential travel time residuals, traditionally used to probe the bulk of the inner core. Preliminary results show that the effect of D" could actually be as strong as that of a few percent anisotropy in the inner core.

OBJECTIVES

The initial objective of this project was to forward model data sensitive to D", a region of unusual seismic heterogeneity known to play an important dynamical, chemical, and possibly electromagnetic role in the Earth. We intended, in particular, to produce a 3-D model of the lower mantle beneath the Central Pacific, a domain where we had previously identified a high degree of heterogeneity.^{1,2}

PROGRESS

We have assembled an extended dataset of S-SKS and SKKS-SKS differential travel time data for the Central Pacific, and by forward modeling, we have developed a family of local lowermost mantle models that provide good fits to these data.

Our approach is to consider the variations with distance of S-SKS and SKKS-SKS travel

time residuals computed with respect to the PREM reference model for a fixed source or station and along narrow azimuthal corridors. We have analyzed residuals for several large events in the Fiji-Tonga-Kermadec Islands source region recorded on a large number of North American stations. By using differential travel times between S and SKS, or SKS and SKKS, we minimize errors due to source mislocation, uncertainty on earthquakes origin times, and heterogeneity in the crust and upper-mantle beneath sources and receivers.

A starting 3-D model was chosen by computing predicted differential travel time residuals for several recent tomographic models, and by selecting the model that gave the closest match to the observed trends (SAW12D).³ Then, by forward modeling of travel time residuals, we progressively perturbed the starting model in two ways:

1. By preserving the spatial distribution of anomalies and only modifying the amplitude of velocity fluctuations in selected high- or low-velocity regions of the model.
2. By slightly shifting their positions laterally when necessary to fit the observations.

We found that lateral shifts on the order of less than 250 km were generally sufficient. We thus obtained, by trial and error, a family of models capable of explaining not only the trends in the travel-time versus distance plots, but also the specific ranges of travel time fluctuations (Fig. 1).

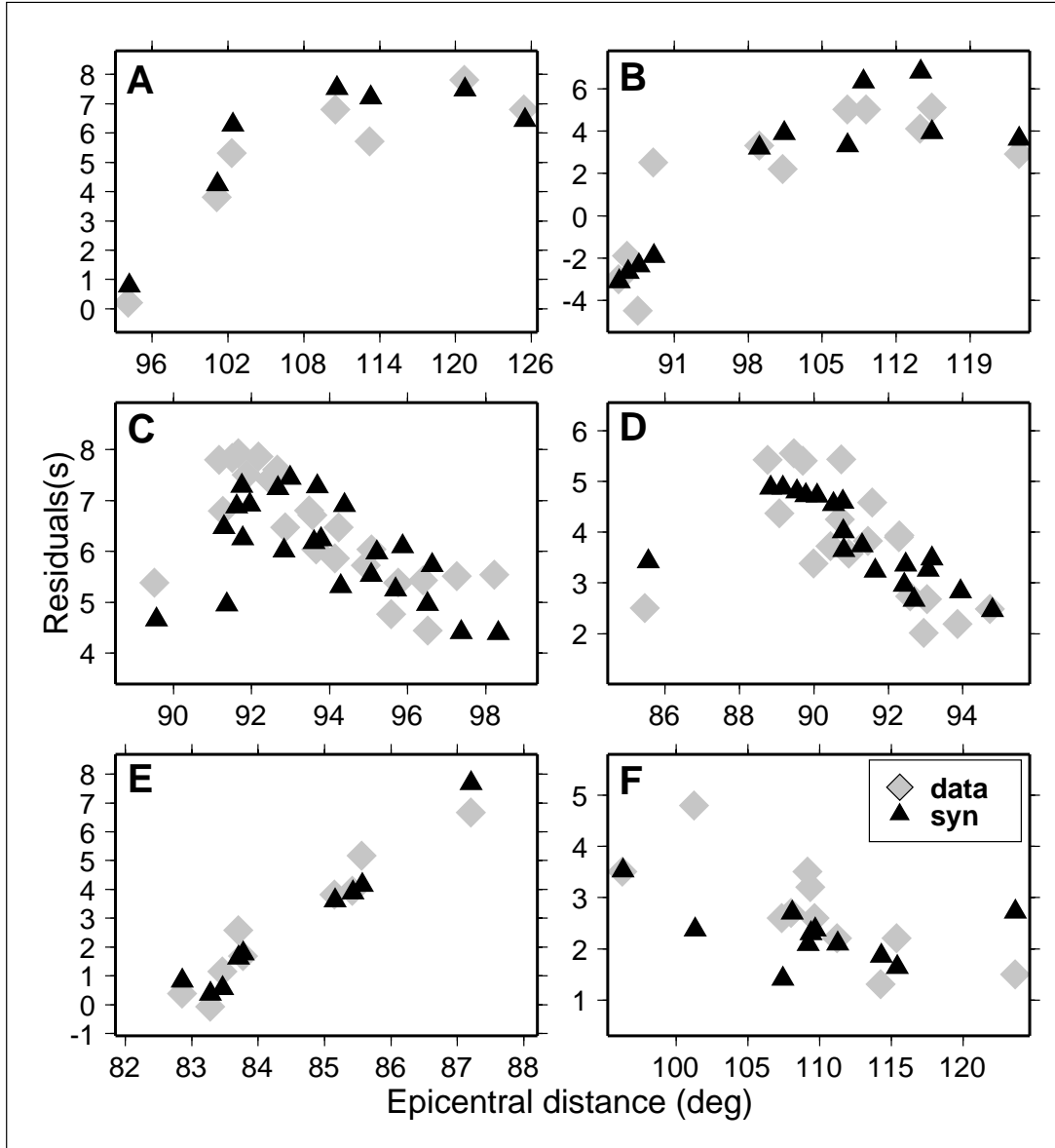


Figure 1. Examples of observed variations of differential travel time residuals as a function of epicentral distance (gray diamonds) along with synthetic predictions (black triangles) computed for our preferred 3-D model.

(A) and (B): Data and predicted residuals for events 97/10/14 and 98/03/29, respectively, and azimuths between 40° and 50° . S penetrates into the slow Pacific anomaly as distance increases, and S -SKS residuals correspondingly increase.

(C) and (D): Same as (A) and (B) for events 92/06/25 and 92/07/11, respectively. The trend is opposite to that observed in (A) and requires a fast region where the S -velocity anomaly reaches +5%.

(E): S -SKS residuals for fixed station COR and several Fiji-Toga-Kermadec Islands events, and azimuths between 35° and 37° .

(F): SKKS-SKS residuals for event 98/03/29, and azimuths between 40° and 60° .⁴

Two prominent features are common to all models in the family. A large slow region at the bottom of the mantle south of Hawaii in the last 1000 km of the mantle is consistently required in order to reasonably fit this type of trend. This anomaly resembles in shape that of the starting tomographic model, but its amplitude needs to be increased to 3.5–4% throughout its domain.

Interestingly, to explain the rapidly decreasing residuals for distances between approximately 90 and 96 degrees, it is necessary to introduce a fast region, adjacent to the large slow anomaly, where the velocity anomaly reaches 4–5% in a small domain that had only a mildly fast anomaly of about 1–2% in the original model.

The large slow region in the mantle beneath the Central Pacific seen in all tomographic models is likely related to a mega-plume generated by thermal boundary layer instabilities at the CMB. The very large velocity anomaly could be in part related to partial melt, but some chemical heterogeneity may be present. The high velocity region documented by our modeling represents a contrast of about 7–8% with respect to adjacent “hot” mantle and cannot be readily explained by thermal effects alone.

A portion of ancient slab lying at the CMB seems unlikely to be responsible for this velocity contrast, because reconstructions of ancient subductions do not predict the presence of remnant lithosphere in this part of D" and because such a fossil slab may not produce a sufficient velocity contrast. A different type of chemical heterogeneity needs to be invoked to explain such a strongly fast and localized anomaly.

The Finite Difference Modeling of Differential Travel Time Residuals

In order to accurately compute differential travel time residuals for a complex heterogeneous

3-D model, it is desirable to use a 3-D finite difference (FD) code. The full 3-D algorithm is unfortunately computationally heavy to use, and we had to limit ourselves to 2-D models. We used several FD codes, and in particular, Shawn Larsen's ELAS3D⁵ to compute S-SKS residuals for several test paths between the Fiji-Tonga-Kermadec Islands source region and stations in North America; we compared those predictions with residuals computed using a 1-D ray tracing.

The difference between the two approaches is less than about 1–2s, which is the typical accuracy of S-SKS residuals measurement. Since the forward modeling of our S-SKS dataset was performed through a trial-and-error approach and required the computation of several thousands of S and SKS travel times, we chose to use the 1-D approach. Having access to the FD codes was nevertheless crucial to test the validity of the 1-D ray tracing.

Possible Effect of Deep Mantle Heterogeneity on Inner Core Studies

In order to study the structure of the bulk of the inner core using PKP(DF), the outer core phase PKP(AB) is often used as a reference phase. PKP(AB-DF) differential residuals are in principle less sensitive than PKP(DF) absolute residuals to mantle structure, but because PKP(AB) and PKP(DF) propagate quite far apart in the deepest mantle, D" could have a non-negligible effect on PKP(AB-DF) residuals.

In light of the S-SKS study, we have started to investigate the potential effect of a strong D" heterogeneity. It seems that most PKP(AB-DF) differential travel time residuals, including those traditionally interpreted as caused by an effect of inner core anisotropy, could actually be explained by deep mantle heterogeneity (Fig. 2, pg. 64).⁶

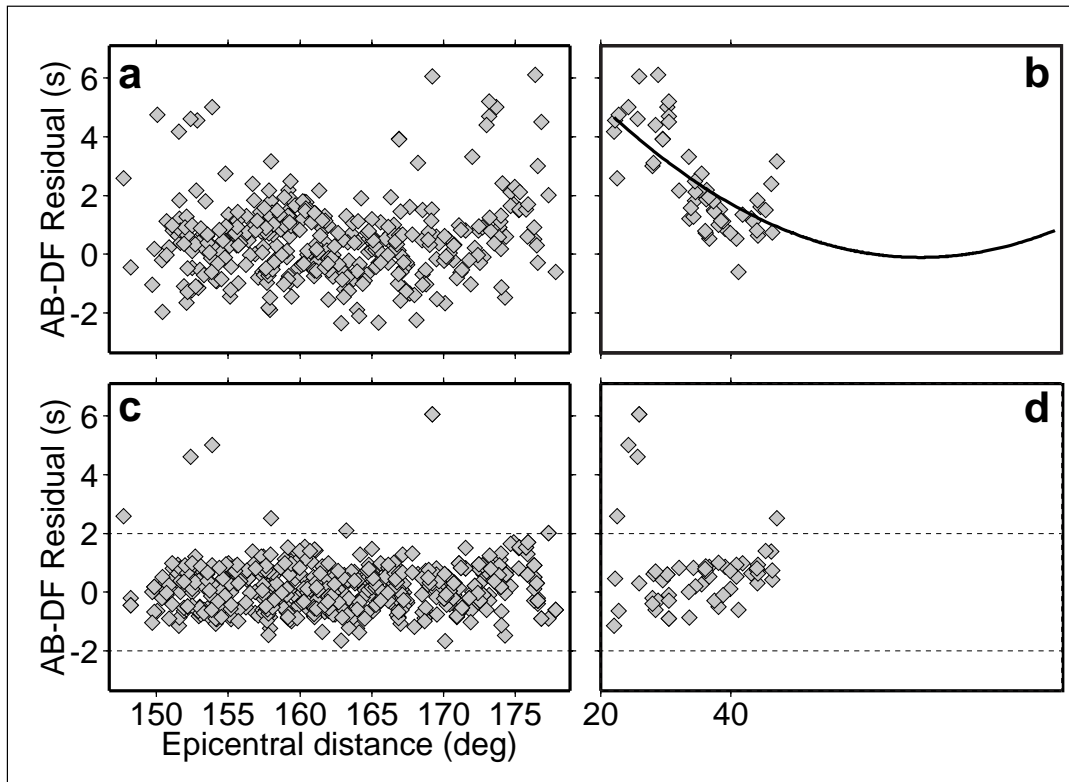


Figure 2. AB-DF differential travel time residuals as a function of epicentral distance (a) and angle ξ of the path in the inner core with respect to the rotation axis (b). The best-fitting second-degree polynomial in $\cos^2\xi$ (solid line) was added in (b) to outline the observed trend. Such a trend is expected, at fixed distance, for models of constant cylindrical anisotropy in the inner core with axis parallel to the rotation axis.

(c) and (d): Same as (a) and (b) after correction for the model discussed in the text. Note that a few large residuals at low ξ remain unexplained. These correspond to South Sandwich Islands paths to stations COL and BILL.⁶

REFERENCES

1. Vinnik, L., L. Bréger, and B. Romanowicz, "Anisotropic Structures at the Base of the Earth's Mantle," *Nature* **393**, 564 (1998).
2. Bréger, L., B. Romanowicz, and L. Vinnik, "Test of Tomographic Models of D" using Differential Travel Time Data," *Geophys. Res. Lett.* **25**, 5 (1998).
3. Li, X.-D., and B. Romanowicz, "Global Mantle Shear Velocity Model Developed using Nonlinear Asymptotic Coupling Theory," *J. Geophys. Res.* **101**, 22245 (1996).
4. Bréger, L., and B. Romanowicz, "Three-Dimensional Structure at the Base of the Mantle beneath the Central Pacific," *Science* **382**, 718 (1998).
5. Larsen, S. C., and C. A. Schultz, "ELAS3D: 2D/3D Elastic Finite-Difference Wave Propagation Code," UCRL-MA-121792, Lawrence Livermore National Laboratory, Livermore, California, 18p (1995).
6. Bréger, L., H. Tkalcic, and B. Romanowicz, "PKP Travel Times: Inner Core Anisotropy or Complex Structure in the Deep Mantle?," revision for *Science*, in prep. (1998).

High-Resolution Study of Inner-Core Rotation (98-GS023)

Principal Investigator: John E. Vidale (UC Los Angeles)

LLNL Collaborator: Doug Dodge

Student: Fei Xu (UC Los Angeles)

The claim that the inner core is rotating¹⁻³ remains controversial. We have undertaken this project to test this claim with array data.

In our first year of work, we collected many recordings from the NORSAR array (located in Norway) of earthquakes in Tonga. We found and reported that the data are numerous and high quality, but even state-of-the-art cross-correlation timing techniques are not sufficient to test for the tiny changes in differential times that comprise the evidence for inner core rotation.⁴ The most striking observation, in fact, is that the PKP waves along this path are amazingly messy, which led us to comment on the kinds of structures probably responsible for the mess.⁵

OBJECTIVE

We are exploring two lines of inquiry this year. First, we are trying to acquire the data from the Yellowknife Array in northern Canada in order to apply our array-based and cross-correlation techniques on new data. These data would sample a path near the one analyzed by Creager and Song.^{1,2} Unfortunately, the guardians of the Yellowknife data are guarding it too well. We haven't seen it yet, despite repeated attempts.

The second line of inquiry is an investigation to find which paths transmit PKP well, and which paths transmit PKP poorly. The answer to this question would help us to learn something about the core-mantle boundary and would tell us which paths are good candidates for testing the reality of inner-core rotation.

PROGRESS

Figure 1 (pg. 66) shows some of the details about the database we have built of PKP phases in the distance range from 110' to 140'. Fei Xu collected more than 10,000 vertical-component seismograms from the FARM-based data collection of Paul Earle (a postdoc at UC Los Angeles). We are systematically checking the distance, depth, and magnitude ranges for which good signal-to-noise ratios are apparent.

Figure 2 (pg. 67) shows the amplitude ratio pattern of PKP divided by PP. Each seismogram is plotted at its midpoint, with an arrow pointing in

the direction of propagation. We are looking for high-amplitude ratios where PKP is propagating unhindered by messy CMB structure, and low-amplitude ratios where PKP is decimated by messy CMB structure. This analysis assumed that PP waves are fairly similar for all paths, an assumption that we are checking by making similar plots of the ratio of PKP to ambient noise and the ratio of PP to ambient noise.

REFERENCES

1. Creager, K. C., "Inner Core Rotation Rate from Small-Scale Heterogeneity and Time Varying Travel Times," *Science* **2(78)**, 1284 (1997).
2. Song, X. D., and P. G. Richards, "Seismological Evidence for Differential Rotation of the Earth's Inner Core," *Nature* **382**, 221 (1996).
3. Su, W. J., A. M. Dziewonski, and R. Jeanloz, "Planet within a Planet: Differential Rotation of the Inner Core of Earth," *Science* **274**, 1883 (1996).
4. Xu, F., J. E. Vidale, and D. A. Dodge, "Checking Inner Core Rotation with a High Quality Path," *Trans., EOS* (abstracts), S22E-05 (1997).
5. Vidale, J. E., and M. A. H. Hedlin, "Evidence for Partial Melt at the Core-Mantle Boundary North of Tonga from the Strong Scattering of Seismic Waves," *Nature* **391**, 682 (1998).

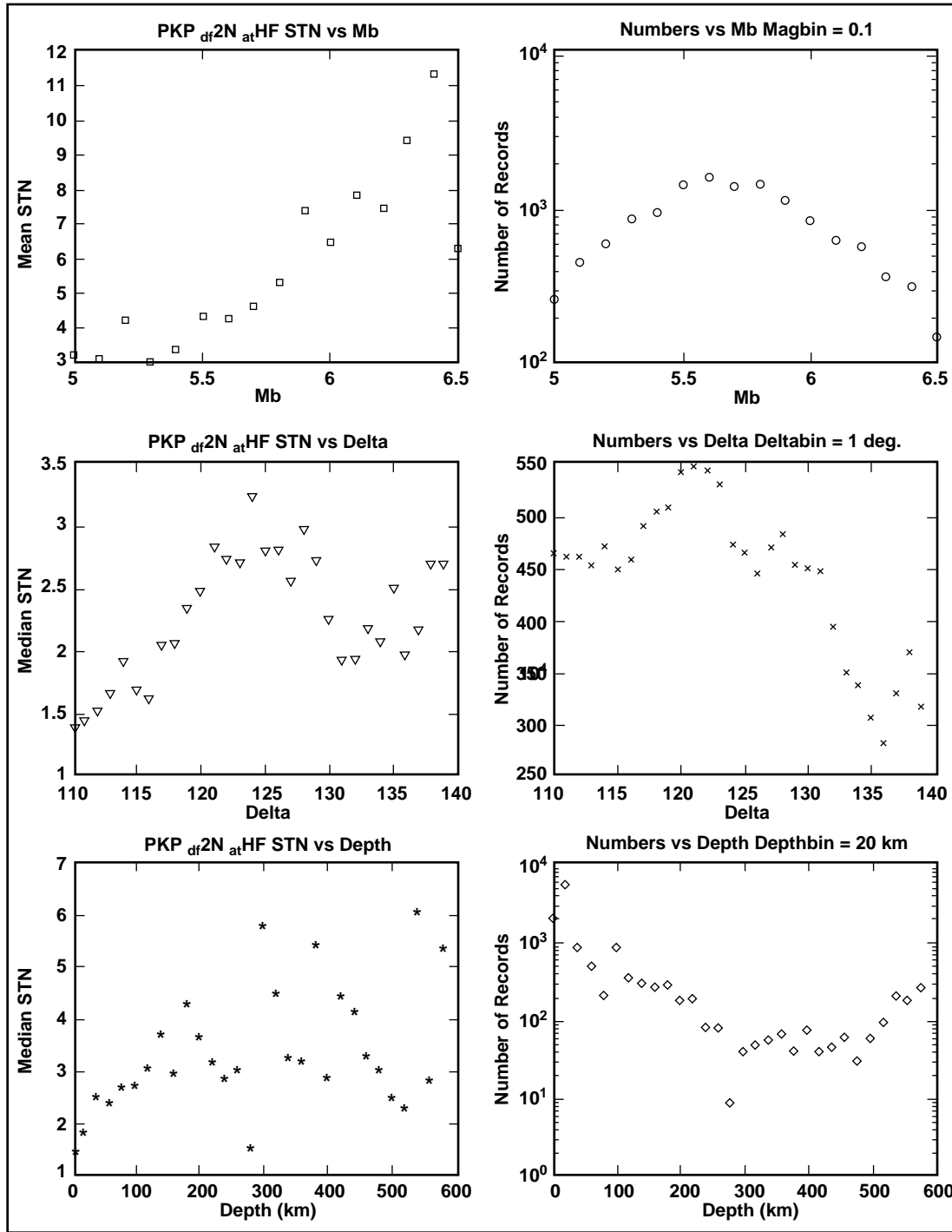


Figure 1. PKP(DF)/noise ratio traces are filtered between 1.0 and 2.5 Hz. Top two panels: left—each point represents an average ratio of PKP(DF) to pre-P noise within each 0.1 Mb bin ($5.0 < Mb < 6.5$); right—trace numbers within each 0.1 Mb bin.

Middle two panels: left—each point represents an average ratio of PKP(DF) to pre-P noise within each 1° distance bin ($110^\circ < \delta < 140^\circ$); right—trace numbers within each 1° distance bin.

Bottom two panels: left—each point represents an average ratio of PKP(DF) to pre-P noise within each 20-km depth bin ($0 \text{ km} < \text{depth} < 600 \text{ km}$); right—trace numbers within each 20-km depth bin.

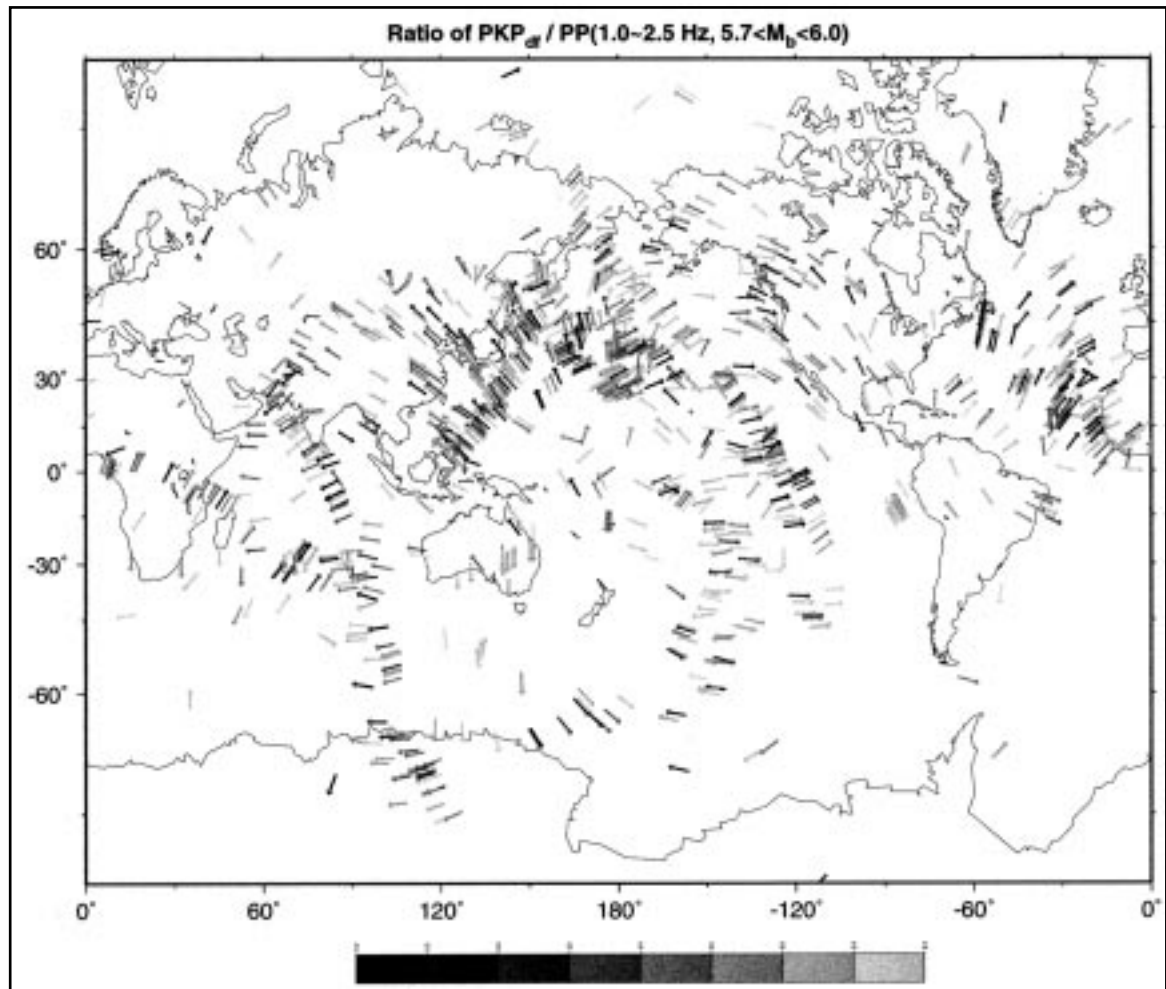


Figure 2. Map view of the amplitude ratio PKP_{df}/PP. The seismograms are filtered between 1.0 ~ 2.5 Hz. The epicentral distance is between 110–140°. The magnitude of the events is between 5.7–6.0.

Controls of U Groundwater Chemistry Constrained by AMS ^{14}C and ^{36}Cl (98-GS029)

Principal Investigator: James B. Gill (UC Santa Cruz)

LLNL Collaborator: Gregory Nimz

Student: Aaron O. Reyes (UC Santa Cruz)

McDowell Valley is a pull-apart basin near Hopland, California, within the San Andreas fault system. Groundwater in McDowell Valley flows through fractured Franciscan bedrock and overlying clayey sediments of the same lithology but lower permeability. The major-ion composition of groundwater in the fractured rocks and sediments is similar. Consequently, the basin is a good site for evaluating the relative role of mixing and flow regime versus time-dependent water-rock reactions in controlling groundwater chemistry. There is similarity in Sr isotope ratios, but substantial difference in the concentration of redox-sensitive species in the two flow systems.

Groundwater in the fractured rocks adjacent to McDowell Valley contains higher concentrations of dissolved oxygen and sulfate, and lower concentrations of arsenic, iron, and manganese than does the more reduced groundwater in the sediments. The oxygenated groundwater in the fractured rocks also has higher concentrations of uranium (0.1–3.3 $\mu\text{g/L}$) and higher $^{234}\text{U}/^{238}\text{U}$ activity ratios (A.R. = 1.65–2.4) relative to the more reduced waters in the Pliocene-Pleistocene sediments (0.008–0.09 $\mu\text{g/L}$ and A.R. < 1.65). Consequently, variation in redox conditions is the principal cause of differences in the groundwater chemistry between the two flow regimes.

^3H , ^{14}C , and ^{36}Cl were measured to constrain water ages. Most samples contain some bomb pulse ^3H and ^{36}Cl , whereas ^{14}C ages are between 3,000 and 40,000 years in the majority of samples. By using groundwater ages, chemical mixing models, and a groundwater flow model, this study will help to determine whether groundwater evolves chemically as it moves from fractured rocks in the hills toward sediments in the valley, or whether the range in chemistries evolve in hydraulically separate flow. The chemical data, in conjunction with hydraulic-head measurements, will identify recharge areas, groundwater-flow paths, and mixing between the flow regimes.

OBJECTIVES

This project used a geochemical approach to unravel the complex groundwater flow that occurs in the McDowell Valley, Hopland, northern California. Geochemical tools including $^{36}\text{Cl}/\text{Cl}$, ^3H , and $^{14}\text{C}/\text{C}$ isotopes were used for temporal constraints, and $^{87}\text{Sr}/^{86}\text{Sr}$, $^{234}\text{U}/^{238}\text{U}$, and element concentrations were used for spatial constraints and as oxidation/reduction indicators. This approach has a two-fold purpose: (1) to unravel complex flow patterns by distinguishing mixing trends from the chemical evolution of waters during flow; and (2) to study the behavior of U iso-

topes in contrasting flow and oxidation state regimes.

The McDowell Valley is a pull-apart basin that is characterized by a dual flow regime, with fracture flow in Franciscan bedrock and porous flow in overlying Pliocene-Pleistocene basin fill.¹ The basin fill is structurally bounded by northwest-southeast-trending strike-slip faults. The different flow regimes affect groundwater flow velocities, residence times, and exposure to the atmosphere. These differences manifest themselves as variations in redox conditions, which affect redox-sensitive elements such as Uranium.

PROGRESS

Eighteen wells and six springs were sampled, and a total of thirty water samples were studied. Some samples were obtained in 1993–94 by the USGS; most were obtained during this award period. All water samples were analyzed for major and trace cations and anions at UCSC. Isotope ratios and concentrations of $\delta^{13}\text{C}$, Sr, and U were also measured at UCSC for selected samples. $^{36}\text{Cl}/\text{Cl}$ ratios and $^{14}\text{C}/\text{C}$ ratios were measured at LLNL for all 1996–97 samples. Results of this work were presented at the December 1998 AGU meeting.^{2,3}

Substantial developmental work was required for the ^{14}C and U measurements. Reyes built a vacuum line at LLNL to extract dissolved inorganic carbon (DIC) from water samples in CO_2 form in order to obtain $\delta^{13}\text{C}$ and $^{14}\text{C}/\text{C}$ ratios for the groundwater samples collected for this study. The line was leak tested, and blanks as low as 0.05% modern carbon ($> 44,000$ y) were obtained.

The line can extract 75–95% of DIC from a water sample after 10 minutes of extraction time. U isotope ratios were successfully measured using TIMS methods for samples with as little as 0.008 ppt U; lower concentrations remained difficult with the sample volumes available.

The elemental concentrations and Sr isotopic ratios indicate that McDowell Valley groundwaters are chemically similar in both fracture and porous flow regimes.

All groundwaters are bicarbonate ($>98\%$ of anions), and most groundwaters are rich in calcium + magnesium ($>75\%$ of cations). Most $^{87}\text{Sr}/^{86}\text{Sr}$ isotope ratios are 0.7061–.7064, indicating an isotopically similar rock matrix in both flow regimes. However, redox-sensitive elements demonstrate that groundwaters in the fracture flow regime are oxidized, while groundwaters in the porous flow regime are partly reduced in some cases and highly reduced in most.

Well waters in the northernmost part of the basin contain the highest concentration of total dissolved solids (TDS). The decrease in TDS to the south suggests dilution by a recharge component. There are redox-related differences within these two chemically contrasting water types, but mixing between two water types characterized by high and low TDS is evident in the concentrations of elements such as Na, K, Sr, Mg, Ca, and B.

$^{36}\text{Cl}/\text{Cl}$ ratios and tritium (^3H) concentrations are good indicators of the modern recharge component. They identify a contribution of young recharge water throughout the northern part of the basin (15–40-year-old precipitation). These waters are thought to be fed into the basin by fracture flow.

The southern part of the basin shows little evidence of young water. ^{14}C ages indicate that the wells located in the northern part of the basin are the oldest, with the spring water having the oldest age of at least 40,000 years. These northernmost waters contain a contribution of both old water, as indicated by the ^{14}C age, and recent recharge (15–40 years old), as indicated by ^3H and $^{36}\text{Cl}/\text{Cl}$. The ^{14}C age of waters in the basin decreases to the south, indicating dilution and freshening in that direction.

Samples with high ($^{234}\text{U}/^{238}\text{U}$) activity ratios (A.R. = 1.65–2.4) are less than 9,000 ^{14}C years old, oxidized, and found in both fracture and porous flow regimes. The samples with low U activity ratios (A.R. = 1.15–1.65) are all found in the porous flow regime, have variable ages, and with one exception, indicate reduced conditions. Differences in uranium concentration are attributed to redox state, with porous flow through sediment being more reduced and having less U in solution. However, the U activity ratios do not conform to expectations because samples in reduced environments do not have higher activity ratios and lower uranium concentrations, as expected.^{4,5}

Models consistent with the geochemical and hydrogeological data are being tested. A three-component mixing system is being assessed in which the water types are: (1) low TDS; (2) high TDS plus low ^3H and $^{36}\text{Cl}/\text{Cl}$; and (3) high TDS plus high ^3H and $^{36}\text{Cl}/\text{Cl}$ (Fig. 1). Each occurs in specific areas of the basin and aquifers. It may be possible to assign unique ages to most water sam-

ples and to use this age information to assess rates of Sr and U isotopic equilibration and redox reactions, thereby distinguishing the effects of rock-water reaction from effects of mixing. Future work will focus on deciphering the evolution of each water type, and interpreting the Sr and U data in light of the mixing and evolution of the different water types.

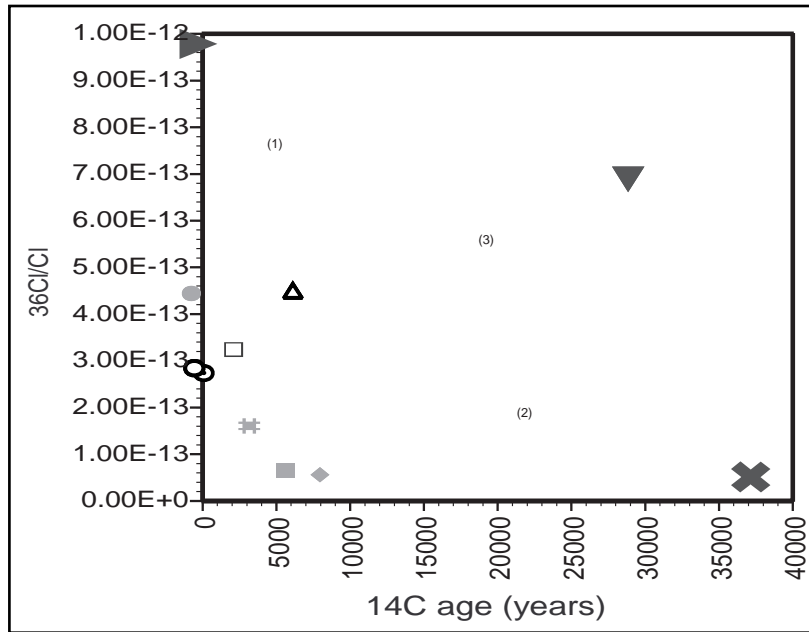


Figure 1. $^{36}\text{Cl}/\text{Cl}$ versus ^{14}C ages for water samples from Hopland wells. Samples from wells in basin sediments are represented by filled symbols. Samples from wells in the Franciscan bedrock are represented by open symbols. Larger dark symbols represent mixing endmembers for water types 1, 2, and 3.

REFERENCES

1. USEPA, "Assessment of the Quality of Water Resources at the Hopland Reservation, Mendocino County, California," prepared by Hopland Band of Pomo Indians with assistance from James B. Tautfest and data collection by USGS Section 305 (b) report (1996).
2. Reyes, A. O., J. B. Gill, J. Tautfest, J. Borchers, and G. Nimz, "Redox Conditions and Isotopic Characteristic of Groundwater in McDowell Valley, Hopland, California," *EOS Trans., Amer. Geophys. Union* 78, Fall Meeting (1997).
3. Reyes, A. O., J. B. Gill, J. Tautfest, J. Borchers, and G. Nimz, "Redox Conditions and Isotopic Characteristic of Groundwater in McDowell Valley, Hopland, California." *EOS Trans., Amer. Geophys. Union* 79, Fall Meeting (1998).
4. Osmond and Cowart, *Uranium-Series Disequilibrium: Applications to Earth, Marine, and Environmental Sciences*, Chapter 9, Ivanovich and Harmon, eds., Calderon Press., Oxford, second edition, pp. 290–333 (1992).
5. Kronfeld, J., and J. A. S. Adams, "Hydrologic Investigations of the Groundwaters of Central Texas using U-234/U-238 Disequilibrium," *J. Hydrology* 22, 77 (1974).

Deformation of Olivine: Comparison of Predictions with Experiments (98-GS031)

Principal Investigator: Hans-Rudolf Wenk (UC Berkeley)

LLNL Collaborator: Bill Durham

Student: Yanxia Xie (UC Berkeley)

Experiments by Zhang and Karato¹ have shown that in simple shear deformation of olivine at low strains, an asymmetric texture develops with a [100] maximum rotated away from the shear direction against the sense of shear. At large strain, where recrystallization is pervasive, the pattern is symmetrical and [100] is parallel to the shear direction.

The deformation texture can be adequately modeled with a viscoplastic self-consistent polycrystal plasticity theory. This model can be expanded to include recrystallization as a balance of boundary migration (growth of relatively undeformed grains at the expense of highly deformed grains) and nucleation (strain-free nuclei replacing highly deformed grains).

If nucleation dominates, the model predicts a change from the asymmetric to the symmetric texture as deformation proceeds and stabilizing in the “easy slip” orientation for the dominant (010)[100] slip system, which is also in accordance with the experiments. This model will be useful to simulate the development of anisotropy in the mantle where olivine is largely recrystallized.

PROGRESS

There is a close relationship between crystal-preferred orientation and anisotropy of physical properties.^{2,3} Whereas the development of preferred orientation during deformation is well understood, recrystallization is still enigmatic.

Based on the premise that dynamic recrystallization is a balance between nucleation and growth, a deformation-based model for recrystallization was developed.⁴ It proposes a phenomenological description of recrystallization with a limited number of empirical parameters with a physical meaning.

Making some assumptions about deformation mechanisms, the hardening behavior, and nucleation and grain growth, it is possible to explain various recrystallization features such as kinetics, some microstructural phenomena, and texture development based on an understanding of deformation.

In geophysics of Earth materials, we are primarily interested in dynamical effects, i.e., if recrystallization takes place while deformation occurs. Therefore, we need a model that deals simultaneously with texture and flow stress evolution due to recrystallization and overall plastic deformation. The self-consistent viscoplastic polycrystal plasticity theory⁵ is a basic ingredient of the recrystallization model because it allows us to determine the relationship between grain orientation and deformation state.

Grains (or orientations) with a high stored energy are likely to nucleate and become dislocation-free grains. They may also instead be invaded by their neighbors, which have a lower stored energy.

Depending on the relative importance of nucleation and boundary migration processes, the recrystallization textures are expected to favor either highly deformed components or less

deformed components. An equivalent strain rate is used as a criterion for nucleation.

The model has been applied to a few systems and has proven to be remarkably robust and reliable. For quartz, it has been possible to explain the asymmetric [0001] maximum in the intermediate strain direction that is frequently observed in mylonitic quartzites and has so far eluded a satisfactory interpretation.⁴ Also, the texture observed in calcite compression experiments with an enigmatic maximum at high-angle positive rhombs could finally be explained as dynamic recrystallization with dominant growth.⁶

In this project, we are applying the recrystallization model to simple shear deformation of olivine.⁷ This is a good example, because simulation results can be compared with the experiments of Zhang and Karato.¹

Olivine, with its low orthorhombic symmetry, has only limited slip systems, and upper bounds compatibility models such as Taylor are not applicable. The self-consistent model has been applied to model deformation of olivine.⁸

The simulated texture shows a characteristic asymmetric maximum in the [100] pole figure, displaced about 30° against the sense of shear

(Fig. 1, bottom). This maximum agrees well with experiments (Fig. 1, top) and corresponds to orientations for which rotation rates are smallest.

Figure 2 shows that during dynamic recrystallization, with recrystallization parameters favoring nucleation, soft orientations nucleate (× symbols), whereas hard orientations grow (+ symbols). Hard orientations are in the center of the pole [100] figure and in the position of the asymmetric deformation maximum.

Soft orientations that nucleate first are in two main concentrations, one near the slip direction (component B) and a second one at high angles to the slip direction (component C). With increasing strain, all old grains disappear.

The nucleated grains at high angles rotate with the sense of shear towards the 30° orientation and slowly disappear. The orientations near the shear direction (component B) concentrate, grow, and nucleate several times. Ultimately, those orientations that represent the “easy slip” orientation for (010)[100] slip dominate the texture.

The pole figures with individual orientations are a good method to illustrate processes. But the best way to compare simulated and experimental textures is again in contoured pole figures.

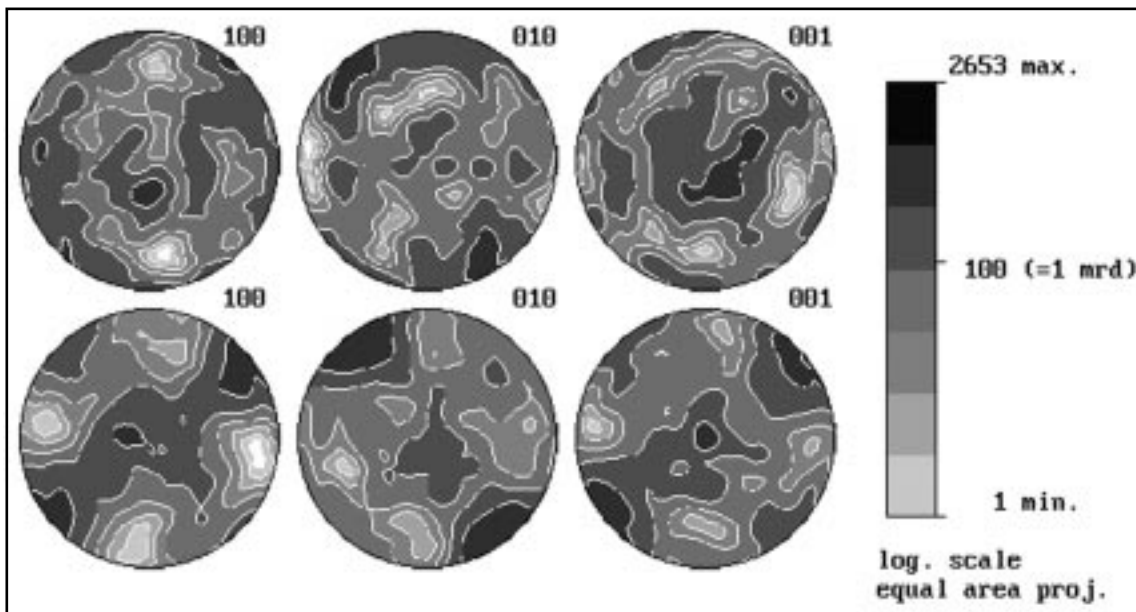


Figure 1. Deformation of olivine in simple shear. Top: experiment; bottom: simulation. Shear plane is horizontal.

The experimental recrystallization texture (Fig. 3, top)¹ is in good accord with the model (Fig. 3, center). Interestingly, these simulated and experimental simple shear olivine textures also conform with textures in mantle peridotites such as from South Africa,⁹ which we measured with SEM-EBSP at Berkeley (Fig. 3, bottom).

The possibility of modeling texture and anisotropy development of olivine polycrystals

during dynamic recrystallization opens many new possibilities: Presently, we are incorporating recrystallization in large finite element models of convective flow in the upper mantle, which we have previously done for deformation only.¹⁰ The research is leading to a better understanding of anisotropy development in the Earth that has become a major concern in seismology.

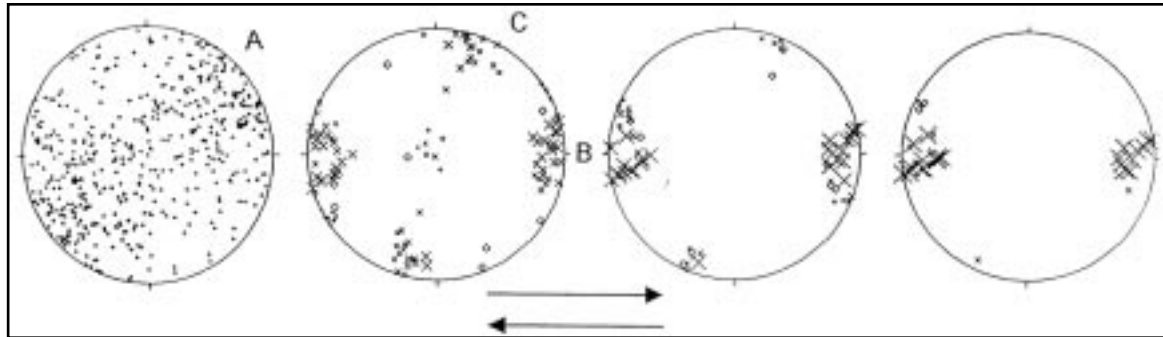


Figure 2. Self-consistent simulations illustrating the evolution of texture in simple shear during deformation by slip (left) and dynamic recrystallization (right). Old grains = +; newly nucleated grains = x. [100] pole figures.

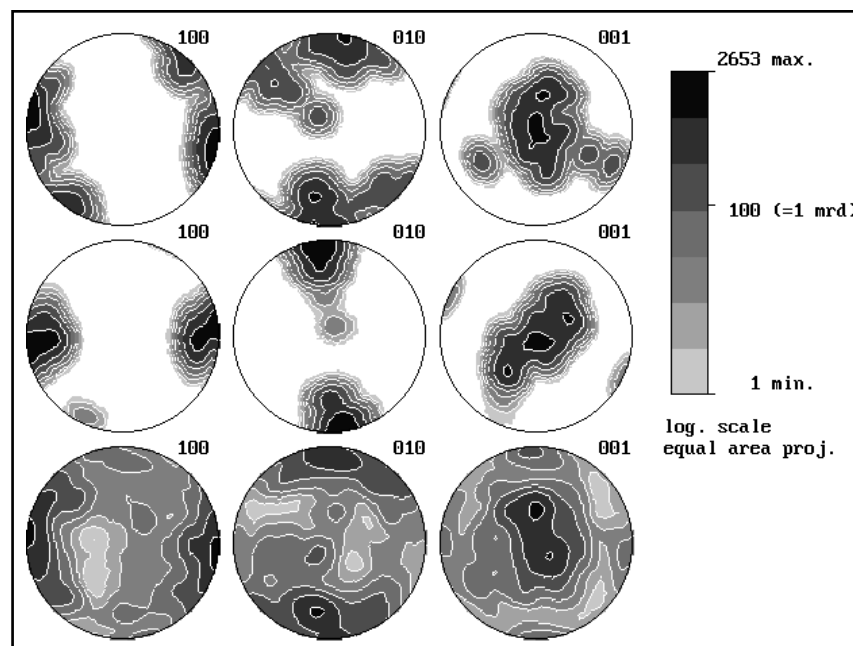


Figure 3. Pole figures of olivine after dynamic recrystallization in simple shear. Top: experiment; middle: simulation; bottom: natural (measured by EBSP). Shear plane is horizontal.

REFERENCES

1. Zhang, S., and S.-I. Karato, "Lattice Preferred Orientation of Olivine Aggregates Deformed in Simple Shear," *Nature* **375**, 774 (1995).
2. Kocks, U. F., C. Tomé, and H.-R. Wenk, *Texture and Anisotropy*, Cambridge Univ. Press (1998).
3. Wenk, H.-R., "A Voyage through the Deformed Earth with the Self-Consistent Model," *Modeling in Materials Science and Engineering*, in prep. (1998).
4. Wenk, H.-R., G. Canova, Y. Brechet, and L. Flaudin, "A Deformation-Based Model for Recrystallization," *Acta Mater.* **45**, 3283 (1997).
5. Canova, G. R., H.-R. Wenk, and A. Molinari, "Deformation Modeling of Multiphase Polycrystals: Case of a Quartz-Mica Aggregate," *Acta Metall.* **40**, 1519 (1992).
6. Lebensohn, R. A., H.-R. Wenk, and C. Tomé, "Modeling Deformation and Recrystallization Textures in Calcite," *Acta Mater.* **46**, 2683 (1998).
7. Wenk, H.-R., and C. N. Tomé, "Modeling Recrystallization of Olivine in Simple Shear," *J. Geophys. Res.*, in prep. (1998).
8. Wenk, H.-R., K. Bennett, G. Canova, and A. Molinari, "Modeling Plastic Deformation of Peridotite with the Self-Consistent Theory," *J. Geophys. Res.* **96B**, 8337 (1991).
9. Rudnick, R. L., W. F. McDonough, and B. W. Chappell, "Carbonatite Metasomatism in the Northern Tanzanian Mantle: Petrographic and Geochemical Characteristics," *EPSL* **114**, 463 (1993).
10. Chastel, Y. B., P. R. Dawson, H.-R. Wenk, and K. Bennett, "Anisotropic Convection with Implications for the Upper Mantle," *J. Geophys. Res.* **98**, 17757 (1993).

Section IV. IGPP–LLNL Seminars

- January 12, 1998
“The Structure of Globular Clusters”
Georges Meylan, European Southern Observatory
- January 16, 1998
“Solar Physics”
Ted Tarbell, Lockheed-Martin
- January 16, 1998
“Global Carbon SI”
Phil Duffy, LLNL
- January 23, 1998
“The Magnetic Propeller in the Cataclysmic Variable AE Aquarii and its Wider Implications”
Mike Eracleous, UC Berkeley
- February 6, 1998
“Europa: New Insights from Galileo”
Paul Geissler, University of Arizona
- February 11, 1998
“Low-Mass Stars and Brown Dwarfs: From Their Physical Properties to Their Galactic Implications”
Gilles Chabrier, Groupe d-Astrophysique, France
- February 13, 1998
“The Emancipation of Slaved Accretion Disks: Do Radiation Torques Cause Disks to Warp and Precess?”
Mitch Begelman, University of Colorado
- February 19, 1998
“Titan’s Haze Distribution at Several Altitudes”
Eliot Young, Southwest Research Institute
- February 20, 1998
“What We Did on Our Summer Vacation: Highlights from the Mars Pathfinder”
Bridget Landry, Jet Propulsion Laboratory
- February 20, 1998
“Visalia Pole Yard”
Roger Aines and Robin Newmark, LLNL
- February 27, 1998
“Dust and Star Formation in UV Bright Galaxies”
Daniela Calzetti, Space Telescope Science Inst.
- March 6, 1998
“Outer Solar System Environments and Inner Solar System Life”
Chris Chyba, University of Arizona
- March 12, 1998
“Probing Black Holes in AGN with X-Ray Observations”
Paul Nandra, NASA/Goddard Space Flight Center
- March 13, 1998
“The Hubble Constant from Gravitational Lens Time Delays”
Paul Schechter, Massachusetts Inst. of Tech.
- March 20, 1998
“Molecular Clouds in the Galactic Center Region”
Tom Wilson, Steward Observatory
- March 20, 1998
“The Macho Project: A Search for Baryonic Dark Matter in the Milky Way”
Charles Alcock, LLNL
- March 27, 1998
“Variations on Globular Cluster Systems”
Markus Kissler-Patig, UC Obs./Lick Obs.
- April 3, 1998
“Probing the Universe at $z > 5$ ”
Daniel Stern, UC Berkeley

- April 10, 1998
“CVs in Globular Clusters: Clues to Stellar,
Binary, and Cluster Evolution”
Josh Grindlay, Harvard-Smithsonian
- April 15, 1998
“Kilohertz QPO—Puzzles and Promises”
Michiel van der Klis, University of Amsterdam
- April 17, 1998
“Are Most QSOs Buried? (Polarization of an
IRAS-Selected AGN Sample)”
Beverly Wills, University of Texas at Austin
- April 24, 1998
“The Physics of Powerful Radio Galaxies and
Their Environments”
Chris Carilli, National Radio Astronomy Obs.
- April 24, 1998
“LLNL’s CTBT R&D: Where We Are and Where
We’re Going”
Jay Zucca, LLNL
- May 1, 1998
“Near-IR Searches for High-Redshift Galaxies”
Andrew Bunker, UC Berkeley
- May 8, 1998
“More on Galaxy Formation from Sub-Galactic
Clumps”
Roger Windhorst, Arizona State University
- May 15, 1998
“Solar Physics and Astrophysics with the High
Energy Solar Spectroscopic Imager (HESSI)”
David Smith, UC Berkeley
- May 22, 1998
“Origin and Evolution of X-Ray Emitting Gas in
Elliptical Galaxies: Cosmological and Environ-
mental Influences”
William Mathews, UC Santa Cruz
- June 5, 1998
“The Hobby-Eberly Telescope Low-Resolution
Spectrograph: Status and Science”
Gary Hill, University of Texas at Austin
- June 19, 1998
“Atmospheric Transport and Fate: Chemical and
Biological Releases in Urban Environment”
Don Ermak, LLNL
- August 28, 1998
“CASTLES: The Lenses, the Sources, and Their
Hosts”
Hans Walter Rix, University of Arizona
- September 4, 1998
“Deconvolution of Astronomical Images and
Spectra: Application to Gravitational Lenses”
Frederic Courbin, University of Liege, France
- September 11, 1998
“Double-Mode RR Lyrae Stars: The Right Lumi-
nosity Scale Indicators”
Geza Kovacs, Konkoly Observatory, Hungary
- September 18, 1998
“Forming the Most Massive Stars”
Margaret Hanson, University of Cincinnati
- September 18, 1998
“Center for Fuels Assessment”
Dave Layton, LLNL
- October 2, 1998
“Gravitational Radiation from Accreting Neutron
Stars: Implications for Millisecond Pulsar For-
mation and LIGO”
Lars Bildsten, UC Berkeley
- October 9, 1998
“Multiple Globular Cluster Populations in Ellipti-
cal Galaxies”
Douglass Geisler, Kitt Peak National Observatory

- October 16, 1998
“Stellar Microscopy: Imaging by Gravitational Microlensing”
Dimitar Sasselov, Harvard-Smithsonian
- October 16, 1998
“Mechanisms for the Impact Delivery of Biochemical Precursors to the Early Earth”
Jennifer Blank, UC Berkeley
- October 23, 1998
“State of Cosmological Tests”
James Peebles, Princeton University
- October 23, 1998
“Near-Field Migration of Radionuclides in Groundwater away from an Underground Nuclear Test”
Andy Tompson and Carol Bruton, LLNL
- October 30, 1998
“The Arecibo Gregorian Upgrade—History and Scientific Prospects”
Paul Goldsmith, Cornell University
- November 6, 1998
“Death of the Dinos (et al.): Physical Effects of the K/T Impact”
H. Jay Melosh, University of Arizona
- November 13, 1998
“The First Stars and Quasars in the Universe”
Abraham Loeb, Harvard University
- November 19, 1998
“Narrow-Line Seyfert 1 Galaxies: A Laboratory for AGN Astrophysics”
Karen Leighly, Columbia University
- November 20, 1998
“The Evolution of Interstellar Dust Out to $z = 0.001$ ”
Geoffrey Clayton, University of Louisiana
- November 20, 1998
“PCMDI: Current and Future Activities”
Jerry Potter, LLNL
- November 30, 1998
“Modeling the Central Parsec of the Milky Way”
Robert Coker, University of Arizona
- December 4, 1998
“Hubble Space Telescope Observations of Jupiter’s Aurora”
John Clarke, University of Michigan
- December 11, 1998
“The Two-Micron All-Sky Survey”
Roc Cutri, California Institute of Technology

Section V. Bibliography

1998

- Alcock, C., Book Review, *Hunting Down the Universe: The Missing Mass, Primordial Black Holes, and Other Dark Matters*, by Michael Hawkins, *Phys. Today* **51**(7), 72 (1998).
- Alcock, C., "The Highest Energy Phenomena in the Universe, Final Report, 95-ERI-008," UCRL-ID-130705, Lawrence Livermore National Laboratory, Livermore, CA (1998).
- Alcock, C., "Microlensing: An Observational Overview," in *Failed Stars and Super Planets: A Report Based on the Workshop on Substellar-Mass Objects*, submitted (1998).
- Alcock, C., R. A. Allsman, D. Alves, R. Anarsi, E. Aubourg, T. A. Axelrod, P. Bareyrne, J.-Ph. Beaulieu, A. Becker, D. P. Bennett, S. Brehin, F. Cavalier, S. Char, K. H. Cook, R. Ferlet, J. Fernandez, K. C. Freeman, K. Griest, Ph. Grison, M. Gros, C. Gry, J. Guibert, M. Lachièze-Rey, B. Laurent, M. J. Lehner, É. L. Lesquoy, C. Magneville, S. L. Marshall, É. Maurice, A. Milsztajn, D. Minniti, M. Moniez, O. Moreau, L. Moscoso, N. Palanque-Delabrouille, B. A. Peterson, M. R. Pratt, L. Prévôt, F. Queinnec, P. J. Quinn, C. Renault, J. Rich, M. Spiro, C. W. Stubbs, W. Sutherland, A. Tomaney, T. Vandehei, A. Vidal-Madjar, L. Vigrous, and S. Zylberajch, "EROS and MACHO Combined Limits on Planetary Mass Dark Matter in the Galactic Halo," *Astrophys. J.* **499**, L9 (1998).
- Alcock, C., R. A. Allsman, D. Alves, T. S. Axelrod, A. C. Becker, A. Basu, L. Baskett, D. P. Bennett, K. H. Cook, K. C. Freeman, K. Griest, J. Guern, M. J. Lehner, S. L. Marshall, D. Minniti, B. A. Peterson, M. R. Pratt, P. J. Quinn, A. W. Rodgers, C. Stubbs, W. Sutherland, T. Vandehei, and D. L. Welch, "The RR Lyrae Population of the Galactic Bulge from the MACHO Database: Mean Colors and Magnitudes," *Astrophys. J.* **492**, 190 (1998).
- Alcock, C., R. A. Allsman, D. A. Alves, T. S. Axelrod, A. C. Becker, D. P. Bennett, A. Basu, L. Baskett, D. P. Bennet, K. H. Cook, K. C. Freeman, K. Griest, A. Gould, J. A. Guern, M. J. Lehner, S. L. Marshall, D. Minniti, B. A. Peterson, P. Popowski, M. R. Pratt, P. J. Quinn, A. W. Rodgers, C. W. Stubbs, W. Sutherland, T. Vandehei, and D. L. Welch (The MACHO Collaboration), "The Zero Point of Extinction toward Baade's Window from RR Lyrae Stars," *Astrophys. J.* **494**, 396 (1998).
- Alcock, C., R. A. Allsman, D. Alves, T. S. Axelrod, A. C. Becker, D. P. Bennett, D. F. Bersier, K. H. Cook, K. C. Freeman, K. Griest, M. J. Lehner, S. L. Marshall, D. Minniti, B. A. Peterson, A. W. Rodgers, W. Sutherland, A. Tomaney, and D. L. Welch, "The MACHO Project Large Magellanic Cloud Variable Star Inventory. VIII. The Recent Star Formation History of the LMC from the Cepheid Period Distribution," *Astron. J.*, submitted (1998).
- Alcock, C., R. A. Allsman, D. Alves, T. S. Axelrod, A. C. Becker, D. P. Bennett, K. H. Cook, A. J. Drake, K. C. Freeman, K. Griest, L. J. King, M. J. Lehner, S. L. Marshall, D. Minniti, B. A. Peterson, M. R. Pratt, P. J. Quinn, S. H. Rhie, A. W. Rodgers, P. B. Stetson, C. W. Stubbs, W. Sutherland, A. Tomaney, and T. Vandehei, "Discovery and Characterization of a Caustic Crossing Microlensing Event in the SMC," *Astrophys. J.*, submitted (1998).

- Alcock, C., R. Allsman, D. Alves, T. Axelrod, A. C. Becker, D. Bennett, K. Cook, A. Drake, K. Freeman, K. Griest, M. Lehner, S. Marshall, D. Minniti, C. A. Nelson, B. Peterson, M. Pratt, P. Quinn, C. Stubbs, W. Sutherland, A. Tomaney, T. Vandehei, and D. Welch, "Calibration of the MACHO Photometry Database," *Proc. Astron. Soc. of the Pacific*, submitted (1998).
- Alcock, C., R. Allsman, D. Alves, T. Axelrod, A. C. Becker, D. Bennett, K. Cook, A. Drake, K. Freeman, K. Griest, M. Lehner, S. Marshall, D. Minniti, B. Peterson, M. Pratt, P. Quinn, A. Rodgers, C. Stubbs, W. Sutherland, A. Tomaney, T. Vandehei, and D. Welch, "Baryonic Dark Matter: The Results from Microlensing Surveys," MACHO Summit Meeting, Canberra, Australia, August 21–28, 1998.
- Alcock, C., R. A. Allsman, D. Alves, T. S. Axelrod, A. C. Becker, D. P. Bennett, K. H. Cook, K. C. Freeman, K. Griest, J. Guern, W. A. Lawson, M. J. Lehner, S. L. Marshall, D. Minniti, B. A. Peterson, K. R. Pollard, M. R. Pratt, P. J. Quinn, A. W. Rodgers, C. W. Stubbs, W. Sutherland, and D. L. Welch, "The MACHO Project LMC Variable Star Inventory. VII: The Discovery of RV Tauri Stars and New Type II Cepheids in the LMC," *Astron. J.* **115**, 1921 (1998).
- Alcock, C., R. A. Allsman, D. Alves, T. S. Axelrod, A. C. Becker, D. P. Bennett, K. H. Cook, K. C. Freeman, K. Griest, M. J. Keane, M. J. Lehner, S. L. Marshall, D. Minniti, B. A. Peterson, M. R. Pratt, P. J. Quinn, A. W. Rodgers, C. W. Stubbs, W. Sutherland, A. B. Tomaney, T. Vandehei, and D. L. Welch, "First Detection of a Gravitational Microlensing Candidate toward the Small Magellanic Cloud," *Astrophys. J. Lett.* **491**, L11 (1998).
- Alcock, C., R. A. Allsman, D. Alves, T. S. Axelrod, A. C. Becker, D. P. Bennett, K. H. Cook, K. C. Freeman, K. Griest, D. W. Kurtz, M. J. Lehner, S. L. Marshall, D. Minniti, B. A. Peterson, M. R. Pratt, P. J. Quinn, A. W. Rodgers, W. Sutherland, A. Tomaney, and D. L. Welch, "The Blazhko Effect in RR Lyrae Stars: Strong Observational Support for the Oblique Pulsator Model in the Three Stars," *Astrophys. J.*, submitted (1998).
- Alcock, C., R. A. Allsman, D. Alves, T. S. Axelrod, D. P. Bennett, P. A. Charles, K. H. Cook, K. C. Freeman, K. Griest, M. J. Lehner, M. Livio, S. L. Marshall, D. Minniti, B. A. Peterson, M. R. Pratt, P. J. Quinn, A. W. Rodgers, K. A. Southwell, C. W. Stubbs, W. Sutherland, and D. L. Welch, "Optical Identification of the LMC Supersoft Source RX J0527.8-6954 from MACHO Project Photometry," *Mon. Not. R. Astron. Soc.* **291**, L13, (1998).
- Alcock, C., R. A. Allsman, D. Alves, T. S. Axelrod, D. P. Bennett, P. A. Charles, K. H. Cook, D. O'Donoghue, K. C. Freeman, K. Griest, J. Guern, M. J. Lehner, M. Livio, S. L. Marshall, D. Minniti, B. A. Peterson, M. R. Pratt, P. J. Quinn, A. W. Rodgers, K. A. Southwell, C. W. Stubbs, W. Sutherland, and D. L. Welch, "Optical Photometry of the Eclipsing Large Magellanic Cloud Supersoft Source CAL 87," *Mon. Not. R. Astron. Soc.* **287**, 699, (1998).
- Alonso, M., D. Minniti, A. A. Zijlstra, and E. Tolstoy, "Infrared Photometry of the Inner Regions of the Dwarf Irregular Galaxy NGC 3109," *Astron. Astrophys.*, submitted (1998).
- Alves D., C. Alcock, K. Cook, S. Marshall, D. Minniti, R. Allsman, T. Axelrod, K. Freeman, B. Peterson, A. Rodgers, K. Griest, T. Vandehei, A. Becker, C. Stubbs, A. Tomaney, D. Bennett, M. Lehner, P. Quinn, M. Pratt, W. Sutherland, and D. Welch, "The MACHO Project LMC Variable Star Inventory: Classical Cepheids and AGB Variables," *Proc. of IAU Joint Discussion No. 24*, "Pulsating Stars—Recent Developments in Theory and Observation," M. Takeuti and D. Sasselov, eds. (1998).

- Alves, D. A., D. W. Hoard, and B. Rodgers, "IRAS 06562-0337, The Ironclad Nebula: A New Young Star Cluster," *Astron. J.* **116**(1), 245 (1998).
- Alves, D. R., and A. Sarajedini, "The Age-Dependent Luminosities of the Red Giant Branch Bump, Asymptotic Giant Branch Bump, and Horizontal Branch Red Clump," *Astrophys. J.*, submitted (1998).
- Arav, N., "Are there Clouds in the BLR? Keck Observations of NGC 4151," Conference on "Structure and Kinematics of Quasar Broad Line Regions," Lincoln, Nebraska, March 22–26, 1998.
- Arav, N., "PG 0946+301: The Rosetta Stone of BALQSOs?," Conference on "Structure and Kinematics of Quasar Broad Line Regions," Lincoln, Nebraska, March 22–26, 1998.
- Arav, N., K. T. Korista, M. de Kool, V. T. Junkkarinen, and M. C. Begelman, "HST Observations of Broad Absorption Line Quasar PG 0946+301," *Astrophys. J.*, submitted (1998).
- Athreya, R. M., V. K. Kapahi, P. J. McCarthy, and W. van Breugel, "Large Rotation Measures in Radio Galaxies at $z > 2$," *Astron. Astrophys.* **329**(3), 809 (1998).
- Bréger, L., and B. Romanowicz, "The Structure of D" in 3D beneath the Central Pacific," SEDI Meeting (1998).
- Bréger, L., B. Romanowicz, and H. Tkalčić, "The Influence of Deep Mantle Heterogeneity of PKP(AB-DF) Differential Travel Times," AGU Fall Meeting (1998).
- Brotherton, M. S., W. van Breugel, R. J. Smith, B. J. Boyle, T. Shanks, S. M. Croom, L. Miller, and R. H. Becker, "Discovery of Radio-Loud Broad Absorption Line Quasars using Ultraviolet Excess and Deep Radio Selection," *Astrophys. J. Lett.*, submitted (1998).
- Brotherton, M. S., B. J. Wills, A. Dey, W. van Breugel, and R. Antonucci, "Spectropolarimetry of 3CR 68.1: A Highly Inclined Quasar," *Astrophys. J.* **501**, 110 (1998).
- Buchalter, A., D. J. Helfand, R. H. Becker, and R. L. White, "Constraining ≥ 0 with the Angular-Size Redshift Relation of Double-Lobed Quasars in the FIRST Survey," *Astrophys. J.* **494**, 503 (1998).
- Connaughton, V., C. R. Robinson, M. L. McCollough, and S. A. Laurent-Muehleisen, "BATSE Observations of BL Lac Objects," BL Lac Phenomenon Conference, Turku, Finland, June 22–26, 1998.
- Cook, K. (ed.), "1998 Observatory Report," *Bull. Am. Astron. Soc.*, submitted (1998).
- Cook, K. H., M. Mateo, E. Olszewski, S. S. Vogt, C. Stubbs, and A. Diercks, "The Systemic Velocity and Internal Kinematics of the Dwarf Galaxy LGS 3: An Optical Foray beyond the Milky Way," *Proc. Astron. Soc. of the Pacific*, submitted (1998).
- De Breuck, C., M. S. Brotherton, H. D. Tran, W. van Breugel, and H. J. A. Röttgering, "Discovery of an Ultra-Steep Spectrum, Highly Polarized Red Quasar at $z = 1.462$," *Astron. J.* **116**(1), 13 (1998).
- De Breuck, C., W. van Breugel, H. Röttgering, and G. Miley, "ATCA Search for the Most Distant Radio Galaxies in the Southern Hemisphere," ATNF Newsletter, submitted (1998).
- de Pater, I., S. G. Gibbard, B. Macintosh, D. Gavel, C. E. Max, A. M. Ghez, E. F. Young, and C. P. McKay, "A Comparison of HST and Keck Data on Titan's Surface," *WPAGU Conf. Proc.*, in press (1998).
- Drinkwater, M. J., and M. D. Gregg, "High Surface Brightness Dwarf Galaxies in the Fornax Cluster," *Mon. Not. R. Astron. Soc.* **296**, L15 (1998).

- Gibbard, S. G., I. de Pater, H. Roe, B. Macintosh, D. Gavel, C. E. Max, K. H. Baines, and A. Ghez, "High-Resolution Infrared Imaging of Neptune from the Keck Telescope," *Icarus*, in prep. (1998).
- Gibbard, S., E. H. Levy, and J. I. Lunine, "Lightning on Neptune," *Icarus*, submitted (1998).
- Gibbard, S. G., B. Macintosh, D. Gavel, C. E. Max, I. de Pater, A. M. Ghez, E. F. Young, and C. P. McKay, "Titan: High-Resolution Speckle Images from the Keck Telescope," *Icarus*, in press (1998).
- Gibbard, S. G., B. Macintosh, C. E. Max, D. Gavel, and I. de Pater, "High-Resolution Speckle Images of Neptune from the Keck Telescope," *Bull. Am. Astron. Soc.* **30**, 1099 (1998).
- Graham, J. R., M. Abrams, C. Bennett, J. Carr, K. Cook, A. Dey, J. Najita, and E. Wishnow, "The Performance and Scientific Rationale for an Infrared Imaging Fourier Transform Spectrograph on a Large Space Telescope," *Proc. Astron. Soc. of the Pacific*, submitted (1998).
- Gregg, M., P. L. Schechter, R. H. Becker, D. J. Helfand, and R. L. White, "The First FIRST Gravitationally Lensed Quasar: FBQ 0951 + 2635," *Astron. J.* **115**, 1371 (1998).
- Gregg, M. D., and M. J. West, "Galaxy Disruption as the Origin of Intracluster Light in the Coma Cluster of Galaxies," *Nature* **396(6711)**, 549 (1998).
- Griest, K., and N. Safizadeh, "The Use of High-Magnification Microlensing Events in Discovering Extrasolar Planets," *Astrophys. J.*, submitted (1998).
- Halpern, J. P., and E. C. Moran, "X-Ray and Optical Spectroscopy of IRAS 20181-2244: Not a Type 2 QSO, But a 'I Zw 1' Object," *Astrophys. J.* **494**, 194 (1998).
- Hwang, D. Q., M. Ryutova, and H. Mclean, "Penetration of a Compressible Magnetized Plasma Object into a Low Beta Target Plasma," *Phys. Plasma*, submitted (1998).
- Kapahi, V. K., R. M. Athreya, C. R. Subrahmanya, J. C. Baker, R. W. Hunstead, P. J. McCarthy, and W. van Breugel, "The Molonglo Reference Catalogue. I. Jy Radio Source Survey. III. Identification of a Complete Quasar Sample," *Astrophys. J. Suppl. Ser.* **118**, 327 (1998).
- Laurent-Muehleisen, S. A., R. H. Becker, W. Brinkmann, J. Seibert, E. D. Feigelson, R. I. Köllgaard, G. Schmidt, and P. Smith, "Four New BL Lac Surveys: Sampling New Populations," BL Lac Phenomenon Conference, Turku, Finland, June 22–26, 1998.
- Laurent-Muehleisen, S. A., R. I. Köllgaard, R. Ciardullo, E. D. Feigelson, W. Brinkmann, and J. Siebert, "Radio-Loud Active Galaxies in the Northern ROSAT All-Sky Survey. III. New Spectroscopic Identifications from the Rass-Green Bank BL Lacertae Survey," *Astrophys. J. Suppl. Ser.* **118(1)**, 127 (1998).
- Lehnert, M. D., and R. H. Becker, "Spectroscopy of the Extended Emission Associated with Two High- z Quasars," *Astron. Astrophys.* **332(2)**, 503 (1998).
- Lehnert, M. D., W. J. M. van Breugel, T. M. Heckman, and G. K. Miley, "HST Imaging of the Host Galaxies of High Redshift Radio-Loud Quasars," *Astrophys. J.*, submitted (1998).
- Macintosh, B., D. Gavel, S. Gibbard, C. E. Max, I. de Pater, A. Ghez, and M. Eckart, "Infrared Speckle Imaging of Io's Volcanoes with 60 km/pixel Resolution," *EOS* **791**, F539 (1998).
- Macintosh, B., D. Gavel, S. Gibbard, C. E. Max, I. de Pater, A. Ghez, and J. Spencer, "Infrared Speckle Imaging of the July/August 1998 Transient Volcano on Io," *Icarus*, in prep. (1998).
- Minniti, D., C. Alcock, R. Allsman, D. Alves, T. Axelrod, A. C. Becker, D. Bennett, K. Cook, A. Drake, K. Freeman, K. Griest, M. Lehner,

- S. Marshall, B. Peterson, M. Pratt, P. Quinn, A. Rodgers, C. Stubbs, W. Sutherland, A. Tomaney, T. Vandehei, and D. Welch, "MACHO RR Lyrae in the Inner Halo and Bulge," MACHO Summit Meeting, Canberra, Australia, August 21–28, 1998.
- Minniti, D., C. Alcock, R. Allsman, D. Alves, T. Axelrod, A. D. Becker, D. Bennett, K. Cook, A. Drake, K. Freeman, K. Griest, M. Lehner, S. Marshall, B. Peterson, M. Pratt, P. Quinn, A. Rodgers, C. Stubbs, W. Sutherland, A. Tomaney, T. Vandehei, and D. Welch, "Variable Stars in the MACHO Bulge Database," International Symposium on Astrophysics, Research, and Science Education, Castel Gandolfo, Italy, June 13–21, 1998.
- Minniti, D., T. R. Bedding, R. Soria, A. Dey, F. R. Marleau, J. Graham, M. Liu, and S. Charlot, "Old Metal-Rich Stars in the Halo of the Giant Elliptical Galaxy NGC 5128," *Nature*, submitted (1998).
- Minniti, D., M. Kissler-Patig, and D. A. Forbes, "Constraints on the Merger Models of Elliptical Galaxies from Their Globular Cluster Systems," *Mon. Not. R. Astron. Soc.* **298**(4), 1123 (1998).
- Minniti, D., T. Vandehei, K. H. Cook, K. Griest, and C. Alcock, "Detection of Lithium in a Main Sequence Bulge Star using Keck I as a 15m Diameter Telescope," *Astrophys. J.* **499**, L175 (1998).
- Minniti, D., and A. A. Zijlstra, "A Dwarf Irregular Galaxy at the Edge of the Local Group: Stellar Populations and Distance of IC 5152," *Astron. J.*, submitted (1998).
- Minniti, D., A. A. Zijlstra, and M. V. Alonso, "Do all Dwarf Irregular Galaxies have Population II Stellar Halos? The Stellar Populations of NGC 3109," *Astron. J.*, submitted (1998).
- Nilsson, K., L. O. Takalo, T. Pursimo, A. Sillanpää, J. Heidt, J. Wagner, S. A. Laurent-Muehleisen, and W. Brinkmann, "The Blue Arc of RGB1745+398: The First Gravitational Arc near a BL Lacertae Object?," *Astrophys. J. Lett.*, submitted (1998).
- Oglesby, D. D., R. J. Archuleta, and S. B. Nielsen, "Dynamic Modeling of Thrust and Normal Faults: Differences in Near-Source Ground Motion," *Seis. Res. Lett.* **69**, 142 (1998).
- Oglesby, D. D., R. J. Archuleta, and S. B. Nielsen, "Dynamic Simulation of Dip-Slip Faulting with Temporally Varying Normal Stress," *Suppl. EOS Trans., Amer. Geophys. Union* **78**, 477 (1997).
- Oglesby, D. D., R. J. Archuleta, and S. B. Nielsen, "Earthquakes on Dipping Faults: The Effects of Broken Symmetry," *Science* **230**, 1055 (1998).
- Oglesby, D. D., R. J. Archuleta, and S. B. Nielsen, "The Dynamics of Dip-Slip Faulting and the Free Surface Interaction," *Suppl. EOS Trans., Amer. Geophys. Union* **79**, 222 (1998).
- Parriott, J., and C. Alcock, "On the Number of Comets around White Dwarf Stars: Orbit Survival during the Late Stages of Stellar Evolution," *Astrophys. J.* **501**, 357 (1998).
- Pentericci, L., H. J. A., Röttgering, G. K. Miley, P. McCarthy, H. Spinrad, W. J. M. van Breugel, and F. Macchetto, "HST Images and Properties of the Most Distant Radio Galaxies," *Astron. Astrophys.*, submitted (1998).
- Pentericci, L., H. J. A., Röttgering, G. K. Miley, P. McCarthy, H. Spinrad, W. J. M. van Breugel, and F. Macchetto, "HST Images of the Extremely Clumpy Radio Galaxy 1138-262 at $z = 2.2$," *Astrophys. J.* **504**, 139 (1998).
- Piatti, A. E., J. J. Claria, E. Bica, D. Geisler, and D. Minniti, "A Photometric and Spectroscopic Study of the Southern Open Clusters Pismis 18, Pismis 19, NGC 6005, and NGC 6253," *Astron. J.* **116**(2), 801 (1998).
- Piechota, T. C., J. A. Dracup, and J. Feddema, "Integrated Hydrologic Modeling of the

- Malibu Creek Watershed,” *EOS Trans., Am. Geophys. Union*, 1998 Spring Meeting (1998).
- Pollitz, F. F., R. Bürgmann, and B. Romanowicz, “Transient Velocity of Oceanic Lithosphere: A Source for External Triggering of Earthquakes,” Southern California Earthquake Center Workshop “Earthquake Stress Triggering, Fault Interaction, and Frictional Failure,” Carmel, California, invited presentation, June 10, 1998.
- Pollitz, F. F., G. Peltzer, and R. Bürgmann, “Interpretation of Long-Term Postseismic Crustal Movements around the 1992 Landers Rupture Zone,” *Am. Geophys. Union*, Fall Meeting, San Francisco, California, invited presentation, December 7, 1998.
- Reyes A. O., “Vacuum Line for Extraction of Dissolved Inorganic Carbon from Natural Water Samples for $^{14}\text{C}/\text{C}$ and $\delta^{13}\text{C}$ Analysis,” in prep. (1998).
- Richards, G. T., D. G. York, B. Yanny, R. I. Köllgaard, S. A. Laurent-Muehleisen, and D. E. Vanden Berk, “Determining the Fraction of Intrinsic C IV Absorption in QSO Absorption Line Systems,” *Astrophys. J.*, submitted (1998).
- Ryutova, M., “Estimate of the Energy Flux from Time-Distance Analysis,” *Astrophys. J. Lett.* **490**, L111 (1998).
- Ryutova, M., and Scherrer, P., “A New Method for Diagnostics of Solar Magnetic Fields and Flows from Time-Distance Analysis,” *Astrophys. J.* **494**, 438 (1998).
- Ryutova, M. P., C. J. Schrijver, R. A. Shine, T. D. Tarbell, T. E. Berger, and A. M. Title, “On the Dynamic of Magnetic Flux Concentrations in Quiet Photospheric Network,” *Astrophys. J.*, submitted (1998).
- Ryutova, M., R. Shine, A. Title, and J. I. Sakai, “A Possible Mechanism for the Origin of Emerging Flux in the Sunspot Moat,” *Astrophys. J.* **492**, 402 (1998).
- Siebert, J., W. Brinkmann, and S. A. Laurent-Muehleisen, “Recent X-Ray Observations of Intermediate BL Lac Objects,” Conference on “BL Lac Phenomenon,” Turku, Finland, June 22–26, 1998.
- Siebert, J., W. Brinkmann, S. A. Laurent-Muehleisen, and M. Matsuoka, “The Broad Band X-Ray Spectra of Intermediate BL Lac Objects,” 32nd COSPAR Scientific Assembly, Nagoya, Japan, July 12–19, 1998.
- Siebert, J., K. M. Leighly, W. Brinkmann, S. A. Laurent-Muehleisen, T. Boller, and M. Matsuoka, “An ASCA Observation of the Radio-Loud Narrow-Line Seyfert 1 Galaxy RGB J0044+193,” *Astron. Astrophys.*, submitted (1998).
- Stanford, S. A., “Elliptical Galaxies in High- z Clusters: How Old are They?,” Conference on “The Birth of Galaxies,” Blois, France, June 29–July 3, 1998.
- Tarbell, T., M. P. Ryutova, and J. Covington, “Heating and Jet Formation by Hydrodynamic Cumulation in Solar Atmosphere,” *Astrophys. J. Lett.*, submitted (1998).
- Tran, H. D., M. S. Brotherton, S. A. Stanford, and W. van Breugel, “Hidden Quasars in Ultraluminous Infrared Galaxies,” IAU Symposium 194, Byurakan, Armenia, August 17–21, 1998.
- Tran, H. D., M. S. Brotherton, S. A. Stanford, W. van Breugel, A. Dey, D. Stern, and R. Antonucci, “A Polarimetric Search for Hidden Quasars in the Three Radio Selected Ultraluminous Infrared Galaxies,” *Astrophys. J.*, submitted (1998).
- Tran, H. D., M. H. Cohen, P. M. Ogle, R. W. Goodrich, and S. D. Alighieri, “Scattered Radiation from Obscured Quasars in Distant Radio Galaxies,” *Astrophys. J.* **500**, 660 (1998).

van Breugel, W. J. M., S. A. Stanford, H. Spinrad, D. Stern, and J. R. Graham, "Morphological Evolution in High Redshift Radio Galaxies and the Formation of Giant Elliptical Galaxies," *Astrophys. J.* **502**, 614 (1998).

1997

Alcock, C., R. A. Allsman, D. Alves, T. S. Axelrod, A. C. Becker, D. P. Bennett, K. H. Cook, K. C. Freeman, K. Griest, J. Guern, M. J. Lehner, S. L. Marshall, D. Minniti, B. A. Peterson, M. R. Pratt, P. J. Quinn, A. W. Rodgers, A. Rorabeck, W. Sutherland, and D. L. Welch, "The MACHO Project LMC Variable Star Inventory. VI. The Second-Overtone Mode of Cepheid Pulsation First/Second Overtone (FO/SO) Beat Cepheids," *Astron. J.* **109**, 1653 (1997).

Alcock, C., R. A. Allsman, D. Alves, T. S. Axelrod, A. C. Becker, D. P. Bennett, K. H. Cook, K. C. Freeman, K. Griest, J. Guern, M. J. Lehner, S. L. Marshall, D. Minniti, B. A. Peterson, M. R. Pratt, P. J. Quinn, A. W. Rodgers, C. Stubbs, W. Sutherland, A. B. Tomaney, T. Vandehei, and D. L. Welch, "Is the Large Magellanic Cloud Microlensing Due to an Intervening Dwarf Galaxy?," *Astrophys. J. Lett.* **490**, L59 (1997).

Kurki-Suonio, H., K. Jedamzik, and G. J. Mathews, "Stochastic Isocurvature Baryon Fluctuations, Baryon Diffusion, and Primordial Nucleosynthesis," *Astrophys. J.* **479**, 31 (1997).

Röttgering, H. J. A., R. van Ojik, G. K. Miley, K. C. Chambers, W. J. M. van Breugel, and S. de Koff, "Spectroscopy of Ultra-Steep-Spectrum Radio Sources: A Sample of $z > 2$ Radio Galaxies," *Astron. Astrophys.* **326**, 505 (1997).

Section VI. Fiscal Year 1999 IGPP–LLNL University Collaborative Research Program

Project No.	UC Campus	Campus Investigators	LLNL Collaborators	Project Title
99-AP001	Berkeley	I. De Pater H. Roe	S. Gibbard D. Gavel B. Macintosh C. Max	Speckle and Adaptive Optics Imaging of Planets and Satellites
99-AP012	Berkeley	J. Rice I. De Pater	C. Alcock	Detection of Occultations
99-GS013	Berkeley	B. Romanowicz	S. Larsen	3D Modeling of Structure in D''
99-GS018	Berkeley	R. Jeanloz	J. Akella	Ultra-High Pressure Melting Studies
99-GS019	Berkeley	K. Nishiizumi L. Wang	R. Finkel	Cosmogenic Nuclide Systematics in Olivine and Calcite
99-AP026	Berkeley	H. Spinrad D. Stern	W. van Breugel	A Search for Red Quasars: The Radio-Loud Quasar Population at $z \geq 3$
99-AP007	Davis	R. Becker	W. van Breugel	A Radio Selected Sample of Active Galactic Nuclei
99-GS005	Los Angeles	A. Yin T. M. Harrison P. Kapp	F. J. Ryerson	Initiation Age and Rate of E-W Extension in Northern Tibet: Implications for the Dynamic Cause of Tibetan Uplift
99-GS006	Los Angeles	S. Mojzsis C. Manning	K. Knauss	The Isotopic and Chemical Composition of Carbonaceous Matter Produced by Serpentinization—An Exploration of a Potential Fischer-Tropsch Type Reaction Process
99-GS010	Los Angeles	T. La Tourrette	I. Hutcheon	Experimental Mineral Diffusion Studies: Constraints on the Thermal Histories of Meteorites and Planetary Formation Timescales
99-GS015	Los Angeles	J. Vidale	D. Dodge	High-Resolution Study of Inner-Core Rotation
99-AP017	Los Angeles	J. Dawson L. Silva	S. Dalhed	Collective Absorption Properties of Neutrinos in Supernovae

Project No.	UC Campus	Campus Investigators	LLNL Collaborators	Project Title
99-GS008	Riverside	L. Owen L. Gualtieri J. Q. Spencer	R. Finkel M. Caffee	Timing of Late Quaternary Glaciation in the Hunza Valley, Karakoram Mountains, Northern Pakistan
99-AP020	San Diego	A. Quirrenbach	C. Max D. Gavel B. Macintosh S. Olivier	First Extragalactic Astronomy with Laser Guide Star Adaptive Optics
99-AP023	San Diego	K. Griest T. Vandehei	C. Alcock	A Full Determination of the MACHO Microlensing Detection Efficiency toward the LMC, SMC, and Bulge
99-GS021	Santa Cruz	Q. Williams H. Scott	F. J. Ryerson	Experimental Constraints on the Chemical Evolution of Icy Satellites
99-GS022	Santa Cruz	T. Lay S. Bilek	W. Walter	Source Effects on Regional Seismic Discriminant Measurements
99-GS025	Santa Cruz	R. Anderson	D. Farber R. Finkel	Cosmogenic Exposure Age Dating of Glacial Deposits in the Cordillero Blanca, Peru: Toward a Detailed Record of Southern Tropical Climate Change
99-GS027	Santa Cruz	J. Revenaugh E. Havens	S. Myers	Collaborative Seismic Investigation of South American Tectosphere
99-GS028	Santa Cruz	S. Schwartz S. Russell	A. Rodgers W. Walters	Seismic Velocity Structure of the North and Central African Lithosphere from Upper Mantle P, PP, S, and SS Waveform Modeling